STRUCTURAL AND FUNCTIONAL STUDIES OF PROTEINS INVOLVED IN MITOCHONDRIAL FUNCTION AND STRUCTURE

By

Yanfeng Zhang

A DISSERTATION

Submitted to
Michigan State University
in partial fulfillment of the requirements
for the degree of

DOCTOR OF PHILOSOPHY

Genetics

2009

ABSTRACT

STRUCTURAL AND FUNCTIONAL STUDIES OF PROTEINS INVOLVED IN MITOCHONDRIAL FUNCTION AND STRUCTURE

Yanfeng Zhang

The dynamics of continuous fission and fusion events maintain normal mitochondrial morphology and reduce the number of functional defects that could lead to a variety of diseases. DLP-1 and MFNs are essential protein components of human mitochondrial fission and fusion machineries, and functional and structural studies of these proteins would increase our understanding of the molecular mechanisms of mitochondrial dynamics, function, and structure.

In this thesis, the biochemical and structural properties of recombinant DLP-1 and selected mutants have been studied. The G350D and R365S mutants in the middle domain severely impair the GTPase activity, but have no significant impact on the protein's oligomeric state, indicating that these two mutations interrupted the intramolecular but not intermolecular interactions, and therefore, the middle domain of DLP-1 is important for the protein activity probably by facilitating appropriate connections between the GTPase domain and the GED. The DLP-1 and the isolated PH-like domain bound free phosphoinositides indicated that DLP-1 may interact with membranes directly by binding acidic phospholipids preferentially phosphoinositides, and the PH-like domain may be responsible for the interactions. Although GTPase activity is abolished, the ΔPH bound to liposomes, which suggested that in addition to the PH-like domain, other regions of DLP-1 may function as lipids-interacting enhancer as well as scaffolds for orienting the PH-like domain into appropriate membrane targeting. Structural studies of DLP-1 and MFNs by way of X-ray crystallography have been

attempted. Molecular protein engineering was designed and performed to improve protein solubility and to increase the likelihood of protein crystallization.

The recently identified (pro)renin receptor ((P)RR) is an important protein molecule for the renin-angiotensin system (RAS), a mechanism regulating blood pressure and cardiovascular function. The (P)RR C-terminus including the cytoplasmic tail is involved in the assembly of the V_0 portion of the vacuolar proton-translocating ATPase. The cytoplasmic tail is short, but functionally important for the pivotal roles of (P)RR in a number of signal transduction pathways that activated by binding of (pro)renin.

Finally, the last 19 amino acids of the (P)RR corresponding to the cytoplasmic tail were fused into the C-terminus of *E. coli* maltose binding protein (MBP), and the chimera was expressed in *E. coli* and purified to homogeneity. Protein crystals, in the presence and absence of the MBP ligand maltose, were obtained, and X-ray diffraction data to 2.0 Å resolution were collected. Despite significantly different unit-cell dimensions and molecular packing, two monomers of the MBP fusion protein were found in the asymmetric unit for both structures. Although the (P)RR cytoplasmic tail appeared as a relatively flexible loop without obvious secondary structural elements, it seemed responsible for the dimerization of MBP fusion protein in the asymmetric unit. The residues in the cytoplasmic tail, particularly the two tyrosines, dominate the interdimer interactions, suggesting a role of the cytoplasmic tail in protein oligomerization.

Dedicated to my beloved: my wife and my parents

ACKNOWLEDGEMENTS

Fist and foremost, I would like to express my sincere gratitude to my advisor, Dr. R. Michael Garavito, for his superb guidance throughout my doctoral program. I would like to thank him for his support, encouragement, patience, and for giving me freedom to pursue all my ideas and interests, and educating me tremendously on protein chemistry.

I would like to thank my graduate committee members, Dr. Shelagh Ferguson-Miller, Dr. James Geiger, and Dr. Katherine W. Osteryoung, for their guidance on my research. I am grateful for their invaluable advice and suggestions.

I would also like to acknowledge present and former Garavito lab members, Dexin Sui, Yi Zheng, Amy Scharmen, Young-Moon Cho, Michael Dumond, Dr. Nicole Webb, Dr. Christine Harman, and Dr. Rachel Powers, for their help and discussions on DNA cloning, protein expression and purification, and crystallography.

I thank Dr. Ling Qin and Jian Liu in the Ferguson-Miller lab for their help on freezing crystals, collecting data, and building molecular models. I would like to thank Dr. David DeWitt for reading my research proposal.

I would like to specially thank Dr. Barbara Sears, Director of Genetics Graduate Program. I am grateful to her for her advice and guidance which helped me tremendously for my personal and academic growth. I thank Jeannine Lee for her help.

I thank staff scientists at LS-CAT at Advanced Photon Source, Argonne National Laboratory, for their training and help with data collections. Dr. Zdzislaw Wawrzak performed the data collection of the apo-form MBP-(P)RR19 crystals.

Finally, I thank my wife, Xiaoli Gao, my parents, and parents-in-law. Without their love and support, none of these would have been accomplished.

TABLE OF CONTENTS

LIST OF TABLES ix

LIST OF FIGURES x

ABBREBIATIONS xiii

CHAPTER 1
BACKGROUND AND INTRODUCTION 1
1.1 Mitochondrial fission and fusion, dynamin-like protein 1, and mitofusins 2
1.1.1 Mitochondrial evolution and function 2
1.1.2 Mitochondrial fission and fusion 3
1.1.3 Molecular mechanisms of Mitochondrial fission and fusion 7
1.2 Renin-angiotensin system, (pro)renin receptor, and the membrane connection 15
1.2.1 Renin-angiotensin systems (RAS) 15
1.2.2 Prorenin and (pro)renin receptor 18
1.2.3 Roles of C-terminus of (P)RR in functions of intracellular compartments 21
1.2.4 Pivotal role of the cytoplasmic domain of (P)RR in signal transduction 22
1.2.5 Interactions of the (P)RR with Promyelocytic Zinc Finger Protein 23
References 26

CHAPTER 2
FUNCTIONAL EXPRESSION OF DLP-1 44
2.1 Introduction 45
2.2 Materials and methods 46
2.3 Results and discussion 50
2.3.1 Protein exprssion and purification 50
2.3.2 GTPase activities 57
2.3.3 Oligomeric states 61
2.3.4 Interactions with lipids and membranes 72
2.4 Conclusion 79
References 81

CHAPTER 3
STRUCTURAL STUDIES OF DLP-1 AND MFN-1 85
3.1 Introduction 86
3.2 Crystallization trials of DLP-1 86
3.3 Protein engineering methods for crystallization enhancement 88
3.3.1 General introduction and rationale 89
3.4 Experimental procedures, results, and discussion on DLP-1 92
3.4.1 Fragments construction 92
3.4.2 Limited proteolysis 98
3.4.3 Surface-entropy reduction 104

3.4.4 Fusion proteins for crystallization aids 110
3.4.5 Homology model of the GTPase domain of DLP-1 115
3.5 MFNs experimental procedures and results 116
3.5.1 Protein expression and purification 116
3.5.2 MFN fragments construction 118
3.5.3 Protein renaturation 125
3.6 Summary 126
References 128

CHAPTER 4
STUDIES ON THE (PRO)RENIN RECEPTOR AND THE PROMYELOCYTIC ZINC FINGER PROTEIN 131
4.1 Introduction 132
4.2 (P)RR wild type protein 133
4.3 Structural determination of the cytoplasmic tail of the (P)RR 136
4.3.1 Experimental procedures 136
4.3.2 Results and discussion 141
4.4 Cloning and expression of the promyelocytic zinc finger protein (PLZF) 172
4.4.1 Experimental procedures 172
4.4.2 Results and discussion 178
4.5 Conclusion 178
References 180

CHAPTER 5
FUTURE DIRECTIONS 189
5.1 Alternative protein expression systems and crystallization screen methods 190
5.2 Further structural studies on (P)RR and roles of tyrosines on the cytoplasmic tail in protein oligomerization and signal transduction 192
References 195

APPENDIX
PRELIMINARY MAPPING OF PLZF FRAGMENTS BINDING TO THE (P)RR CYTOPLASMIC TAIL 197

LIST OF TABLES

Table 2.1 Specific GTPase activity of DLP-1 WT and mutants 53

Table 2.2 Calculated molecular weight of DLP-1 WT and mutants by gel filtration..... 71

Table 2.3 Illustration of the binding strength of DLP-1 WT and the PH-like domain to each phospholipids by FAT-Western blot analysis 74

Table 4.1 Data-collection and processing statistics 163

Table 4.2 Potential hydrogen bonds formed between two MBP-(P)RR19 monomers... 169

LIST OF FIGURES

Figure 1.1 Dynamin superfamily members in animals and plants.....6

Figure 1.2 Schematic nonproteolytic activation of prorenin bound to the (pro)renin receptor.....20

Figure 2.1 Sequence alignments of partial GTPase domain (upper) and the middle domain (lower) of dynamin related proteins..... 52

Figure 2.2 Purification of DLP-1 WT and mutants 54

Figure 2.3 GTPase activity of purified DLP-1 WT and mutants by malachite green colorimetric assay 55

Figure 2.4 Schematic model of DLP-1 intramolecular interactions 60

Figure 2.5 Size exclusion chromatography of DLP-1 WT and mutants..... 66

Figure 2.6 FAT-Western blot analysis of phospholipids binding by DLP-1 WT and the PH-like domain 73

Figure 2.7 Liposome-binding of DLP-1 WT and mutants..... 77

Figure 3.1 Comparison of secondary structure predictions of DLP-1 from PSI-PRED and SABLE severs by visualizing the predictions.....94

Figure 3.2 Multiple-sequence alignments of DLP-1..... 95

Figure 3.3 Schematic illustration of DLP-1 constructs..... 99

Figure 3.4 SDS-PAGE analysis of Limited proteolysis of DLP-1 by different proteases 101

Figure 3.5 Mass determination of the DLP-1 proteolytic fragment by mass spectrometry 102

Figure 3.6 Surface-entropy prediction of DLP-1 indicating that the PH-like domain contains many residue clusters with high conformational entropy..... 103

Figure 3.7 Illustration of designed RMG series expression vectors. 106

Figure 3.8 Homology model of the GTPase domain of DLP-1 116

Figure 3.9 Expression and purification of MFN-1 in *E.coli.* 119

Figure 3.10 Size exclusion chromatography of MFN-1 by a Superdex 200 10/30 column 121

Figure 3.11 Multiple-sequence alignments of MFN-1 by T-Coffee and ESPript..... 122

Figure 3.12 Comparison of secondary structure predictions of MFN-1 from PSI-PRED and SABLE severs by visualizing the predictions 124

Figure 3.13 Schematic illustration of MFN-1 constructs..... 125

Figure 4.1 Putative crystals of the (pro)renin receptor in hanging drops 136

Figure 4.2 SDS-PAGE of MBP-(P)RR19 purification by amylose column..... 143

Figure 4.3 Purification of the MBP-(P)RR19 by ion exchange chromatography..... 144

Figure 4.4 Accurate molecular weight of purified MBP-(P)RR19 measured by mass spectrometry..... 147

Figure 4.5 Crystals of apo-MBP-(P)RR19 from hanging drop vapor diffusion..... 149

Figure 4.6 Crystals of ligand-bound MBP-(P)RR19 151

Figure 4.7 Structure of MBP-(P)RR19 with maltose bound..... 152

Figure 4.8 Structure of MBP-(P)RR19 without maltose 153

Figure 4.9 The (P)RR19 in a *2Fo-Fc* electron-density map contoured at one standard deviation above the mean density..... 154

Figure 4.10 Dimeric interface of apo-MBP-(P)RR19 is mediated by hydrogen bonds formed by residues from (P)RR19 peptide 155

Figure 4.11 Dimeric interface of ligand-bound-MBP-(P)RR19 is predominated by hydrogen bonds formed by residues from (P)RR19 peptide 158

Figure 4.12 Size exclusion chromatography of MBP-(P)RR19 161

Figure 4.13 Structure of the (P)RR cytoplasmic tail..... 170

Figure 4.14 Purification of PLZF fragments by Ni-NTA column 175

Figure A1 Binding of the PLZF RD2 domain to the MBP-(P)RR19 199

Figure A2 Binding of the PLZF BTB domain to the MBP-(P)RR19 200

Figure A3 Binding of the PLZF zinc finger domain to the MBP-(P)RR19..... 201

Figure A4 Purification of *E. coli* maltose-binding protein (MBP) by ion exchange chromatography 202

Figure A5 Binding of the PLZF RD2 domain to the MBP 202

(Images in this dissertation are presented in color)

ABBREVIATIONS

ACE: Angiotensin-converting enzyme

ADL2: Arabidopsis dynamin-like protein 2

Ang: Angiotensin

AT: Angiotensin receptor

BAR: Bin/amphiphysin/Rvs domain

BDLP: Cyanobacterial dynamin-like protein

BTB: Bric-a-brac domain

DLP-1: Dynamin-like protein 1

Dnm1: Dynamin-like protein in yeast

DsRed: A red fluorescent protein from Discosoma sp. reef coral

DTT: Dithiothreitol

Dyn A: *Dictyostelium discoideum* dynamin A

ER: Endoplasmic reticulum

Fzo: Fuzzy onion protein

GAP: GTPase-activating protein

GED: GTPase effector domain

GEF: Guanine nucleotide-exchange factors

GST: Glutathione-S-transferase

hGBP1: Human Guanylate-binding protein 1

HR: Heptad repeat region

IPTG: Isopropyl β-D-1-thiogalactopyranoside

LB: Luria-Bertani media

M6P/IGF2R: Mannose 6-phosphate/insulin-like growth factor II receptor

MBP: Maltose-binding protein

MBP-(P)RR19: (P)RR19 fused in the C-terminus of MBP

MFN: Mitofusin

MtDNA: Mitochondrial DNA

PA: Phosphatidic acid

Pfu: *Pyrococcus furiosus*

PH: Pleckstrin-homology domain

PI3K: Phosphatidylinositol-3 kinase

PI(4)P: Phosphatidylinositol 4-phosphate

PIs: Phosphoinositides

PLZF: Promyelocytic Zinc Finger Protein

PRD: Proline-rich domain

(Pro)renin: Prorenin and renin

(P)RR: Prorenin and renin receptor

(P)RR19: The last 19 amino acid of (P)RR encoding the cytoplasmic tail

PS: Phosphatidylserine

ΔPH: DLP1 mutant that the PH-like domain is deleted

RAS: Renin-angiotensin system

RD2: Second repressor domain

Sarcosyl: N-lauryl-sarcosine

SH: Src homology domain

TM: Transmembrane domain

CHAPTER 1

Background and introduction

1.1 Mitochondrial fission and fusion, dynamin-like protein 1 and mitofusins

1.1.1 Mitochondrial evolution and function

Mitochondria are essential organelles of eukaryotes. It is generally believed that mitochondria were originally derived from prokaryotes by endosymbiosis (Osteryoung and Nunnari 2003; Dyall, Brown et al. 2004; Gray, Lang et al. 2004; Dolezal, Likic et al. 2006; Embley and Martin 2006). The evolutionary scenario is that an aerobic prokaryote (probably an alpha-proteobacterium) was first engulfed by an ancestor of eukaryotes about 1.5 billion years ago. Then, the two organisms developed a symbiotic relationship in which the host provides nutrients for the endosymbiont and takes advantage of the energy generated by the endosymbiont through aerobic respiration. After years of adaptation and evolution, genome reduction eventually occurred by which most genes of the endosymbiont were lost, while some were transferred to nucleus of the host. One of the key events of endosymbiotic organelle biogenesis is the development of mitochondrial division machinery for reproduction. Another key step is evolution of a protein translocation mechanism that allows movement of nuclear-encoded proteins into the mitochondria.

The main function of mitochondria is to produce energy for cellular activities by the process of oxidative phosphorylation (OXPHOS). Maintenance of normal mitochondrial function is essential for cellular energy metabolism. Dysfunction of nuclear-encoded or mitochondrial DNA (mtDNA)–encoded mitochodrial genes results in various mitochondrial diseases such as autosomal dominant optical atrophy, Charcot-Marie-Tooth

(CMT) type 2A, Friedreich's ataxia (FRDA), and Kearns-Sayre syndrome (KSS) (Chinnery and Schon 2003; Newmeyer and Ferguson-Miller 2003; Rotig, Lebon et al. 2004; Zeviani and Di Donato 2004; Sato, Nakada et al. 2006; Debray, Lambert et al. 2008). Mitochondrial diseases damage a wide range of organs, including brain, heart, and muscles, and impact the progression of disease states such as diabetes, heart disease, kidney failure, mental and developmental defects.

1.1.2 Mitochondrial fission and fusion

Mitochondria exist as highly dynamic tubular networks, which are thought to be the normal morphological state. The dynamic morphology is maintained by tightly regulated fission and fusion processes (Osteryoung 2000; Osteryoung 2001; Chen, Chomyn et al. 2005; Okamoto and Shaw 2005; Heath-Engel and Shore 2006; Santel 2006; Cerveny, Tamura et al. 2007; Hoppins, Lackner et al. 2007; Berman, Pineda et al. 2008; Santel and Frank 2008; Benard and Karbowski 2009; Hoppins and Nunnari 2009). The balance between the fusion and fission events regulates the morphology of mitochondria throughout the cell cycle stages. During cell division, the mitochondria divide and are distributed to daughter cells. They also undergo continuous fusion to process genetic recombination with one another to prevent dysfunction arising from mutated genes. Disruption of fission machinery causes formation of clusters that contain elongated, interconnected mitochondria (Smirnova, Griparic et al. 2001; Yoon, Krueger et al. 2003; Stojanovski, Koutsopoulos et al. 2004). Disruption of fusion results in fragmentation of

normal mitochondria (Chen, Detmer et al. 2003; Chen, Chomyn et al. 2005).

Although still controversial, mitochondrial fission and fusion have been suggested to be involved in apoptosis, a form of programmed cell death that is essential for embryonic development (Perfettini, Roumier et al. 2005; Youle and Karbowski 2005; Parone and Martinou 2006; Cheng, Leach et al. 2008; Jeong and Seol 2008; Suen, Norris et al. 2008). The remarkable morphological characteristic of mitochondria during apoptosis is that they are fragmented, which indicates that the mitochondrial fission is related to apoptosis. Disruption of protein components of the fission machinery before induction of apoptosis not only inhibits mitochondrial fission, but also affects apoptosis (Frank, Gaume et al. 2001; Lee, Jeong et al. 2004). Overexpression of the fission proteins induces apoptosis (James, Parone et al. 2003). On the other hand, upregulation of the mitochondrial fusion machinery inhibits apoptosis (Sugioka, Shimizu et al. 2004).

The human mtDNA is 16.6 kb in size and it is circular and double stranded. It encodes 13 respiratory chain subunits, 22 transfer RNAs and 2 ribosomal RNAs (Anderson, Bankier et al. 1981). Other protein components of the respiratory chain are encoded by the nuclear DNA. Theoretically, normal mitochondria are thought to contain wild type mtDNAs. In reality, the mtDNA is a mixture of wild type and mutated mtDNA (heteroplasmy) (Sato, Nakada et al. 2006). Because mtDNA has a much higher mutation rate than nuclear DNA, the extensive and continuous fusion among mitochondria may be a specific defense mechanism to complement mutated mtDNA and prevent mitochondria diseases. However, cells only tolerate the mtDNA mutation within a specific level. Once

a particular threshold of the content of mutated mtDNA is passed, normal functions of the respiratory chain are disrupted and mitochondria-related diseases would occur (Zeviani 2004; Sato, Nakada et al. 2006).

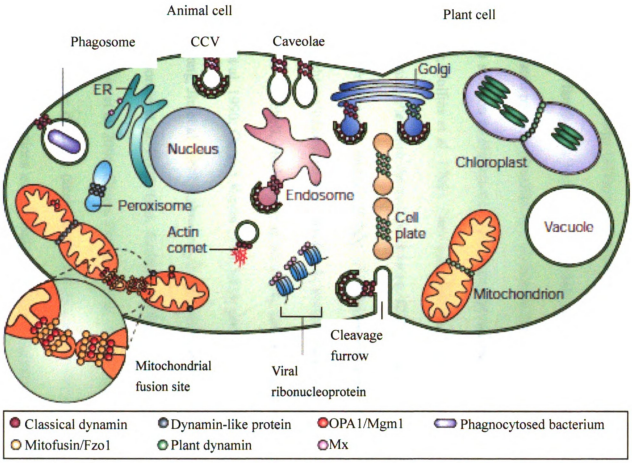

Figure 1.1: Dynamin superfamily members in animals and plants. This figure shows the variety of function taken on by the dynamin family of protein. As can bee seen, the dynamin-like protein-1 (DLP-1) and mitofusin 1 are exclusively involved in mitochondrial fission and fusion reactions. Taken from Praefcke, G. J. and H. T. McMahon "The dynamin superfamily: universal membrane tubulation and fission molecules?" Nat Rev Mol Cell Biol **5**(2): 133-47.

1.1.3 Molecular mechanisms of mitochondrial fission and fusion

1.1.3.1 Dynamin superfamily

Correct mitochondrial mechanisms depend on the functions of dynamin-related proteins, which are large GTPases in the dynamin superfamily (Fig. 1.1). Proteins in the dynamin superfamily can be divided into two major groups: classical dynamins and dynamin-related proteins (Praefcke and McMahon 2004). Classical dynamins are proteins involved in scission of clathrin-coated vesicles during endocytosis (Grigliatti, Hall et al. 1973; Obar, Collins et al. 1990). They have five identifiable domains: GTPase domain, Middle domain, Pleckstrin-homology domain (PH domain), GTPase effector domain (GED) and Proline-rich domain (PRD). The dynamin-related proteins are involved in various membrane tubulation and remodeling events mainly involving fission and fusion of organelles (Staeheli, Horisberger et al. 1984; Staeheli, Haller et al. 1986; Rothman, Raymond et al. 1990; Gu and Verma 1996; Hales and Fuller 1997; Hermann, Thatcher et al. 1998; Kang, Jin et al. 1998; Labrousse, Zappaterra et al. 1999; Santel and Fuller 2001; Olichon, Emorine et al. 2002; Gao, Kadirjan-Kalbach et al. 2003; Santel, Frank et al. 2003; Gao, Sage et al. 2006; Glynn, Froehlich et al. 2008; Glynn, Yang et al. 2009). They lack one or more domains (such as the PH domain or the PRD) or have additional domains (such as insertions or organelle-localization signals) compared to the classical dynamins.

Oligomerization plays an essential role in the functions of proteins in the dynamin family. Most of them form ring-like or helical structures that bind to the target membrane

and stimulate GTPase activity. Two models have been proposed for molecular functions of proteins in the dynamin family. One is that the stimulated GTP hydrolysis upon membrane binding results in a conformational change to generate mechanical force, which facilitate the membrane constriction and scission (Sweitzer and Hinshaw 1998). The opposing model is that GTPase activity regulates the function of other molecules that are actually involved in the membrane fission and remodeling (Scheffzek, Ahmadian et al. 1997; Sever, Muhlberg et al. 1999; Sever, Damke et al. 2000). However, the exact mechanism remains controversial.

Dynamin family GTPases are unique, and are clearly different from canonical small GTPases such as Ras-like and heterotrimeric GTP-binding proteins. They are much larger (70-100 kDa) containing a large GTPase domain (30-40 kDa), and have relatively lower affinity for guanine nucleotides. They are stable in the absence of guanine nucleotides but have high turnover rates of GTP (Schweins, Geyer et al. 1995; Binns, Helms et al. 2000; McEwen, Gee et al. 2001). The GTPase activity of proteins in the dynamin family is regulated by self-oligomerization, while canonical small GTPases require guanine nucleotide-exchange factors (GEF) and GTPase-activating protein (GAP) to catalyze GTPase activity. All of these properties distinguish them from canonical small GTPases.

1.1.3.2 Mitochondrial fission and DLP-1

Human mitochondrial fission is regulated by dynamin-like protein 1 (DLP-1), which represents a class of highly conserved GTPases (Dnm1 in yeast / Drp1 in *C.elegans*)

(Hales and Fuller 1997; Hermann, Thatcher et al. 1998; Smirnova, Shurland et al. 1998; Bleazard, McCaffery et al. 1999; Labrousse, Zappaterra et al. 1999; Smirnova, Griparic et al. 2001). The molecular mechanism of mtichondrial fission is mostly studied in yeast. In yeast, in addition to Dnm1, Mdv1 and Fis1 are required to form fission complexes that catalyze mitochondrial fission (Fekkes, Shepard et al. 2000; Mozdy, McCaffery et al. 2000; Tieu and Nunnari 2000; Cerveny, McCaffery et al. 2001; Lackner, Horner et al. 2009). Fis1 is an outer mitochondrial membrane protein with the C-terminus inserted into the membrane and the N-terminus forming a tetratricopeptide repeat domain (TPR) that faces the cytoplasm (Suzuki, Neutzner et al. 2005). Mdv1 is a WD-40 repeat-containing protein which probably functions as a molecular adaptor to mediate the formation of fission complex (Tieu, Okreglak et al. 2002; Lackner, Horner et al. 2009). It is believed that the membrane-anchored Fis1 recruits Mdv1 first, and then this Fis1-Mdv1 complex consequently recruits Dnm1 (Mozdy, McCaffery et al. 2000; Cerveny, McCaffery et al. 2001; Tieu, Okreglak et al. 2002; Karren, Coonrod et al. 2005). In humans, DLP-1 mediated mitochondrial fission has been thought to have a mechanism similar to that of yeast. The structure of human Fis1 (hFis1) has been shown to be similar to that of Fis1 in yeast (Suzuki, Jeong et al. 2003; Dohm, Lee et al. 2004; Suzuki, Neutzner et al. 2005). However, the homologue of Mdv1 has not been identified in humans.

DLP-1 also undergoes various posttranslational modifications for regulation of mitochondrial fission. cAMP-dependant protein kinase-dependent phosphorylation on residues in the C-terminus affects the DLP-1 GTPase activity, promotes mitochondrial

fission in mitotic cells, and alters mitochondria morphology (Chang and Blackstone 2007; Cribbs and Strack 2007; Taguchi, Ishihara et al. 2007). Nitric oxide can trigger mitochondrial fission, synaptic loss, and neuronal damage, possibly due to the S-nitrosylation of DLP-1 (Cho, Nakamura et al. 2009). The mitochondrial E3 ubiquitin ligase MARCH V regulates mitochondrial fission by facilitating DLP-1 binding to actual mitochondrial division sites (Nakamura, Kimura et al. 2006; Yonashiro, Ishido et al. 2006; Karbowski, Neutzner et al. 2007). In addition, small ubiquitin-like modifier (SUMO) proteins are reported to be involved in the DLP-1 mediated mitochondrial fission (Harder, Zunino et al. 2004; Di Bacco and Gill 2006; Wasiak, Zunino et al. 2007; Zunino, Schauss et al. 2007).

DLP-1 is comprised of four domains: an N-terminal GTPase domain (1-340 aa) with conserved GTP-binding motifs; a middle domain (341-500 aa) with a potential role in self-assembly; an insertion (501-607 aa) of unknown function (a "putative" PH-like domain); and a GED (608-710 aa) with potential roles in not only self-assembly, but also cooperative stimulation of GTPase activity.

The GTPase domain contains conserved G1-G4 GTP-binding motifs, which are spread over the whole domain. Based on the crystal structure of other GTP-binding proteins (Pai, Krengel et al. 1990; Vetter and Wittinghofer 2001), the G1 motif, or P-loop ($G_{32}XXXXG_{37}K_{38}S_{39}$ in DLP-1) is involved in the binding of phosphates, while the G2 motif (T_{59} in DLP-1) coordinates magnesium ion and water for catalysis. The G3 motif ($D_{156}XXG_{159}$ in DLP-1) is hydrogen-bonded with gamma-phosphates of GTP. The G4

motif ($T/N_{215}K/R_{216X}D_{218}$ in DLP-1) coordinates the base and ribose. Conformational change caused by hydrolysis of GTP occurs in the switch 1 and switch 2 regions, which overlap with the G2 and G3 motif, respectively. Mutation of DLP-1-K38A abolishes the GTPase activity of DLP-1 *in vitro*, and overexpression of DLP-1-K38A in COS-7 cells markedly reduces the mitochondrial fission (Yoon, Pitts et al. 2001; Zhu, Patterson et al. 2004). Experiments using labeled GTP have demonstrated that DLP-1-K38A binds but does not hydrolyze or release GTP (Yoon, Pitts et al. 2001). The crystal structures of the GTPase domain of *Dictyostelium discoideum* dynamin A (Dyn A) and rat dynamin 1 have shown that the overall fold is similar with but larger than those of the canonical GTPase (Niemann, Knetsch et al. 2001; Reubold, Eschenburg et al. 2005). The structures display an eight-stranded beta-sheet with six parallel and two antiparallel strands surrounded by nine helices.

The PH domain of classical dynamins is involved in binding to negatively charged lipid membranes. The single PH domain of dynamin binds to the lipids with a relatively low affinity compared to other PH domains. The oligomerized PH domains lead to strong binding of dynamins to the membranes (Klein, Lee et al. 1998; Lemmon and Ferguson 2000). The crystal structure of the PH domain of classical dynamin shows a seven-stranded beta sheet followed by an alpha helix in the C-terminus. Three variable loops form a positive surface that may be sites for interaction with lipids (Ferguson, Lemmon et al. 1994). For DLP-1, sequence analysis does not indicate any region that shows a high degree of homology to the PH domains of classical dynamins or other PH

domains. However, DLP-1 has been shown to tubulate membrane *in vitro* (Yoon, Pitts et al. 2001). Although this behavior is reminiscent of the PH domain in classical dynamins, whether DLP-1 binds to specific lipids and which DLP-1 domain is critical for membrane binding remain unknown.

The middle domain and the GED of classical dynamins are thought to be important for oligomerization and subsequent multimerization (Zhang and Hinshaw 2001). In yeast, Mutant Dnm1-G_{385}D, which contains a point mutation in the middle domain of Dnm1, fails to self-assemble and forms stable dimers (Ingerman, Perkins et al. 2005). This mutation inhibits mitochondrial fission but still can interact with the fission complex containing Mdv1 and Fis1 (Bhar, Karren et al. 2006). Point mutaions in the middle domain of the human dynamin forms a dimer instead of a tetramer and fails to integrate into higher order structures under conditions which stimulate assembly. The dimeric form also markedly reduces the GTPase activity of the dynamin (Ramachandran, Surka et al. 2007).

The GED of DLP-1 has a potential role in not only self-assembly, but also cooperative stimulation of GTPase activity. The crystal structure of a member of the dynamin family, human Guanylate-binding protein 1 (hGBP1) in both nucleotide-free and GTP analogue GppNHp-bound forms has been solved (Prakash, Praefcke et al. 2000; Prakash, Renault et al. 2000). hGBP1 is a protein induced by gamma-interferon to mediate antiviral pathway (Anderson, Carton et al. 1999). Unlike DLP-1, hGBP1 lacks the PH-like domain. The structure is composed of two parts: the large global domain that is the GTPase

domain, and the long, purely alpha-helical domain that contains the Middle domain and the GED. The structure also reveals that the GED forms a long helix that folds back to interact with the helical bundle in the middle domain, and contacts the global GTPase domain. The three-dimensional map of classical dynamin determined from cryo-electron micrographs at a resolution of 20 ′ suggested a similar structural property (Zhang and Hinshaw 2001). Yeast two-hybrid experiments showed that the GED of DLP-1 strongly interacts with the middle and GTPase domains. Mutant DLP-1-$K_{679}A$, which contains a mutation in the GED of DLP-1, impairs the GTPase activity and affects the intra- and intermolecular interactions (Zhu, Patterson et al. 2004). The crystal structure of the GTPase domain of DynA reveals a hydrophobic groove, suggesting a GED interacting site (Niemann, Knetsch et al. 2001). The crystal structure of the GTPase domain of rat dynamin 1 also supports the model that the C-terminus, probably GED, folds back to stimulate GTPase activity (Reubold, Eschenburg et al. 2005). However, elucidation of how the GED is involved in the assembly and the stimulation of GTPase activity will require the detailed structure of the full-length protein.

1.1.3.3 Mitochondrial fusion and MFNs

Mitochondrial outer membrane fusion is mediated by mitofusins (MFNs), belonging to a group of highly conserved mitochodrial transmembrane GTPase homologues (yFzo1 in yeast / Fzo in *Drosophila*) (Hales and Fuller 1997; Hermann, Thatcher et al. 1998; Santel and Fuller 2001). The two mammalian MFNs, MFN-1 and MFN-2 share the same

structural motifs with 77% sequence similarity (Santel, Frank et al. 2003). They contain four domains: an N-terminal GTPase domain (1-370 aa in MFN-1) with conserved GTP-binding motifs; two heptad repeat regions, HR1 (371-580 aa in MFN-1) and HR2 (630-741 aa in MFN-1), with the HR2 forming a dimeric, antiparallel coiled coil that mediates tethering of adjacent mitochondria (Koshiba, Detmer et al. 2004); and a bipartite transmembrane domain, or TM (581-629 aa in MFN-1). Structural and biochemical studies have established that the MFNs are anchored in the mitochondrial outer membrane with both N- and C-terminus exposed to the cytosol (Rojo, Legros et al. 2002). MFN-1 and MFN-2 may play both redundant and distinct roles in mitochondrial fusion in a GTPase activity-dependent manner (Ishihara, Eura et al. 2004; Chen, Chomyn et al. 2005).

Similar to those of DLP-1, the conserved G1-G4 GTP-binding motifs of the GTPase domain of MFNs are spread over the entire domain. GTP hydrolysis has been shown to be important for MFN-1 mediated tethering of mitochondria (Ishihara, Eura et al. 2004). Mutant MFN-1-$K_{88}T$, which contains a mutation in the G1 motif of the GTPase domain, blocks the ability of overexpressed MFN-1 to induce formation of elongated networks of mitochondria (Santel, Frank et al. 2003). Overexpression of mutant MFN-1-$T_{109}A$, containing a mutation in the G2 motif, results in fragmentation of mitochondria (Santel, Frank et al. 2003).

The HR1, HR2, and TM of MFN-2 are found to be important for mitochondrial targeting. Deletion of any one of these domains caused partial localization to

mitochondria and significant amounts of protein remained in the cytosol (Rojo, Legros et al. 2002). The crystal structure of a part of HR2 ($HR2_{660-735}$) of MFN-1 revealed that it forms a dimeric antiparallel coiled coil that is 95 ' long (Koshiba, Detmer et al. 2004). Mutant $HR2_{660-735}$ $L_{691}P$ and $L_{705}P$ reduce the stability of the HR2 coiled coil and mutants MFN-1-$L_{691}P$ and MFN-1-$L_{705}P$ cannot restore mitochondrial tubules in MFN-null cells to the extent that with wide-type MFN-1, indicating that the HR2 coiled coil is important for the mitochondrial fusion (Koshiba, Detmer et al. 2004). It is believed that HR2 functions as a mitochondrial fusion tether (Rojo, Legros et al. 2002; Koshiba, Detmer et al. 2004). The crystal structure of cyanobacterial DLP (BDLP) in both nucleotide-free and GDP-associated conformation provided structural insights into the functional mechanisms of dynamins (Low and Lowe 2006). Sequence analysis shows that the BDLP is closed related to the *Arabidopsis* chloroplast FZO-like protein (FZL) (Gao, Sage et al. 2006), suggesting a bacterial ancestry of dynamins (Low and Lowe 2006).

Based on the best-studied virus-mediated fusion and vesicle fusion mechanism, and genetic and structural studies of MFNs, it has been proposed that MFNs form complexes *in trans* that mediate homotypic interactions between adjacent mitochondria and are likely directly involved in outer membrane fusion (Koshiba, Detmer et al. 2004; Griffin, Detmer et al. 2006).

1.2 Renin-angiotenisn system, (pro)renin receptor, and the membrane connection

1.2.1 Renin-angiotensin system (RAS)

The renin-angiotensin system (RAS) is an incompletely understood mechanism regulating blood pressure, cardiac and vascular function. The aspartyl protease, renin, which is released by kidney, cleaves the angiotensinogen to generate the decapeptide angiotensin (Ang) I. The inactive Ang I was further processed by the angiotensin-converting enzyme (ACE) to an active octopeptide, Ang II. Ang II interacts with cell membrane receptors AT1 and AT2, which belong to the G protein-coupled receptor family, to active downstream signal pathways and regulate blood pressure and cardiovascular modeling.

Renin is considered to catalyze the rate-limiting step of RAS to generate the precursor of active end product, Ang I (Ang I; Asp^{1}-Arg^{2}-Val^{3}-Tyr^{4}-Ile^{5}-His^{6}-Pro^{7}-Phe^{8}-His^{9}-Leu^{10}) (de Gasparo, Catt et al. 2000). The X-ray crystal structure shows that the general fold of renin is comprised of two homologous domains (Sielecki, Hayakawa et al. 1989). The active site and ligand-binding motif are located in between the two domains (Rahuel, Priestle et al. 1991). The two major catalytic residues Asp 32 and Asp 215 are in each part. Renin cleaves the Leu^{10} -Val^{11} peptide bond and releases Ang I. The ACEs bind Ang I and cleave off the two C-terminal residues and create active Ang II. The heptapeptide Ang-(1-7) and dodecapeptide Ang-(1-12) are among those angiotensins discovered recently and involved in different signal transduction pathways.

The signals of renin and angiotensins were mediated by two major G protein-coupled receptors, AT1 and AT2. Although Ang II binds to both AT1 and AT2, the majority of the Ang II signal was transducted by AT1 (Timmermans, Wong et al. 1993). The $G_{q/11}$ family

of G proteins dominates the downstream interactions of AT1 (Wang, Jayadev et al. 1995). The G_0, $G_{11/12}$, and $G_{12/13}$ are other G protein interaction partners of the AT1 (Shirai, Takahashi et al. 1995; Ushio-Fukai, Griendling et al. 1998; Fujii, Onohara et al. 2005). Besides G proteins, AT1 also interacts with beta arrestins to activate a mitogen activated protein kinase (MAPK) cascade (McDonald, Chow et al. 2000; Tohgo, Pierce et al. 2002). The AT1 receptor-associated protein (ATRAP), the epidermal growth factor (EGF) receptor, and the nicotinamide adenine dinucleotide phosphate oxidase (NADPH)-generated reactive oxygen species (ROS) are other partners with which AT1 interacts (Griendling, Minieri et al. 1994; Sabri, Govindarajan et al. 1998; Daviet, Lehtonen et al. 1999; Zuo, Ushio-Fukai et al. 2005; Mehta and Griendling 2007; Tamura, Tanaka et al. 2007). The blood pressure regulation mechanisms that mediated the AT2 receptor are less understood. AT2 interacts with G_i (Kang, Richards et al. 1995). The vasodilation effect mediated by the cascade of bradykinin (BK), nitric oxide (NO), and cGMP is thought to be induced by AT2 (Siragy and Carey 1996; Siragy, Jaffa et al. 1996; Siragy and Linden 1996).

Since renin, ACE, and AT1 and AT2 are the major protein components of the RAS system, inactivating renin or ACE or blocking the Ang II-receptor interaction are current therapeutic strategies in hypertension drug development. According to molecular modeling and X-ray crystal structure of the active site of renin, a number of renin inhibitors have been created for direct renin inhibition (Rahuel, Priestle et al. 1991; Rahuel, Rasetti et al. 2000; Holsworth, Powell et al. 2005; Tice, Xu et al. 2009). These

inhibitors occupy the active site of renin so that its substrate angiotensinogen could not bind and be processed. One of the representative direct renin inhibitors is aliskiren which has a very high binding affinity for renin (Rahuel, Rasetti et al. 2000; Wood, Maibaum et al. 2003). RAS blockers such as ACE inhibitors or Ang II AT1 blockers cause accumulation of Ang I and decrease of Ang II. However, they also stimulate the renin activity probably because of disruption of the feedback loop which inhibits renin (Vander and Geelhoed 1965; Bing 1973; Borghi, Boschi et al. 1993; Roig, Perez-Villa et al. 2000; Azizi and Menard 2004).

1.2.2 Prorenin and (pro)renin receptor

Prorenin is the renin inactive precursor and it has a 43-amino acid prosegment in the N-terminus(Fukamizu, Nishi et al. 1988; Inagami 1991; Morris 1992; Morris 1992). The prosegment has been thought to block the interaction between the active site and angiotensins (Baxter, James et al. 1989; Heinrikson, Hui et al. 1989; Shiratori, Nakagawa et al. 1990). Prorenin can be activated proteolytically by cleaving off the prosegment or non-proteolytically at low pH, low temperature or by interaction with specific antibodies (Sealey and Laragh 1975; Derkx, von Gool et al. 1976; Leckie and McGhee 1980; Derkx, Schalekamp et al. 1987; Pitarresi, Rubattu et al. 1992; Reudelhuber, Brechler et al. 1998; Suzuki, Hatano et al. 1999). The presence of non-proteolytic activation has led to the identification of the "gate" and "handle" regions in the prosegment which may control prorenin activation (Suzuki, Hayakawa et al. 2003). In blood, the level of prorenin is

about 10 times higher that that of renin (Sealey, Glorioso et al. 1986; Leckie, Birnie et al. 1994). However, the exact function of the circulating prorenin remains unclear.

There are two proteins that are generally accepted to be (pro)renin receptors. One is the mannose 6-phosphate/insulin-like growth factor II receptor (M6P/IGF2R) (van Kesteren, Danser et al. 1997; van den Eijnden, Saris et al. 2001). The M6P/IGF2R binds renin and prorenin but does not stimulate any protein activity. However, on binding to the M6P/IGF2R, prorenin is processed to renin by removing the prosegment. Therefore, the M6P/IGF2R is considered as a clearance receptor of (pro)renin (van den Eijnden, Saris et al. 2001; Saris, van den Eijnden et al. 2002).

The second recently identified receptor is the (pro)renin receptor ((P)RR) (Nguyen, Delarue et al. 2002). The (P)RR binds both renin and prorenin and it increases the renin catalytic activity of converting angiotensinogen to Ang I up to four fold (Nguyen, Delarue et al. 2002; Nabi, Kageshima et al. 2006). Moreover, binding of (P)RR probably causes a conformational change of prorenin prosegment to activate the prorenin (Nguyen, Delarue et al. 2002; Batenburg, Krop et al. 2007) (Fig. 1.2). One controversial hypothesis is that the "gate" region of T_7FKR and the "handle" region of I_{11}FLKR on the prosegment of prorenin may be critical for its binding to the (P)RR (Suzuki, Hayakawa et al. 2003). The (P)RR gene encodes a 350-amino acid protein with a short signal peptide in N-terminus, a putative 20-amino acid transmembrane region near the C-terminus, and a short 19-amino acid cytoplasmic tail.

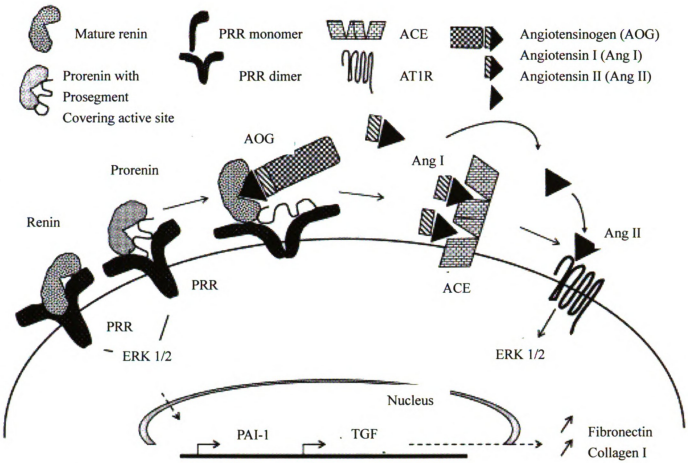

Figure 1.2: Schematic nonproteolytic activation of prorenin bound to the (pro)renin receptor. Either renin or (pro)renin can bind to the (pro)renin receptor and activate the ERK1/2 pathway, but (pro)renin can also autoactivate, which allows it to cleave angiotensinogen. Taken from Nguyen, G. "The (pro)renin receptor: pathophysiological roles in cardiovascular and renal pathology." Curr. Opin. Nephrol. Hyperten. 16(2): 129-133.

1.2.3 Roles of the C-terminus of (P)RR in functions of intracellular compartments

The N-terminal extracellular domain of the (P)RR receptor displays no sequence similarity to any known protein, but the C-terminal domain of (P)RR is highly homologous to ATP6M8-9, a highly conserved accessory protein involved in the assembly of the V_0 portion of the vacuolar proton-translocating ATPase (V-ATPases) (Ludwig, Kerscher et al. 1998). As a consequence, (P)RR is also known as ATP6AP2 (adaptor protein type II vacuolar H^+-ATPase). The V-ATPases play essential roles in regulating cytoplasmic pH maintenance and the acidifying intracellular compartments including endosomes, lysosomes and secretory vesicles (Nishi and Forgac 2002). Some important cellular activities such as endocytosis, intracellular targeting of lysosomal enzymes, protein processing and degradation, and small molecule trafficking, are functioned by the V-ATPases (Stevens and Forgac 1997; Forgac 1999; Bowman and Bowman 2000; Nishi and Forgac 2002).

The ATP6M8-9 is a 70 amino acid portion of the (P)RR C-terminus, which includes a small portion of the extracellular domain, the transmembrane region, and the cytoplasmic tail. How the (P)RR is cleaved and which molecule(s) is involved remain unclear, although the arginine 277 is the putative cutting site for the protease furin (Bader 2007). The (P)RR is also present in lower species that do not have RAS such as *C. elegans* and Drosophila. The protein sequence of the extracellular part before the putative cutting site shows little homology between vertebrates' and invertebrates' (P)RR, although high sequence similarity was observed among mammals' (P)RR. However, The C-terminus

after the putative cutting site exhibits about 40% - 50% sequence identity (Bader 2007). Moreover, a mutation of (P)RR caused X-linked mental retardation and epilepsy syndrome in humans (Ramser, Abidi et al. 2005). Zebrafish with mutant (P)RR died in early development (Amsterdam, Nissen et al. 2004) and mouse embryonic stem cells that are deficient for the (P)RR could not generate chimeras after injection into blastocysts (Burckle and Bader 2006). These results indicate that besides roles in binding (pro)renin, the (P)RR may be involved in other important cellular functions and the conserved C-terminus ATP6M8-9 may be a major component in those functions. Therefore, it has been hypothesized that the (P)RR was evolved from an old version of ATP6M8-9 that was essential for basic cellular functions (Burckle and Bader 2006). The extracelluar domain adapted to a new environment and evolved to take over new function of binding (pro)renin.

1.2.4 Pivotal role of the cytoplasmic domain of the (P)RR in signal transduction

On binding of (pro)renin to (P)RR, a series of signal transduction pathways are triggered that are independent of the RAS pathway. The binding of renin to (P)RR induces phosphorylation of serine and tyrosine residues on the (P)RR and activates the extracellular signal-regulated kinases (ERK) 1/2 and stimulate growth factor TGF-β 1 and plasminogen activator inhibitor-1 (PAI1) (Nguyen, Delarue et al. 2002; Huang, Wongamorntham et al. 2006; Huang, Noble et al. 2007; Sakoda, Ichihara et al. 2007; Feldt, Batenburg et al. 2008). Small interfering RNA targeting the (P)RR abolished those

stimulations indicating the (P)RR is involved in these signaling pathways. In cardiomyocytes, prorenin binding activates the p38 mitogen-activated protein kinase (MAPK) in a concentration-dependent manner and simultaneously phosphorylates Hsp-27 (Saris, t Hoen et al. 2006). Although short, the cytoplasmic domain is the only region that is exposed to a downstream receptor molecule, suggesting that it is a very important mediator of these signal transduction mechanisms.

The (P)RR was first reported to localize on the cell surface (Nguyen, Delarue et al. 2002). However, later research indicated that the (P)RR is mainly localized in the intracellular perinuclear region, with a minor portion on the cell membrane (Saris, t Hoen et al. 2006; Schefe, Menk et al. 2006; Feldt, Maschke et al. 2008). The sequence analysis of the (P)RR revealed two putative intracellular targeting motifs which are in the cytoplasmic tail (Burckle and Bader 2006), a tyrosine-based motif Y^{335}DSI and a C-terminal dibasic motif K^{346}IRMD. The Yxxϕ (where x is a random residue and ϕ is a large hydrophobic residue) is typical for protein sorting to endosomes and lysosomes. The K(x)Kxx or R(x)Rxx are conventional ER retention/retrieval signals. Although further experimental evidence is needed, the intracellular location may be another cellular function of the (P)RR that has not yet been elucidated. The signal sequences on the cytoplasmic tail may also play an important role in the protein localization.

1.2.5 Interactions of the (P)RR with Promyelocytic Zinc Finger Protein

The transcriptional factor Promyelocytic Zinc Finger Protein (PLZF) was identified as

a downstream partner that interacts with the cytoplasmic domain of the (P)RR by yeast two-hybrid screening and coimmunoprecipitation (Schefe, Menk et al. 2006; Danser, Batenburg et al. 2008; Schefe, Unger et al. 2008). The PLZF belongs to the family of Kruppel-type zinc finger proteins (Chowdhury, Deutsch et al. 1987). It is a transcriptional repressor involved in regulating cell cycle and growth suppression, and has been suggested in limb development, differentiation of myeloid cells, and spermatogenesis (Melnick and Licht 1999; Yeyati, Shaknovich et al. 1999; Barna, Hawe et al. 2000; Takahashi and Licht 2002). The human PLZF has a Broad-Complex, Tramtrack, and Bric-a-brac (BTB), or Poxvirus and Zinc Finger (POZ) domain in the N-terminal 120 amino acids, a central second repressor domain (RD2) of about 250 amino acids, and nine C2H2 Kruppel-type zinc fingers in the C-terminus. The BTB domains in transcription factors are usually involved in regulation of gene expression by controlling the chromatin conformation (Albagli, Dhordain et al. 1995). The RD2 contains a proline-rich region, which may be responsible for protein-protein interactions (Li, English et al. 1997; Melnick, Westendorf et al. 2000). The zinc fingers are responsible for DNA binding, or interactions with RNA or other protein partners. The X-ray crystal structure of the BTB domain of human PLZF revealed a tightly intertwined dimer with about 25% of the monomer surface involved in the hydrophobic interface (Ahmad, Engel et al. 1998).

On binding of (pro)renin by (P)RR, the PLZF is activated and translocated to the nucleus to be recruited to the cis element of the (P)RR promoter. The transcription of the (P)RR is repressed by the activated PLZF and therefore, a short negative feedback loop

was created (Schefe, Menk et al. 2006). These results support a novel signal transduction pathway in which (pro)renin, (P)RR, and PLZF are involved. This negative feedback pathway, which downregulates the (P)RR expression, explains why accumulation of (pro)renin during renin inhibitor exposure does not increase the (P)RR activity to a significant level. Activation of (P)RR will cause a six-fold increase in recruitment of PLZF to (P)RR promoter region and therefore prevent further (P)RR activation through suppression of (P)RR expression (Schefe, Menk et al. 2006). Direct interaction of PLZF with the cytoplasmic domain of the (P)RR was demonstrated by the yeast two-hybrid study and coimmunoprecipitation with truncated (P)RR fragments (Schefe, Menk et al. 2006). However, which region(s) of the PLZF is responsible for the interaction remains unclear.

Together with PLZF, the promoter activity of the p85α subunit of the phosphatidylinositol-3 kinase (PI3K-p85α) was stimulated by 45% (Schefe, Menk et al. 2006). Nuclear PLZF binds to the PI3K-p85α consensus sequence and positively regulate the gene. The PI3K-p85α is a protein involved in activation of protein synthesis and cardiac hypertrophy (Senbonmatsu, Saito et al. 2003). What the exact roles of the (P)RR-PLZF-PI3K-p85α pathway are in cellular function remain unclear.

References

Ahmad, K. F., C. K. Engel and G. G. Prive (1998). "Crystal structure of the BTB domain from PLZF." Proc Natl Acad Sci U S A **95**(21): 12123-8.

Albagli, O., P. Dhordain, C. Deweindt, G. Lecocq and D. Leprince (1995). "The BTB/POZ domain: a new protein-protein interaction motif common to DNA- and actin-binding proteins." Cell Growth Differ **6**(9): 1193-8.

Amsterdam, A., R. M. Nissen, Z. Sun, E. C. Swindell, S. Farrington and N. Hopkins (2004). "Identification of 315 genes essential for early zebrafish development." Proc Natl Acad Sci U S A **101**(35): 12792-7.

Anderson, S., A. T. Bankier, B. G. Barrell, M. H. de Bruijn, A. R. Coulson, J. Drouin, I. C. Eperon, D. P. Nierlich, B. A. Roe, F. Sanger, P. H. Schreier, A. J. Smith, R. Staden and I. G. Young (1981). "Sequence and organization of the human mitochondrial genome." Nature **290**(5806): 457-65.

Anderson, S. L., J. M. Carton, J. Lou, L. Xing and B. Y. Rubin (1999). "Interferon-induced guanylate binding protein-1 (GBP-1) mediates an antiviral effect against vesicular stomatitis virus and encephalomyocarditis virus." Virology **256**(1): 8-14.

Azizi, M. and J. Menard (2004). "Combined blockade of the renin-angiotensin system with angiotensin-converting enzyme inhibitors and angiotensin II type 1 receptor antagonists." Circulation **109**(21): 2492-9.

Bader, M. (2007). "The second life of the (pro)renin receptor." J Renin Angiotensin Aldosterone Syst **8**(4): 205-8.

Barna, M., N. Hawe, L. Niswander and P. P. Pandolfi (2000). "Plzf regulates limb and axial skeletal patterning." Nat Genet **25**(2): 166-72.

Batenburg, W. W., M. Krop, I. M. Garrelds, R. de Vries, R. J. de Bruin, C. A. Burckle, D. N. Muller, M. Bader, G. Nguyen and A. H. Danser (2007). "Prorenin is the endogenous agonist of the (pro)renin receptor. Binding kinetics of renin and prorenin in rat vascular smooth muscle cells overexpressing the human (pro)renin receptor." J Hypertens **25**(12): 2441-53.

Baxter, J. D., M. N. James, W. N. Chu, K. Duncan, M. A. Haidar, C. T. Carilli and T. L. Reudelhuber (1989). "The molecular biology of human renin and its gene." Yale J

Biol Med **62**(5): 493-501.

Benard, G. and M. Karbowski (2009). "Mitochondrial fusion and division: Regulation and role in cell viability." Semin Cell Dev Biol **20**(3): 365-74.

Berman, S. B., F. J. Pineda and J. M. Hardwick (2008). "Mitochondrial fission and fusion dynamics: the long and short of it." Cell Death Differ **15**(7): 1147-52.

Bhar, D., M. A. Karren, M. Babst and J. M. Shaw (2006). "Dimeric Dnm1-G385D interacts with Mdv1 on mitochondria and can be stimulated to assemble into fission complexes containing Mdv1 and Fis1." J Biol Chem **281**(25): 17312-20.

Bing, J. (1973). "Rapid marked increase in plasma renin in rats treated with inhibitors of the renin system. Effects of 1-sar-8-ala-angiotensin II and of a synthetic converting enzyme inhibitor (nonapeptide, SQ 20.881) on normal and adrenalectomized rats." Acta Pathol Microbiol Scand A **81**(3): 376-8.

Binns, D. D., M. K. Helms, B. Barylko, C. T. Davis, D. M. Jameson, J. P. Albanesi and J. F. Eccleston (2000). "The mechanism of GTP hydrolysis by dynamin II: a transient kinetic study." Biochemistry **39**(24): 7188-96.

Bleazard, W., J. M. McCaffery, E. J. King, S. Bale, A. Mozdy, Q. Tieu, J. Nunnari and J. M. Shaw (1999). "The dynamin-related GTPase Dnm1 regulates mitochondrial fission in yeast." Nat Cell Biol **1**(5): 298-304.

Borghi, C., S. Boschi, E. Ambrosioni, G. Melandri, A. Branzi and B. Magnani (1993). "Evidence of a partial escape of renin-angiotensin-aldosterone blockade in patients with acute myocardial infarction treated with ACE inhibitors." J Clin Pharmacol **33**(1): 40-5.

Bowman, E. J. and B. J. Bowman (2000). "Cellular role of the V-ATPase in Neurospora crassa: analysis of mutants resistant to concanamycin or lacking the catalytic subunit A." J Exp Biol **203**(Pt 1): 97-106.

Burckle, C. and M. Bader (2006). "Prorenin and its ancient receptor." Hypertension **48**(4): 549-51.

Cerveny, K. L., J. M. McCaffery and R. E. Jensen (2001). "Division of mitochondria requires a novel DMN1-interacting protein, Net2p." Mol Biol Cell **12**(2): 309-21.

Cerveny, K. L., Y. Tamura, Z. Zhang, R. E. Jensen and H. Sesaki (2007). "Regulation of

mitochondrial fusion and division." Trends Cell Biol **17**(11): 563-9.

Chang, C. R. and C. Blackstone (2007). "Cyclic AMP-dependent protein kinase phosphorylation of Drp1 regulates its GTPase activity and mitochondrial morphology." J Biol Chem **282**(30): 21583-7.

Chen, H., A. Chomyn and D. C. Chan (2005). "Disruption of fusion results in mitochondrial heterogeneity and dysfunction." J Biol Chem **280**(28): 26185-92.

Chen, H., S. A. Detmer, A. J. Ewald, E. E. Griffin, S. E. Fraser and D. C. Chan (2003). "Mitofusins Mfn1 and Mfn2 coordinately regulate mitochondrial fusion and are essential for embryonic development." J Cell Biol **160**(2): 189-200.

Cheng, W. C., K. M. Leach and J. M. Hardwick (2008). "Mitochondrial death pathways in yeast and mammalian cells." Biochim Biophys Acta **1783**(7): 1272-9.

Chinnery, P. F. and E. A. Schon (2003). "Mitochondria." J Neurol Neurosurg Psychiatry **74**(9): 1188-99.

Cho, D. H., T. Nakamura, J. Fang, P. Cieplak, A. Godzik, Z. Gu and S. A. Lipton (2009). "S-nitrosylation of Drp1 mediates beta-amyloid-related mitochondrial fission and neuronal injury." Science **324**(5923): 102-5.

Chowdhury, K., U. Deutsch and P. Gruss (1987). "A multigene family encoding several "finger" structures is present and differentially active in mammalian genomes." Cell **48**(5): 771-8.

Cribbs, J. T. and S. Strack (2007). "Reversible phosphorylation of Drp1 by cyclic AMP-dependent protein kinase and calcineurin regulates mitochondrial fission and cell death." EMBO Rep **8**(10): 939-44.

Danser, A. H., W. W. Batenburg, J. H. van Esch and M. Krop (2008). "Prorenin anno 2008." J Mol Med **86**(6): 655-8.

Daviet, L., J. Y. Lehtonen, K. Tamura, D. P. Griese, M. Horiuchi and V. J. Dzau (1999). "Cloning and characterization of ATRAP, a novel protein that interacts with the angiotensin II type 1 receptor." J Biol Chem **274**(24): 17058-62.

de Gasparo, M., K. J. Catt, T. Inagami, J. W. Wright and T. Unger (2000). "International union of pharmacology. XXIII. The angiotensin II receptors." Pharmacol Rev **52**(3): 415-72.

Debray, F. G, M. Lambert and G A. Mitchell (2008). "Disorders of mitochondrial function." Curr Opin Pediatr **20**(4): 471-82.

Derkx, F. H., M. P. Schalekamp and M. A. Schalekamp (1987). "Two-step prorenin-renin conversion. Isolation of an intermediary form of activated prorenin." J Biol Chem **262**(6): 2472-7.

Derkx, F. H., J. M. von Gool, G J. Wenting, R. P. Verhoeven, A. J. Man in 't Veld and M. A. Schalekamp (1976). "Inactive renin in human plasma." Lancet **1**(7984): 496-9.

Di Bacco, A. and G Gill (2006). "SUMO-specific proteases and the cell cycle. An essential role for SENP5 in cell proliferation." Cell Cycle **5**(20): 2310-3.

Dohm, J. A., S. J. Lee, J. M. Hardwick, R. B. Hill and A. G Gittis (2004). "Cytosolic domain of the human mitochondrial fission protein Fis1 adopts a TPR fold." Proteins-Structure Function and Genetics **54**(1): 153-156.

Dolezal, P., V. Likic, J. Tachezy and T. Lithgow (2006). "Evolution of the molecular machines for protein import into mitochondria." Science **313**(5785): 314-8.

Dyall, S. D., M. T. Brown and P. J. Johnson (2004). "Ancient invasions: from endosymbionts to organelles." Science **304**(5668): 253-7.

Embley, T. M. and W. Martin (2006). "Eukaryotic evolution, changes and challenges." Nature **440**(7084): 623-30.

Fekkes, P., K. A. Shepard and M. P. Yaffe (2000). "Gag3p, an outer membrane protein required for fission of mitochondrial tubules." J Cell Biol **151**(2): 333-40.

Feldt, S., W. W. Batenburg, I. Mazak, U. Maschke, M. Wellner, H. Kvakan, R. Dechend, A. Fiebeler, C. Burckle, A. Contrepas, A. H. Jan Danser, M. Bader, G Nguyen, F. C. Luft and D. N. Muller (2008). "Prorenin and renin-induced extracellular signal-regulated kinase 1/2 activation in monocytes is not blocked by aliskiren or the handle-region peptide." Hypertension **51**(3): 682-8.

Feldt, S., U. Maschke, R. Dechend, F. C. Luft and D. N. Muller (2008). "The putative (pro)renin receptor blocker HRP fails to prevent (pro)renin signaling." J Am Soc Nephrol **19**(4): 743-8.

Ferguson, K. M., M. A. Lemmon, J. Schlessinger and P. B. Sigler (1994). "Crystal structure at 2.2 A resolution of the pleckstrin homology domain from human

dynamin." Cell **79**(2): 199-209.

Forgac, M. (1999). "Structure and properties of the vacuolar (H+)-ATPases." Journal of Biological Chemistry **274**(19): 12951-12954.

Frank, S., B. Gaume, E. S. Bergmann-Leitner, W. W. Leitner, E. G. Robert, F. Catez, C. L. Smith and R. J. Youle (2001). "The role of dynamin-related protein 1, a mediator of mitochondrial fission, in apoptosis." Dev Cell **1**(4): 515-25.

Fujii, T., N. Onohara, Y. Maruyama, S. Tanabe, H. Kobayashi, M. Fukutomi, Y. Nagamatsu, N. Nishihara, R. Inoue, H. Sumimoto, F. Shibasaki, T. Nagao, M. Nishida and H. Kurose (2005). "Galpha12/13-mediated production of reactive oxygen species is critical for angiotensin receptor-induced NFAT activation in cardiac fibroblasts." J Biol Chem **280**(24): 23041-7.

Fukamizu, A., K. Nishi, T. Cho, M. Saitoh, K. Nakayama, H. Ohkubo, S. Nakanishi and K. Murakami (1988). "Structure of the rat renin gene." J Mol Biol **201**(2): 443-50.

Gao, H., D. Kadirjan-Kalbach, J. E. Froehlich and K. W. Osteryoung (2003). "ARC5, a cytosolic dynamin-like protein from plants, is part of the chloroplast division machinery." Proc Natl Acad Sci U S A **100**(7): 4328-33.

Gao, H., T. L. Sage and K. W. Osteryoung (2006). "FZL, an FZO-like protein in plants, is a determinant of thylakoid and chloroplast morphology." Proc Natl Acad Sci U S A **103**(17): 6759-64.

Glynn, J. M., J. E. Froehlich and K. W. Osteryoung (2008). "Arabidopsis ARC6 coordinates the division machineries of the inner and outer chloroplast membranes through interaction with PDV2 in the intermembrane space." Plant Cell **20**(9): 2460-70.

Glynn, J. M., Y. Yang, S. Vitha, A. J. Schmitz, M. Hemmes, S. Y. Miyagishima and K. W. Osteryoung (2009). "PARC6, a novel chloroplast division factor, influences FtsZ assembly and is required for recruitment of PDV1 during chloroplast division in Arabidopsis." Plant J.

Gray, M. W., B. F. Lang and G. Burger (2004). "Mitochondria of protists." Annu Rev Genet **38**: 477-524.

Griendling, K. K., C. A. Minieri, J. D. Ollerenshaw and R. W. Alexander (1994). "Angiotensin II stimulates NADH and NADPH oxidase activity in cultured

vascular smooth muscle cells." Circ Res **74**(6): 1141-8.

Griffin, E. E., S. A. Detmer and D. C. Chan (2006). "Molecular mechanism of mitochondrial membrane fusion." Biochim Biophys Acta **1763**(5-6): 482-9.

Grigliatti, T. A., L. Hall, R. Rosenbluth and D. T. Suzuki (1973). "Temperature-sensitive mutations in Drosophila melanogaster. XIV. A selection of immobile adults." Mol Gen Genet **120**(2): 107-14.

Gu, X. and D. P. Verma (1996). "Phragmoplastin, a dynamin-like protein associated with cell plate formation in plants." Embo J **15**(4): 695-704.

Hales, K. G. and M. T. Fuller (1997). "Developmentally regulated mitochondrial fusion mediated by a conserved, novel, predicted GTPase." Cell **90**(1): 121-9.

Harder, Z., R. Zunino and H. McBride (2004). "Sumo1 conjugates mitochondrial substrates and participates in mitochondrial fission." Curr Biol **14**(4): 340-5.

Heath-Engel, H. M. and G. C. Shore (2006). "Mitochondrial membrane dynamics, cristae remodelling and apoptosis." Biochim Biophys Acta **1763**(5-6): 549-60.

Heinrikson, R. L., J. Hui, H. Zurcher-Neely and R. A. Poorman (1989). "A structural model to explain the partial catalytic activity of human prorenin." Am J Hypertens **2**(5 Pt 1): 367-80.

Hermann, G. J., J. W. Thatcher, J. P. Mills, K. G. Hales, M. T. Fuller, J. Nunnari and J. M. Shaw (1998). "Mitochondrial fusion in yeast requires the transmembrane GTPase Fzo1p." J Cell Biol **143**(2): 359-73.

Holsworth, D. D., N. A. Powell, D. M. Downing, C. Cai, W. L. Cody, J. M. Ryan, R. Ostroski, M. Jalaie, J. W. Bryant and J. J. Edmunds (2005). "Discovery of novel non-peptidic ketopiperazine-based renin inhibitors." Bioorganic & Medicinal Chemistry **13**(7): 2657-2664.

Hoppins, S., L. Lackner and J. Nunnari (2007). "The machines that divide and fuse mitochondria." Annu Rev Biochem **76**: 751-80.

Hoppins, S. and J. Nunnari (2009). "The molecular mechanism of mitochondrial fusion." Biochim Biophys Acta **1793**(1): 20-6.

Huang, Y., N. A. Noble, J. Zhang, C. Xu and W. A. Border (2007). "Renin-stimulated

TGF-beta1 expression is regulated by a mitogen-activated protein kinase in mesangial cells." Kidney Int **72**(1): 45-52.

Huang, Y., S. Wongamorntham, J. Kasting, D. McQuillan, R. T. Owens, L. Yu, N. A. Noble and W. Border (2006). "Renin increases mesangial cell transforming growth factor-beta1 and matrix proteins through receptor-mediated, angiotensin II-independent mechanisms." Kidney Int **69**(1): 105-13.

Inagami, T. (1991). "Purification of renin and prorenin." Hypertension **18**(3): 241-51.

Ingerman, E., E. M. Perkins, M. Marino, J. A. Mears, J. M. McCaffery, J. E. Hinshaw and J. Nunnari (2005). "Dnm1 forms spirals that are structurally tailored to fit mitochondria." J Cell Biol **170**(7): 1021-7.

Ishihara, N., Y. Eura and K. Mihara (2004). "Mitofusin 1 and 2 play distinct roles in mitochondrial fusion reactions via GTPase activity." J Cell Sci **117**(Pt 26): 6535-46.

James, D. I., P. A. Parone, Y. Mattenberger and J. C. Martinou (2003). "hFis1, a novel component of the mammalian mitochondrial fission machinery." J Biol Chem **278**(38): 36373-9.

Jeong, S. Y. and D. W. Seol (2008). "The role of mitochondria in apoptosis." BMB Rep **41**(1): 11-22.

Kang, J., E. M. Richards, P. Posner and C. Sumners (1995). "Modulation of the delayed rectifier K+ current in neurons by an angiotensin II type 2 receptor fragment." Am J Physiol **268**(1 Pt 1): C278-82.

Kang, S. G, J. B. Jin, H. L. Piao, K. T. Pih, H. J. Jang, J. H. Lim and I. Hwang (1998). "Molecular cloning of an Arabidopsis cDNA encoding a dynamin-like protein that is localized to plastids." Plant Mol Biol **38**(3): 437-47.

Karbowski, M., A. Neutzner and R. J. Youle (2007). "The mitochondrial E3 ubiquitin ligase MARCH5 is required for Drp1 dependent mitochondrial division." J Cell Biol **178**(1): 71-84.

Karren, M. A., E. M. Coonrod, T. K. Anderson and J. M. Shaw (2005). "The role of Fis1p-Mdv1p interactions in mitochondrial fission complex assembly." J Cell Biol **171**(2): 291-301.

Klein, D. E., A. Lee, D. W. Frank, M. S. Marks and M. A. Lemmon (1998). "The pleckstrin homology domains of dynamin isoforms require oligomerization for high affinity phosphoinositide binding." J Biol Chem **273**(42): 27725-33.

Koshiba, T., S. A. Detmer, J. T. Kaiser, H. Chen, J. M. McCaffery and D. C. Chan (2004). "Structural basis of mitochondrial tethering by mitofusin complexes." Science **305**(5685): 858-62.

Labrousse, A. M., M. D. Zappaterra, D. A. Rube and A. M. van der Bliek (1999). "C. elegans dynamin-related protein DRP-1 controls severing of the mitochondrial outer membrane." Mol Cell **4**(5): 815-26.

Lackner, L. L., J. S. Horner and J. Nunnari (2009). "Mechanistic analysis of a dynamin effector." Science **325**(5942): 874-7.

Leckie, B. J., G. Birnie and R. Carachi (1994). "Renin in Wilms' tumor: prorenin as an indicator." J Clin Endocrinol Metab **79**(6): 1742-6.

Leckie, B. J. and N. K. McGhee (1980). "Reversible activation-inactivation of renin in human plasma." Nature **288**(5792): 702-5.

Lee, Y. J., S. Y. Jeong, M. Karbowski, C. L. Smith and R. J. Youle (2004). "Roles of the mammalian mitochondrial fission and fusion mediators Fis1, Drp1, and Opa1 in apoptosis." Mol Biol Cell **15**(11): 5001-11.

Lemmon, M. A. and K. M. Ferguson (2000). "Signal-dependent membrane targeting by pleckstrin homology (PH) domains." Biochem J **350 Pt 1**: 1-18.

Li, J. Y., M. A. English, H. J. Ball, P. L. Yeyati, S. Waxman and J. D. Licht (1997). "Sequence-specific DNA binding and transcriptional regulation by the promyelocytic leukemia zinc finger protein." J Biol Chem **272**(36): 22447-55.

Low, H. H. and J. Lowe (2006). "A bacterial dynamin-like protein." Nature **444**(7120): 766-9.

Ludwig, J., S. Kerscher, U. Brandt, K. Pfeiffer, F. Getlawi, D. K. Apps and H. Schagger (1998). "Identification and characterization of a novel 9.2-kDa membrane sector-associated protein of vacuolar proton-ATPase from chromaffin granules." J Biol Chem **273**(18): 10939-47.

McDonald, P. H., C. W. Chow, W. E. Miller, S. A. Laporte, M. E. Field, F. T. Lin, R. J.

Davis and R. J. Lefkowitz (2000). "Beta-arrestin 2: a receptor-regulated MAPK scaffold for the activation of JNK3." Science **290**(5496): 1574-7.

McEwen, D. P., K. R. Gee, H. C. Kang and R. R. Neubig (2001). "Fluorescent BODIPY-GTP analogs: real-time measurement of nucleotide binding to G proteins." Anal Biochem **291**(1): 109-17.

Mehta, P. K. and K. K. Griendling (2007). "Angiotensin II cell signaling: physiological and pathological effects in the cardiovascular system." Am J Physiol Cell Physiol **292**(1): C82-97.

Melnick, A. and J. D. Licht (1999). "Deconstructing a disease: RARalpha, its fusion partners, and their roles in the pathogenesis of acute promyelocytic leukemia." Blood **93**(10): 3167-215.

Melnick, A. M., J. J. Westendorf, A. Polinger, G. W. Carlile, S. Arai, H. J. Ball, B. Lutterbach, S. W. Hiebert and J. D. Licht (2000). "The ETO protein disrupted in t(8;21)-associated acute myeloid leukemia is a corepressor for the promyelocytic leukemia zinc finger protein." Mol Cell Biol **20**(6): 2075-86.

Morris, B. J. (1992). "Molecular biology of renin. I: Gene and protein structure, synthesis and processing." J Hypertens **10**(3): 209-14.

Morris, B. J. (1992). "Molecular biology of renin. I: Gene and protein structure, synthesis and processing." Journal of Hypertension **10**(3): 209-14.

Mozdy, A. D., J. M. McCaffery and J. M. Shaw (2000). "Dnm1p GTPase-mediated mitochondrial fission is a multi-step process requiring the novel integral membrane component Fis1p." J Cell Biol **151**(2): 367-80.

Nabi, A. H., A. Kageshima, M. N. Uddin, T. Nakagawa, E. Y. Park and F. Suzuki (2006). "Binding properties of rat prorenin and renin to the recombinant rat renin/prorenin receptor prepared by a baculovirus expression system." Int J Mol Med **18**(3): 483-8.

Nakamura, N., Y. Kimura, M. Tokuda, S. Honda and S. Hirose (2006). "MARCH-V is a novel mitofusin 2- and Drp1-binding protein able to change mitochondrial morphology." EMBO Rep **7**(10): 1019-22.

Newmeyer, D. D. and S. Ferguson-Miller (2003). "Mitochondria: releasing power for life and unleashing the machineries of death." Cell **112**(4): 481-90.

Nguyen, G., F. Delarue, C. Burckle, L. Bouzhir, T. Giller and J. D. Sraer (2002). "Pivotal role of the renin/prorenin receptor in angiotensin II production and cellular responses to renin." J Clin Invest **109**(11): 1417-27.

Niemann, H. H., M. L. Knetsch, A. Scherer, D. J. Manstein and F. J. Kull (2001). "Crystal structure of a dynamin GTPase domain in both nucleotide-free and GDP-bound forms." Embo J **20**(21): 5813-21.

Nishi, T. and M. Forgac (2002). "The vacuolar (H+)-ATPases--nature's most versatile proton pumps." Nat Rev Mol Cell Biol **3**(2): 94-103.

Obar, R. A., C. A. Collins, J. A. Hammarback, H. S. Shpetner and R. B. Vallee (1990). "Molecular cloning of the microtubule-associated mechanochemical enzyme dynamin reveals homology with a new family of GTP-binding proteins." Nature **347**(6290): 256-61.

Okamoto, K. and J. M. Shaw (2005). "Mitochondrial morphology and dynamics in yeast and multicellular eukaryotes." Annu Rev Genet **39**: 503-36.

Olichon, A., L. J. Emorine, E. Descoins, L. Pelloquin, L. Brichese, N. Gas, E. Guillou, C. Delettre, A. Valette, C. P. Hamel, B. Ducommun, G. Lenaers and P. Belenguer (2002). "The human dynamin-related protein OPA1 is anchored to the mitochondrial inner membrane facing the inter-membrane space." FEBS Lett **523**(1-3): 171-6.

Osteryoung, K. W. (2000). "Organelle fission. Crossing the evolutionary divide." Plant Physiol **123**(4): 1213-6.

Osteryoung, K. W. (2001). "Organelle fission in eukaryotes." Curr Opin Microbiol **4**(6): 639-46.

Osteryoung, K. W. and J. Nunnari (2003). "The division of endosymbiotic organelles." Science **302**(5651): 1698-704.

Pai, E. F., U. Krengel, G. A. Petsko, R. S. Goody, W. Kabsch and A. Wittinghofer (1990). "Refined Crystal-Structure of the Triphosphate Conformation of H-Ras P21 at 1.35 a Resolution - Implications for the Mechanism of Gtp Hydrolysis." Embo Journal **9**(8): 2351-2359.

Parone, P. A. and J. C. Martinou (2006). "Mitochondrial fission and apoptosis: an ongoing trial." Biochim Biophys Acta **1763**(5-6): 522-30.

Perfettini, J. L., T. Roumier and G. Kroemer (2005). "Mitochondrial fusion and fission in the control of apoptosis." Trends Cell Biol **15**(4): 179-83.

Pitarresi, T. M., S. Rubattu, R. Heinrikson and J. E. Sealey (1992). "Reversible cryoactivation of recombinant human prorenin." J Biol Chem **267**(17): 11753-9.

Praefcke, G. J. and H. T. McMahon (2004). "The dynamin superfamily: universal membrane tubulation and fission molecules?" Nat Rev Mol Cell Biol **5**(2): 133-47.

Prakash, B., G. J. Praefcke, L. Renault, A. Wittinghofer and C. Herrmann (2000). "Structure of human guanylate-binding protein 1 representing a unique class of GTP-binding proteins." Nature **403**(6769): 567-71.

Prakash, B., L. Renault, G. J. Praefcke, C. Herrmann and A. Wittinghofer (2000). "Triphosphate structure of guanylate-binding protein 1 and implications for nucleotide binding and GTPase mechanism." Embo J **19**(17): 4555-64.

Rahuel, J., J. P. Priestle and M. G. Grutter (1991). "The crystal structures of recombinant glycosylated human renin alone and in complex with a transition state analog inhibitor." J Struct Biol **107**(3): 227-36.

Rahuel, J., V. Rasetti, J. Maibaum, H. Rueger, R. Goschke, N. C. Cohen, S. Stutz, F. Cumin, W. Fuhrer, J. M. Wood and M. G. Grutter (2000). "Structure-based drug design: the discovery of novel nonpeptide orally active inhibitors of human renin." Chem Biol **7**(7): 493-504.

Ramachandran, R., M. Surka, J. S. Chappie, D. M. Fowler, T. R. Foss, B. D. Song and S. L. Schmid (2007). "The dynamin middle domain is critical for tetramerization and higher-order self-assembly." Embo J **26**(2): 559-66.

Ramser, J., F. E. Abidi, C. A. Burckle, C. Lenski, H. Toriello, G. Wen, H. A. Lubs, S. Engert, R. E. Stevenson, A. Meindl, C. E. Schwartz and G. Nguyen (2005). "A unique exonic splice enhancer mutation in a family with X-linked mental retardation and epilepsy points to a novel role of the renin receptor." Hum Mol Genet **14**(8): 1019-27.

Reubold, T. F., S. Eschenburg, A. Becker, M. Leonard, S. L. Schmid, R. B. Vallee, F. J. Kull and D. J. Manstein (2005). "Crystal structure of the GTPase domain of rat dynamin 1." Proc Natl Acad Sci U S A **102**(37): 13093-8.

Reudelhuber, T. L., V. Brechler, I. Jutras, C. Mercure and D. Methot (1998). "Proteolytic and non-proteolytic activation of prorenin." Adv Exp Med Biol **436**: 229-38.

Roig, E., F. Perez-Villa, M. Morales, W. Jimenez, J. Orus, M. Heras and G. Sanz (2000). "Clinical implications of increased plasma angiotensin II despite ACE inhibitor therapy in patients with congestive heart failure." Eur Heart J **21**(1): 53-7.

Rojo, M., F. Legros, D. Chateau and A. Lombes (2002). "Membrane topology and mitochondrial targeting of mitofusins, ubiquitous mammalian homologs of the transmembrane GTPase Fzo." J Cell Sci **115**(Pt 8): 1663-74.

Rothman, J. H., C. K. Raymond, T. Gilbert, P. J. O'Hara and T. H. Stevens (1990). "A putative GTP binding protein homologous to interferon-inducible Mx proteins performs an essential function in yeast protein sorting." Cell **61**(6): 1063-74.

Rotig, A., S. Lebon, E. Zinovieva, J. Mollet, E. Sarzi, J. P. Bonnefont and A. Munnich (2004). "Molecular diagnostics of mitochondrial disorders." Biochim Biophys Acta **1659**(2-3): 129-35.

Sabri, A., G. Govindarajan, T. M. Griffin, K. L. Byron, A. M. Samarel and P. A. Lucchesi (1998). "Calcium- and protein kinase C-dependent activation of the tyrosine kinase PYK2 by angiotensin II in vascular smooth muscle." Circ Res **83**(8): 841-51.

Sakoda, M., A. Ichihara, Y. Kaneshiro, T. Takemitsu, Y. Nakazato, A. H. Nabi, T. Nakagawa, F. Suzuki, T. Inagami and H. Itoh (2007). "(Pro)renin receptor-mediated activation of mitogen-activated protein kinases in human vascular smooth muscle cells." Hypertens Res **30**(11): 1139-46.

Santel, A. (2006). "Get the balance right: mitofusins roles in health and disease." Biochim Biophys Acta **1763**(5-6): 490-9.

Santel, A. and S. Frank (2008). "Shaping mitochondria: The complex posttranslational regulation of the mitochondrial fission protein DRP1." IUBMB Life **60**(7): 448-55.

Santel, A., S. Frank, B. Gaume, M. Herrler, R. J. Youle and M. T. Fuller (2003). "Mitofusin-1 protein is a generally expressed mediator of mitochondrial fusion in mammalian cells." J Cell Sci **116**(Pt 13): 2763-74.

Santel, A. and M. T. Fuller (2001). "Control of mitochondrial morphology by a human

mitofusin." J Cell Sci **114**(Pt 5): 867-74.

Santel, A. and M. T. Fuller (2001). "Control of mitochondrial morphology by a human mitofusin." Journal of Cell Science **114**(5): 867-874.

Saris, J. J., P. A. t Hoen, I. M. Garrelds, D. H. Dekkers, J. T. den Dunnen, J. M. Lamers and A. H. Jan Danser (2006). "Prorenin induces intracellular signaling in cardiomyocytes independently of angiotensin II." Hypertension **48**(4): 564-71.

Saris, J. J., M. M. van den Eijnden, J. M. Lamers, P. R. Saxena, M. A. Schalekamp and A. H. Danser (2002). "Prorenin-induced myocyte proliferation: no role for intracellular angiotensin II." Hypertension **39**(2 Pt 2): 573-7.

Sato, A., K. Nakada and J. Hayashi (2006). "Mitochondrial dynamics and aging: Mitochondrial interaction preventing individuals from expression of respiratory deficiency caused by mutant mtDNA." Biochim Biophys Acta **1763**(5-6): 473-81.

Schefe, J. H., M. Menk, J. Reinemund, K. Effertz, R. M. Hobbs, P. P. Pandolfi, P. Ruiz, T. Unger and H. Funke-Kaiser (2006). "A novel signal transduction cascade involving direct physical interaction of the renin/prorenin receptor with the transcription factor promyelocytic zinc finger protein." Circ Res **99**(12): 1355-66.

Schefe, J. H., T. Unger and H. Funke-Kaiser (2008). "PLZF and the (pro)renin receptor." J Mol Med **86**(6): 623-7.

Scheffzek, K., M. R. Ahmadian, W. Kabsch, L. Wiesmuller, A. Lautwein, F. Schmitz and A. Wittinghofer (1997). "The Ras-RasGAP complex: structural basis for GTPase activation and its loss in oncogenic Ras mutants." Science **277**(5324): 333-8.

Schweins, T., M. Geyer, K. Scheffzek, A. Warshel, H. R. Kalbitzer and A. Wittinghofer (1995). "Substrate-assisted catalysis as a mechanism for GTP hydrolysis of p21ras and other GTP-binding proteins." Nat Struct Biol **2**(1): 36-44.

Sealey, J. E., N. Glorioso, J. Itskovitz and J. H. Laragh (1986). "Prorenin as a reproductive hormone. New form of the renin system." Am J Med **81**(6): 1041-6.

Sealey, J. E. and J. H. Laragh (1975). ""Prorenin" in human plasma?" Circ Res **36**(6 Suppl 1): 10-6.

Senbonmatsu, T., T. Saito, E. J. Landon, O. Watanabe, E. Price, Jr., R. L. Roberts, H. Imboden, T. G. Fitzgerald, F. A. Gaffney and T. Inagami (2003). "A novel

angiotensin II type 2 receptor signaling pathway: possible role in cardiac hypertrophy." Embo J **22**(24): 6471-82.

Sever, S., H. Damke and S. L. Schmid (2000). "Dynamin:GTP controls the formation of constricted coated pits, the rate limiting step in clathrin-mediated endocytosis." J Cell Biol **150**(5): 1137-48.

Sever, S., A. B. Muhlberg and S. L. Schmid (1999). "Impairment of dynamin's GAP domain stimulates receptor-mediated endocytosis." Nature **398**(6727): 481-6.

Shirai, H., K. Takahashi, T. Katada and T. Inagami (1995). "Mapping of G protein coupling sites of the angiotensin II type 1 receptor." Hypertension **25**(4 Pt 2): 726-30.

Shiratori, Y., S. Nakagawa, H. Hori, K. Murakami and H. Umeyama (1990). "Protein modeling of human prorenin using the molecular dynamics method." J Mol Graph **8**(3): 163-7, 150.

Sielecki, A. R., K. Hayakawa, M. Fujinaga, M. E. Murphy, M. Fraser, A. K. Muir, C. T. Carilli, J. A. Lewicki, J. D. Baxter and M. N. James (1989). "Structure of recombinant human renin, a target for cardiovascular-active drugs, at 2.5 A resolution." Science **243**(4896): 1346-51.

Siragy, H. M. and R. M. Carey (1996). "The subtype-2 (AT2) angiotensin receptor regulates renal cyclic guanosine 3', 5'-monophosphate and AT1 receptor-mediated prostaglandin E2 production in conscious rats." J Clin Invest **97**(8): 1978-82.

Siragy, H. M., A. A. Jaffa, H. S. Margolius and R. M. Carey (1996). "Renin-angiotensin system modulates renal bradykinin production." Am J Physiol **271**(4 Pt 2): R1090-5.

Siragy, H. M. and J. Linden (1996). "Sodium intake markedly alters renal interstitial fluid adenosine." Hypertension **27**(3 Pt 1): 404-7.

Smirnova, E., L. Griparic, D. L. Shurland and A. M. van der Bliek (2001). "Dynamin-related protein Drp1 is required for mitochondrial division in mammalian cells." Mol Biol Cell **12**(8): 2245-56.

Smirnova, E., D. L. Shurland, S. N. Ryazantsev and A. M. van der Bliek (1998). "A human dynamin-related protein controls the distribution of mitochondria." Molecular Biology of the Cell **9**: 197a-197a.

Staeheli, P., O. Haller, W. Boll, J. Lindenmann and C. Weissmann (1986). "Mx protein: constitutive expression in 3T3 cells transformed with cloned Mx cDNA confers selective resistance to influenza virus." Cell **44**(1): 147-58.

Staeheli, P., M. A. Horisberger and O. Haller (1984). "Mx-dependent resistance to influenza viruses is induced by mouse interferons alpha and beta but not gamma." Virology **132**(2): 456-61.

Stevens, T. H. and M. Forgac (1997). "Structure, function and regulation of the vacuolar (H+)-ATPase." Annu Rev Cell Dev Biol **13**: 779-808.

Stojanovski, D., O. S. Koutsopoulos, K. Okamoto and M. T. Ryan (2004). "Levels of human Fis1 at the mitochondrial outer membrane regulate mitochondrial morphology." J Cell Sci **117**(Pt 7): 1201-10.

Suen, D. F., K. L. Norris and R. J. Youle (2008). "Mitochondrial dynamics and apoptosis." Genes Dev **22**(12): 1577-90.

Sugioka, R., S. Shimizu and Y. Tsujimoto (2004). "Fzo1, a protein involved in mitochondrial fusion, inhibits apoptosis." J Biol Chem **279**(50): 52726-34.

Suzuki, F., Y. Hatano, T. Nakagawa, K. Terazawa, A. Gotoh, U. M. Nasir, Y. Ishida and Y. Nakamura (1999). "Non-proteolytic activation of human prorenin by anti-prorenin prosegment (pf#1: 1P-15P) antiserum." Biosci Biotechnol Biochem **63**(3): 550-4.

Suzuki, F., M. Hayakawa, T. Nakagawa, U. M. Nasir, A. Ebihara, A. Iwasawa, Y. Ishida, Y. Nakamura and K. Murakami (2003). "Human prorenin has "gate and handle" regions for its non-proteolytic activation." J Biol Chem **278**(25): 22217-22.

Suzuki, M., S. Y. Jeong, M. Karbowski, R. J. Youle and N. Tjandra (2003). "The solution structure of human mitochondria fission protein Fis1 reveals a novel TPR-like helix bundle." Journal of Molecular Biology **334**(3): 445-458.

Suzuki, M., A. Neutzner, N. Tjandra and R. J. Youle (2005). "Novel structure of the N terminus in yeast Fis1 correlates with a specialized function in mitochondrial fission." J Biol Chem **280**(22): 21444-52.

Sweitzer, S. M. and J. E. Hinshaw (1998). "Dynamin undergoes a GTP-dependent conformational change causing vesiculation." Cell **93**(6): 1021-9.

Taguchi, N., N. Ishihara, A. Jofuku, T. Oka and K. Mihara (2007). "Mitotic

phosphorylation of dynamin-related GTPase Drp1 participates in mitochondrial fission." J Biol Chem **282**(15): 11521-9.

Takahashi, S. and J. D. Licht (2002). "The human promyelocytic leukemia zinc finger gene is regulated by the Evi-1 oncoprotein and a novel guanine-rich site binding protein." Leukemia **16**(9): 1755-62.

Tamura, K., Y. Tanaka, Y. Tsurumi, K. Azuma, A. Shigenaga, H. Wakui, S. Masuda and M. Matsuda (2007). "The role of angiotensin AT1 receptor-associated protein in renin-angiotensin system regulation and function." Curr Hypertens Rep **9**(2): 121-7.

Tice, C. M., Z. Xu, J. Yuan, R. D. Simpson, S. T. Cacatian, P. T. Flaherty, W. Zhao, J. Guo, A. Ishchenko, S. B. Singh, Z. Wu, B. B. Scott, Y. Bukhtiyarov, J. Berbaum, J. Mason, R. Panemangalore, M. G. Cappiello, D. Muller, R. K. Harrison, G. M. McGeehan, L. W. Dillard, J. J. Baldwin and D. A. Claremon (2009). "Design and optimization of renin inhibitors: Orally bioavailable alkyl amines." Bioorg Med Chem Lett **19**(13): 3541-5.

Tieu, Q. and J. Nunnari (2000). "Mdv1p is a WD repeat protein that interacts with the dynamin-related GTPase, Dnm1p, to trigger mitochondrial division." J Cell Biol **151**(2): 353-66.

Tieu, Q., V. Okreglak, K. Naylor and J. Nunnari (2002). "The WD repeat protein, Mdv1p, functions as a molecular adaptor by interacting with Dnm1p and Fis1p during mitochondrial fission." J Cell Biol **158**(3): 445-52.

Timmermans, P. B. M. W. M., P. C. Wong, A. T. Chiu, W. F. Herblin, P. Benfield, D. J. Carini, R. J. Lee, R. R. Wexler, J. A. M. Saye and R. D. Smith (1993). "Angiotensin-Ii Receptors and Angiotensin-Ii Receptor Antagonists." Pharmacol Rev **45**(2): 205-251.

Tohgo, A., K. L. Pierce, E. W. Choy, R. J. Lefkowitz and L. M. Luttrell (2002). "beta-Arrestin scaffolding of the ERK cascade enhances cytosolic ERK activity but inhibits ERK-mediated transcription following angiotensin AT1a receptor stimulation." J Biol Chem **277**(11): 9429-36.

Ushio-Fukai, M., K. K. Griendling, M. Akers, P. R. Lyons and R. W. Alexander (1998). "Temporal dispersion of activation of phospholipase C-beta 1 and -gamma isoforms by angiotensin II in vascular smooth muscle cells - Role of alpha(q/11), alpha(12), and beta gamma G protein subunits." Journal of Biological Chemistry

273(31): 19772-19777.

van den Eijnden, M. M., J. J. Saris, R. J. de Bruin, E. de Wit, W. Sluiter, T. L. Reudelhuber, M. A. Schalekamp, F. H. Derkx and A. H. Danser (2001). "Prorenin accumulation and activation in human endothelial cells: importance of mannose 6-phosphate receptors." Arterioscler Thromb Vasc Biol **21**(6): 911-6.

van Kesteren, C. A., A. H. Danser, F. H. Derkx, D. H. Dekkers, J. M. Lamers, P. R. Saxena and M. A. Schalekamp (1997). "Mannose 6-phosphate receptor-mediated internalization and activation of prorenin by cardiac cells." Hypertension **30**(6): 1389-96.

Vander, A. J. and G. W. Geelhoed (1965). "Inhibition of renin secretion by angiotensin. II." Proc Soc Exp Biol Med **120**(2): 399-403.

Vetter, I. R. and A. Wittinghofer (2001). "The guanine nucleotide-binding switch in three dimensions." Science **294**(5545): 1299-304.

Wang, C., S. Jayadev and J. A. Escobedo (1995). "Identification of a domain in the angiotensin II type 1 receptor determining Gq coupling by the use of receptor chimeras." J Biol Chem **270**(28): 16677-82.

Wasiak, S., R. Zunino and H. M. McBride (2007). "Bax/Bak promote sumoylation of DRP1 and its stable association with mitochondria during apoptotic cell death." J Cell Biol **177**(3): 439-50.

Wood, J. M., J. Maibaum, J. Rahuel, M. G. Grutter, N. C. Cohen, V. Rasetti, H. Ruger, R. Goschke, S. Stutz, W. Fuhrer, W. Schilling, P. Rigollier, Y. Yamaguchi, F. Cumin, H. P. Baum, C. R. Schnell, P. Herold, R. Mah, C. Jensen, E. O'Brien, A. Stanton and M. P. Bedigian (2003). "Structure-based design of aliskiren, a novel orally effective renin inhibitor." Biochem Biophys Res Commun **308**(4): 698-705.

Yeyati, P. L., R. Shaknovich, S. Boterashvili, J. Li, H. J. Ball, S. Waxman, K. Nason-Burchenal, E. Dmitrovsky, A. Zelent and J. D. Licht (1999). "Leukemia translocation protein PLZF inhibits cell growth and expression of cyclin A." Oncogene **18**(4): 925-34.

Yonashiro, R., S. Ishido, S. Kyo, T. Fukuda, E. Goto, Y. Matsuki, M. Ohmura-Hoshino, K. Sada, H. Hotta, H. Yamamura, R. Inatome and S. Yanagi (2006). "A novel mitochondrial ubiquitin ligase plays a critical role in mitochondrial dynamics." Embo J **25**(15): 3618-26.

Yoon, Y., E. W. Krueger, B. J. Oswald and M. A. McNiven (2003). "The mitochondrial protein hFis1 regulates mitochondrial fission in mammalian cells through an interaction with the dynamin-like protein DLP1." Mol Cell Biol **23**(15): 5409-20.

Yoon, Y., K. R. Pitts and M. A. McNiven (2001). "Mammalian dynamin-like protein DLP1 tubulates membranes." Mol Biol Cell **12**(9): 2894-905.

Youle, R. J. and M. Karbowski (2005). "Mitochondrial fission in apoptosis." Nat Rev Mol Cell Biol **6**(8): 657-63.

Zeviani, M. (2004). "Mitochondrial disorders." Suppl Clin Neurophysiol **57**: 304-12.

Zeviani, M. and S. Di Donato (2004). "Mitochondrial disorders." Brain **127**(Pt 10): 2153-72.

Zhang, P. and J. E. Hinshaw (2001). "Three-dimensional reconstruction of dynamin in the constricted state." Nat Cell Biol **3**(10): 922-6.

Zhu, P. P., A. Patterson, J. Stadler, D. P. Seeburg, M. Sheng and C. Blackstone (2004). "Intra- and intermolecular domain interactions of the C-terminal GTPase effector domain of the multimeric dynamin-like GTPase Drp1." J Biol Chem **279**(34): 35967-74.

Zunino, R., A. Schauss, P. Rippstein, M. Andrade-Navarro and H. M. McBride (2007). "The SUMO protease SENP5 is required to maintain mitochondrial morphology and function." J Cell Sci **120**(Pt 7): 1178-88.

Zuo, L., M. Ushio-Fukai, S. Ikeda, L. Hilenski, N. Patrushev and R. W. Alexander (2005). "Caveolin-1 is essential for activation of Rac1 and NAD(P)H oxidase after angiotensin II type 1 receptor stimulation in vascular smooth muscle cells: role in redox signaling and vascular hypertrophy." Arterioscler Thromb Vasc Biol **25**(9): 1824-30.

CHAPTER 2

Functional expression of DLP-1

2.1 Introduction

Functional and structural studies on DLP-1 would shed light onto the molecular mechanisms of mitochondrial fission, increasing our understanding of mitochondrial defects and prevent human diseases. The middle domain and the GED of dynamins and related proteins are considered to be important for protein intra- and intermolecular interactions (Shin, Takatsu et al. 1999; Smirnova, Shurland et al. 1999; Zhang and Hinshaw 2001; Zhu, Patterson et al. 2004). Mutations in the yeast homolog Dnm1 and the human dynamin have been showed to impair the protein GTPase activities and disrupt the protein oligomeric states (Ingerman, Perkins et al. 2005; Ramachandran, Surka et al. 2007). However, the functions of the DLP-1 middle domain on protein GTPase activities and oligomerization have not been directly studied.

The dynamins also bind to lipids, particularly to negatively charged phospholipids, primarily through their PH domains (Klein, Lee et al. 1998; Lemmon and Ferguson 2000). Usually the regions between the middle domains and the GEDs of dynamin-related proteins are topologically analogous to the dynamin PH domain, and these regions contain high content of positively charged residues that have the potential to interact with negatively charged membrane lipids. However, for the dynamin-related proteins, there is no domain or motif that is obviously similar to the canonical PH domain in dynamin. DLP-1 binds and tubulates membranes (Yoon, Pitts et al. 2001), but the specificities of the binding and what region(s) is responsible for the binding remain unclear.

Finally, one bottleneck that impacts protein structural studies, especially

membrane-interacting proteins of large size, such as DLP-1, is obtaining sufficient amounts of highly purified protein suitable for functional and structural studies. Towards solving the issues mentioned above, this chapter describes the recombinant DLP-1 expression and purification, and biochemical analyses for functional characterizations and future structural studies.

2.2 Materials and methods

2.2.1 DNA Cloning of DLP-1 and Mutants - The DNA encoding for wild type human DLP-1 isoform 2, the GTPase domain (1-307aa), and the PH-like domain (497-607aa) were amplified from cDNA IMAGE (clone ID 3882922) by PCR. The PCR amplification was comprised of 35 cycles of denaturing at 94 °C for 30 sec, annealing at 55 °C for 45 sec, and elongation at 72 °C for 2 min and 30 sec for wild type DLP-1; 1 min for the GTPase domain; and 40 sec for the PH-like domain, followed by 72 °C for 10 min. The PCR products were purified by QIAquick PCR purification kit (QIAGEN), digested with restriction enzymes Afl III and XhoI. The pLW01 expression vector digested with NcoI (Compatible with Afl III) and XhoI together with digested PCR products was transformed into *E.coli* DH5α competent cells. Positive clones growing from LB plates containing 100 μg/ml ampicillin were picked, and plasmid DNAs were isolated and sequenced. Site-directed mutagenesis was performed using GeneEditor *in vitro* site-directed mutagenesis system (Promega).

2.2.2 Protein Expression and Purification - The sequenced plasmid was transformed into expression host *E. coli* C41 (DE3) competent cells. A fresh single colony from the selection plate was inoculated into 100 ml LB media containing 100 μg/ml antibiotic at 37 °C with shaking at 200 rpm for overnight. Twenty ml of this culture was transferred into 1 L fresh LB media and the cells were grown at 37 °C until the OD_{600} reached to 0.8-1.0. The cells were then induced by adding 0.05 mM IPTG and incubated with shaking at room temperature for 17 hrs. Cells were harvested by centrifugation and stored at –80 °C.

To purify DLP-1 wild type and mutant proteins, the cell pellets were resuspended in Buffer A (50 mM sodium phosphate, 300 mM NaCl, 250 mM sucrose, 10% glycerol, 10 mM β-mercaptoethanol, 0.1 mM EDTA, pH 8.0). After sonication, the crude cell extract was centrifuged at 4 °C for 20 min at 12,000×g. The supernatant was loaded onto a pre-equilibrated column containing 20 ml Ni-NTA agarose slurry. The column was washed with buffer B (50 mM sodium phosphate, 300 mM NaCl, 10% glycerol, 10 mM β-mercaptoethanol, 20 mM imidazole, pH 8.0). The protein bound column was eluted by Buffer C (50 mM sodium phosphate, 300 mM NaCl, 10% glycerol, 10 mM β-mercaptoethanol, 200 mM imidazole, pH 8.0). The protein eluates were pooled and concentrated to 1 ml by Amicon ultra centrifugal filter molecular cutoff (Millipore).

2.2.3 Ion Exchange and Size Exclusion Chromatography – Ion exchange chromatography was performed to further purify target proteins and remove

contaminants. The pooled and concentrated eluates from Ni-NTA were loaded onto a 1 ml HiTrap Q ion exchanger (Amersham Biosciences) pre-equilibrated with Buffer D (20 mM Tris-HCl, pH 8.5). Protein was eluted off the column with a linear concentration gradient of NaCl from 0 to 1 M, at a flow rate of 1 ml/min. The peak fractions containing highly purified target protein were pooled and concentrated.

The oligomeric states of wild type DLP-1 and mutants were determined by analytical size exclusion chromatography. A Superdex 200 10/30 GL or Superdex 75 10/30 GL column was pre-equilibrated with buffer F (20 mM HEPES, 150 mM NaCl, 5% glycerol, pH 7.2). The protein was loaded onto the column and eluted at a rate of 0.5 ml/min. Fractions containing homogenous protein was combined and concentrated. Protein concentration was estimated by Bradford assay using bovine serum albumin as standard. For SDS-PAGE analysis, samples were electrophoresed on precast NuPAGE 4-12% Bis-Tris polyacrylamide gels (Invitrogen) and visualized with Coomassie blue staining and by Western blotting.

2.2.4 Measurement of GTPase Activity - The GTPase activities of DLP-1 wild type, the GTPase domain, the G350D, the R365S, the ΔPH, and the K38A were measured using a Malachite Green phosphate assay kit (Bioassay systems) at room temperature. The reaction included 1μM purified target protein with 0.05% bovine serum albumin, 16μM GTP, and 2 mM $MgCl_2$ with Buffer F in an 800μL volume. At different time points, 200μL malachite green reagent was added to stop the reaction and the mixture was

incubated at room temperature for 10 minutes to allow color to develop. Absorbance at 650 nm was measured spectrophotometrically, and the amount of released inorganic phosphate was determined by using a standard curve of known phosphate concentrations. All data points represent an average of at least three independent measurements.

2.2.5 Lipid-Protein Interactions - FAT-Western blot assay was used to investigate the interaction of DLP-1 with free lipids. Membrane strips (Invitrogen) pre-spotted with phospholipids were blocked using TBS-T-BSA buffer (10 mM Tris-HCl, 150 mM NaCl, 0.1% Tween 20, 3% fatty acid-free BSA, pH 8.0) for 1 h at room temperature. Two μg/mL of target protein were incubated with TBS-T-BSA buffer at 4 °C overnight. The membrane strips were washed three times and soaked into TBS-T-BSA with an anti-hexaHis mouse monoclonal antibody (Clontech) at a 1:1,000 dilution at 4 °C overnight. The membranes were then washed three times and incubated with secondary antibody at a 1:5,000 dilution in TBS-T-BSA for 1 h at room temperature. After another three-time washing, the target protein was detected by using the standard Western Lightning Chemiluminescence Reagent (PerkinElmer LAS Inc.).

Further protein-lipids interactions were analyzed by liposome-binding assays. The lipids consist of phosphatidylcholine, phosphatidylserine, or phosphoinositides were incubated in TBS buffer (50 mM Tris-HCl, 100 mM NaCl, pH 7.0) at 37 °C for 1 h. After vortexing for 5 min, the solution was centrifuged at 20,000×g at 4 °C. The pellet containing 200 μg liposomes was resuspended in 100 μl TBS followed by adding 10

μg/mL of protein. The binding reaction was performed by incubating the mixture at 30 °C for 30 min. The solution was centrifuged at 20,000×g at 4 °C and the distribution of target proteins was determined by SDS-PAGE and Western blotting using an anti-hexaHis mouse monoclonal antibody (at 1:5,000 dilution) and anti-mouse antibody (at 1:10,000 dilution).

2.3 Results and Discussion

2.3.1 Protein Expression and Purification - To produce high-yield recombinant proteins for functional and structural analysis, several aspects regarding membrane-associated protein expression in *E. coli* were considered. First, a small 3.4 kb, hexa-histidine tagged vector with high copy numbers, pLW01, was selected as an expression vector. The pLW01 was generated based on pET-23d and pBluescript II KS + vectors and was successfully used to express membrane protein P450 in *E. coli* (Bridges, Gruenke et al. 1998). Second, the *E. coli* C41 (DE3) strain was chosen as expression host. Although DLP-1 exists primarily in the cytoplasm, it functions as a membrane-interacting protein and probably binds to mitochondrial membranes. The C41 strain is a derivative of *E. coli* BL21 (DE3) and can allow high-yield expression of membrane proteins, probably because of the formation of internal membranes (Miroux and Walker 1996; Arechaga, Miroux et al. 2000). Third, the growth conditions including temperature and concentration of the inducer (IPTG) were optimized to reduce the rate of protein synthesis and minimize formation of inclusion bodies. With these optimizations, about 10

mg DLP-1 protein was purified from 1 L bacterial culture.

Several DLP-1 mutant species with deletions or point mutations were also recombinantly expressed and purified for investigation of impacts of specific domains or key amino acids on the biochemical properties of DLP-1. I have aligned the DLP-1 protein sequence with its homologues from other organisms and analyzed the secondary structure to determine possible essential residues and domain boundaries. Except the putative PH-like domain, other regions of the protein are highly conserved and contain regular secondary structures with combination of helices and strands (data not shown). However, no obvious secondary structures or sequence conservation were identified in the PH-like domain. Therefore, I isolated the PH-like domain and also created DLP-1 ΔPH in which the PH-like domain was deleted, to investigate whether the domain has effects on DLP-1 biochemical functions. In addition, the GTPase domain was isolated to analyze whether other domains are required for the DLP-1 full GTPase activity and whether the GTPase domain is critical for protein oligomerization. The G350 and the R365 are located in the middle domain and are conserved in dynamin and a number of dynamin-related proteins (Fig. 2.1). These two residues in DLP-1 homologues were previously reported to be important for protein function including oligomerization and GTPase activities (Ingerman, Perkins et al. 2005; Bhar, Karren et al. 2006; Ramachandran, Surka et al. 2007). The K38A was used as a control to evaluate the GTPase activities of other DLP-1 species. The K38 is conserved in dynamin and related proteins (Fig. 2.1). It is located in the GTP/GDP binding motif of the GTPase domain and

is critical for the GTP hydrolysis. Mutation of K38A was previously reported to abolish the DLP-1 GTPase activity (Yoon, Pitts et al. 2001; Zhu, Patterson et al. 2004). The schematic demonstration of these mutants is shown in Fig. 2.2A. With considerations of DNA cloning and protein expression methods as described above, all the recombinant DLP-1 species were purified to near homogeneity by Ni-NTA column and ion exchange chromatography (Fig. 2.2B).

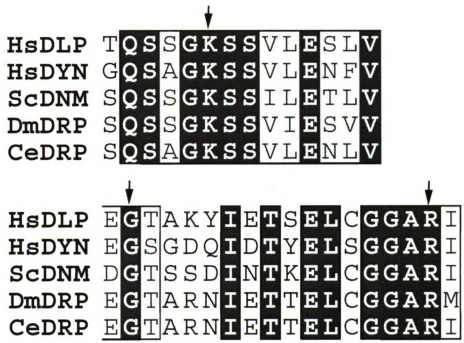

Figure 2.1: Sequence alignments of partial GTPase domain (upper) and the middle domain (lower) of dynamin related proteins. HsDLP, *H. sapiens* DLP-1; HsDYN, *H. sapiens* Dynamin; ScDNM, *S. cerevisiae* Dnm1p; DmDRP, *D. melanogaster* dynamin related protein; CeDRP, *C. elegans* dynamin related protein. The K38, G350, and R365 of DLP-1 were indicated by arrows.

Table 2.1: Specific GTPase activity of DLP-1 WT and mutants. The specific activities were measured based on the linear regions of the reactions.

Protein	Specific Activity
DLP-1 WT	0.90 μM GTP / min / μM protein
GTPase domain (1-307)	0.35 μM GTP / min / μM protein
R365S	0.12 μM GTP / min / μM protein
G350D	0.10 μM GTP / min / μM protein

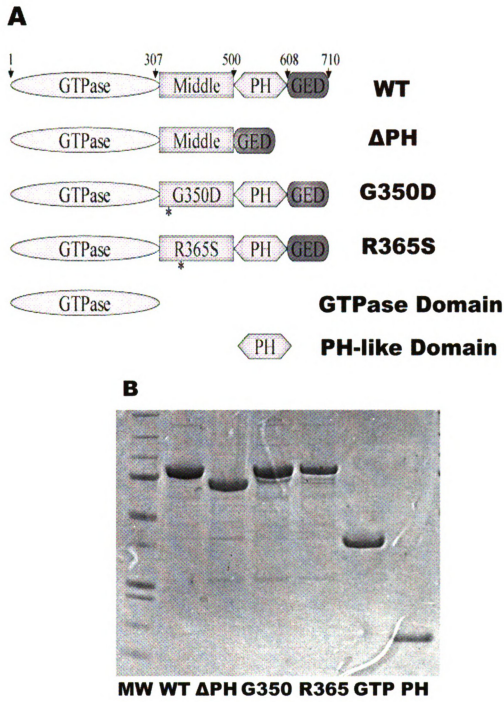

Figure 2.2: Purification of DLP-1 WT and mutants. (A) Schematic illustration of constructs. ΔPH, DLP-1 lacking 501-607 aa; G350D and R365S, DLP-1 with a point mutation at G350 and R365, respectively; GTPase domain, DLP-1 1-307 aa; PH-like domain, DLP-1 501-607aa. (B) SDS-PAGE analysis of purified recombinant DLP-1 WT and mutants. From left to right: molecular weight markers; DLP-1 WT; ΔPH; G350D; R365S; the GTPase domain; the PH-like domain.

Figure 2.3: GTPase activity of purified DLP-1 WT and mutants by malachite green colorimetric assay. (A) GTP hydrolysis by DLP-1 WT. The data were plotted as time (min) vs. released phosphate (μM). Square, DLP-1 WT; triangle, DLP-1 K38A; (B) GTP hydrolyzed by DLP-1 WT and mutants. The data were plotted as time (min) vs. hydrolyzed GTP/total GTP (%). Squares, WT; triangles, the GTPase domain; stars, R365S; circles, G350D; rhomboids, ΔPH. All data points represent an average of at least three independent measurements.

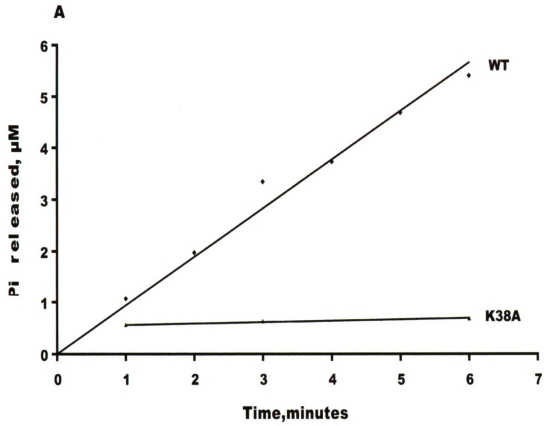
A
Pi released, µM
Time,minutes
WT
K38A
0
1
2
3
4
5
6
7

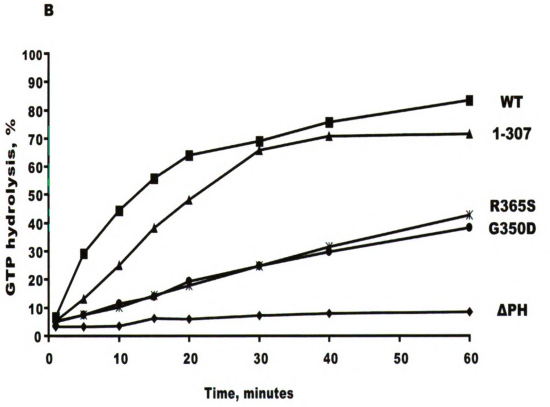
B
GTP hydrolysis, %
Time, minutes
WT
1-307
R365S
G350D
ΔPH
0
10
20
30
40
50
60
70
80
90
100

2.3.2 GTPase Activities – The full-length DLP-1 showed efficient GTPase activity (Fig. 2.3A and Table 2.1) as apposed to the GTPase null mutant K38A, which is consistent with previous studies (Yoon, Pitts et al. 2001; Zhu, Patterson et al. 2004). The isolated GTPase domain demonstrated lower activity than the full-length protein (Fig. 2.3B and Table 2.1). Although the GTPase domain is supposed to provide enzymatic function, its lower activity measured in this experiment suggests roles of other domains in the DLP-1 full GTPase activity. Presumably it is the lack of GED that is probably responsible for the reduced GTPase domain activity based on previous reports about roles of the GED of dynamins or related proteins in GTPase activity.

Although controversial, the GED of dynamin was considered to have GTPase activating protein (GAP) activity (Muhlberg, Warnock et al. 1997; Sever, Muhlberg et al. 1999). Direct interactions between the GTPase domain and the GED of dynamin were demonstrated by yeast two-hybrid studies (Smirnova, Shurland et al. 1999). Meanwhile, the crystal structures of the GTPase domains of *Dictyostlium* dynamin A and rat dynamin 1 revealed a hydrophobic groove suggesting a putative GED interacting site (Niemann, Knetsch et al. 2001; Reubold, Eschenburg et al. 2005). Although strong interactions between the GTPase domain and the GED of DLP-1 was not detected directly by yeast two-hybrid assay, point mutations in the GEDs of DLP-1 or yeast DNM1 were reported to cause a reduction of GTPase activity probably by interfering the interactions of GED with the middle domain and further the GTPase domain (Shin, Takatsu et al. 1999; Fukushima, Brisch et al. 2001; Zhu, Patterson et al. 2004). Therefore, The possible roles

of the C-terminus, particularly the GED in the DLP-1, on GTPase activity may explain a relatively low activity of the GTPase domain. Our results from another aspect, demonstrated that the GED is important for the full GTPase activity of DLP-1.

Both the G350D and the R365S mutations showed much lower GTPase activities (Fig. 2.3B and Table 2.1). Since these two mutations are not physically located in the GTPase domain, it is possible that they affect the protein activity by interfering with the intramolecular interactions, particularly between the middle domain and the GED so that the GED could not reach effectively to the GTPase domain (Fig. 2.4B). The crystal structure of a member of the dynamin superfamily, human guanylate-binding protein 1 (hGBP1) showed that the GED folds back interacting with the middle domain and extends to the GTPase domain (Prakash, Praefcke et al. 2000; Prakash, Renault et al. 2000). The three-dimensional map of dynamin from cryo-electron micrographs suggested a similar structural property of a "stalk" region constituted by the middle domain and the GED (Zhang and Hinshaw 2001). In addition, yeast two-hybrid assays of dynamins and related proteins showed direct interactions between the GED and the middle domain (Shin, Takatsu et al. 1999; Smirnova, Shurland et al. 1999; Zhu, Patterson et al. 2004). Therefore, The two mutations may cause conformational changes in the middle domain of DLP-1 and interfere the intramolecular interactions and further affect the GTPase activity.

The results that the two point mutations have lower activities than isolated GTPase domain indicated that besides affecting the interactions between the GED and the GTPase

domain, other local protein structures that are important for the activity may also be affected. Given the fact that the two residues are close, the similar low activities that both point mutations exhibited indicated that they may fall in the same functional or structural group. Meanwhile, to my knowledge, for the first time, I demonstrated that the middle domain is important to the DLP-1 GTPase activity.

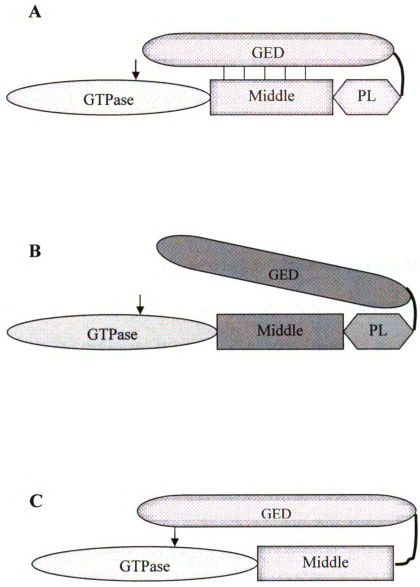

Figure 2.4: Schematic model of DLP-1 intramolecular interactions. GTPase: the GTPase domain; Middle: the middle domain; PL: the PH-like domain. Arrow: active site the GTPase domain (A) wild type DLP-1. The lines show the interactions between the middle domain and the GED. (B) G350D or R365S. (C) ΔPH.

Surprisingly, deletion of the PH-like domain abolished the GTPase activity (Fig. 2.3B). It is hard to interpret this result since the GTPase domain is intact in the ΔPH. A possible interpretation is that deletion of the PH-like domain forces the GED to fold back from the very end of the middle domain instead of from the end of the PH-like domain as in full-length DLP-1. This structure change makes the C-terminus of the GED reaching further than normal to the GTPase domain and blocking the active site of the GTPase domain (Fig. 2.4C).

The GTPase activities of dynamins can be largely stimulated by assembly into higher order structures from tetramers at low ionic strength environments or in presence of specific phospholipids (Warnock, Hinshaw et al. 1996; Barylko, Binns et al. 1998; Stowell, Marks et al. 1999). I have attempted to measure the stimulated GTPase activity of wild type DLP-1. At low ionic state of 20 mM NaCl, DLP-1 formed a structure larger than its native size (data not shown). However, no stimulated GTPase activity was observed either in low ionic state or in presence of phospholipids (data not shown). These observations may be accounted for by the fact that particular components of the fission complex or specific mitochondrial membrane structures may be required for the stimulation of DLP-1 GTPase activity.

2.3.3 Oligomeric States – Since the GTPase domain, the G350D, the R365S, and the ΔPH demonstrated reduced GTPase activities, I was interested in studying the oligomeric states of these species to analyze whether the decreased activities have relationships with

protein oligomerization. For the middle domain, intermolecular interactions of dynamin were previously reported to be important for the protein oligomerization and further assembly (Smirnova, Shurland et al. 1999; Zhang and Hinshaw 2001). The yeast mutation equivalent to DLP-1 G350D and the human dynamin mutation equivalent to DLP-1 R365S have been showed to impair the protein GTPase activities and disrupt the multimeric or tetrameric protein states to dimeric state (Ingerman, Perkins et al. 2005; Ramachandran, Surka et al. 2007). Therefore, I sought to determine whether the reduced GTPase activities of the G350D and the R365S are caused by disruption of protein oligomerization. For the GTPase domain and the PH-like domain, I am interested in their oligomeric states for investigating whether the domains are critical for full-length protein oligomerization.

DLP-1 exists primarily as tetramers in the cytosol and forms higher order structures once binding to membranes (Shin, Takatsu et al. 1999; Zhu, Patterson et al. 2004). Our size exclusion chromatography results showed that the full-length DLP-1 can be isolated as a size of about 350 kDa, corresponding to the tetrameric state (Fig. 2.5A and Table 2.2), consistent with previous reports (Shin, Takatsu et al. 1999; Zhu, Patterson et al. 2004). Similarly, the G350D and the R365S were eluted also at about 350 kDa (Fig. 2.5B, C and Table 2.2), displaying stable tetrameric forms that are almost indistinguishable from that of the wild type protein. These results suggested that the G350D and the R365S mutations do not seem to affect the intermolecular interactions, and the reduced GTPase activities do not appear to be caused by loss of protein quaternary structures. Although

the middle domain may be important for not only protein activities, but also protein oligomerization, mutations in these two positions may not be strong enough to alter the intermolecular interactions. However, they are sufficient to show that the middle domain of DLP-1 is important for protein activities, and the untouched protein oligomeric states support our interpretation about the reduced GTPase activities of the G350D and R365S that alteration of intramolecular interactions caused by possible conformational changes in the middle domain may be responsible for decreased activities (Fig. 2.4A).

Unlike the DLP-1 G350D and R365S which keep uninfluenced oligomeric states, the equivalent mutations in yeast DNM1 and human dynamin was disrupted to dimers compared to the wild type multimers and tetramers, respectively (Ingerman, Perkins et al. 2005; Ramachandran, Surka et al. 2007). Although these proteins are functionally similar, difference in protein natures may explain the distinct effects of equivalent mutations on protein oligomerization. For example, compared to the tetrameric DLP-1 found in cytosol or *in vitro* (Shin, Takatsu et al. 1999; Zhu, Patterson et al. 2004), the Dnm1 aggregates in cytosol and was isolated as multimers likely 8-12 mers (Ingerman, Perkins et al. 2005). Therefore, it is possible that either DLP-1 forms relatively stronger tetramers, or other residues evolved in DLP-1 that is critical for the dimer to tetramer transition.

In addition, the reduced GTPase activities with untouched tetrameric forms that the two middle domain mutations G350D and R365S exhibited are similar with the phenotypes reported previously for the mutation in the DLP-1 GED, K679A (Zhu, Patterson et al. 2004). Because of the intramolecular interactions between the middle

domain and the GED, mutations on either side would disrupt the similar interactions and cause similar defective "open" state. The parallel phenotypes of mutations from different locations may provide another evidence that the middle domain interacts with the GED.

The isolated GTPase domain (1-307aa) was characterized as 35 kDa, a monomeric size by exclusion chromatography (Fig. 2.5D and Table 2.2), indicating that probably this domain is not involved in DLP-1 oligomerization. Lack of oligomerization may be another factor responsible for the reduced activity of the isolated GTPase domain. In addition, during testing possible domain boundary of the GTPase domain, I also isolated the 1-323aa and 1-340aa fragments because secondary structure prediction suggested a long helix ending at residue 323 and sequence alignments favored residue 340 as the domain boundary (data not shown). However, although these fragments were purified, they aggregated when analyzed by size exclusion chromatography (data not shown). This may suggest that the part from residue 308 to 340 is involved in the formation of middle domain helix bundle and inclusion of this part into the isolated GTPase domain may cause the hydrophobic region exposed to solvent.

Taking the activities and protein oligomerization results of the isolated GTPase domain, the G350D, and the R365S, our findings support the idea that the GED plays roles in the protein GTPase activity. And proper intramolecular interactions with the middle domain are important for normal GED functions on DLP-1 activity.

Because deletion of the PH-like domain abolished the GTPase activity, I was interested in investigating the oligomeric state of the DLP-1 ΔPH to determine whether the loss of

activity was caused by collapse of the overall protein structure without the PH-like domain, and whether the PH-like domain is critical for the full-length protein oligomerization. The chromatography results showed that the ΔPH exists as about 300 kDa, stable tetramers without any sign of quaternary structure being disrupted (Fig. 2.5E and Table 2.2), indicating that deletion of the PH-like domain does not affect the protein oligomerization.

Figure 2.5: Size exclusion chromatography of DLP-1 WT and mutants. Panels A, B, C, and E show chromatography on a Superdex 200 10/30 gel filtration column; panels D and F show chromatography on a Superdex 75 10/30 gel filtration column. (A) DLP-1 WT; (B) G350D; (C) R365S; (D) the GTPase domain; (E) ΔPH; (F) the PH-like domain; (G) Kav versus molecular weight plot of protein standards. The standards were plotted as K_{av} vs. molecular weight. K_{av} was obtained by the formula of $K_{av} = (V_e-V_0)/(V_t-V_0)$, where V_e is the elution volume of each molecular weight markers, V_0 the void volume, and V_t total volume of the column.

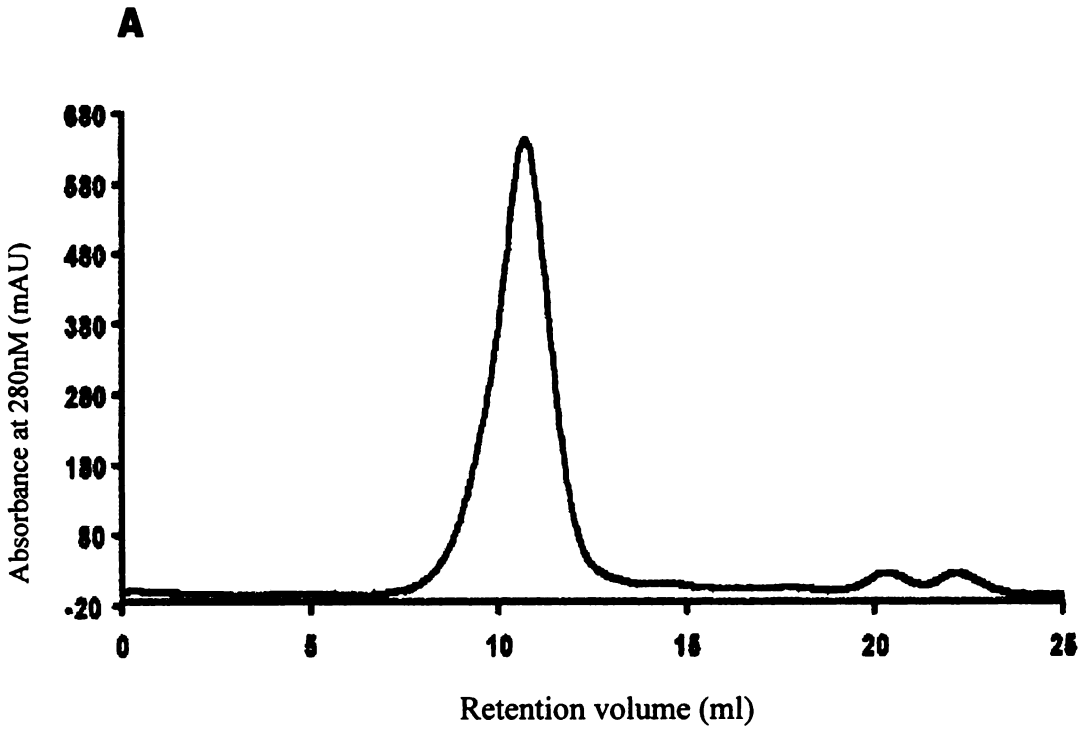
A
Absorbance at 280nM (mAU)
680
580
480
380
280
180
80
-20
0
5
10
15
20
25
Retention volume (ml)

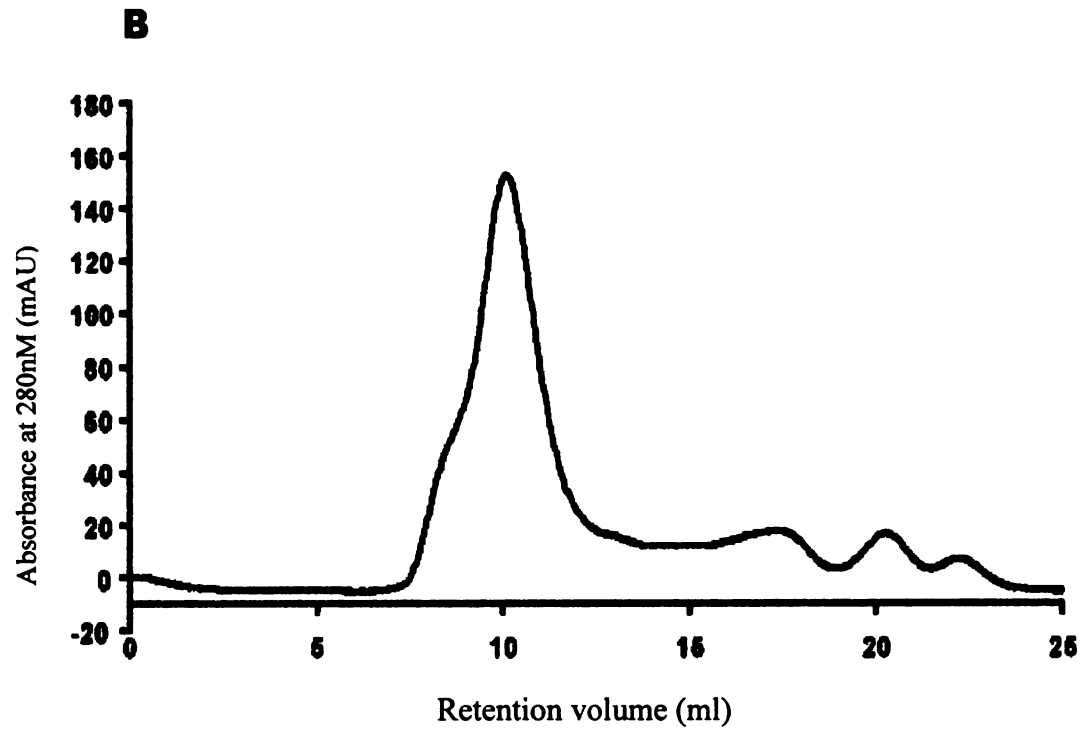
B
Absorbance at 280nM (mAU)
180
160
140
120
100
80
60
40
20
0
-20
0
5
10
15
20
25
Retention volume (ml)

Figure 2.5 continued

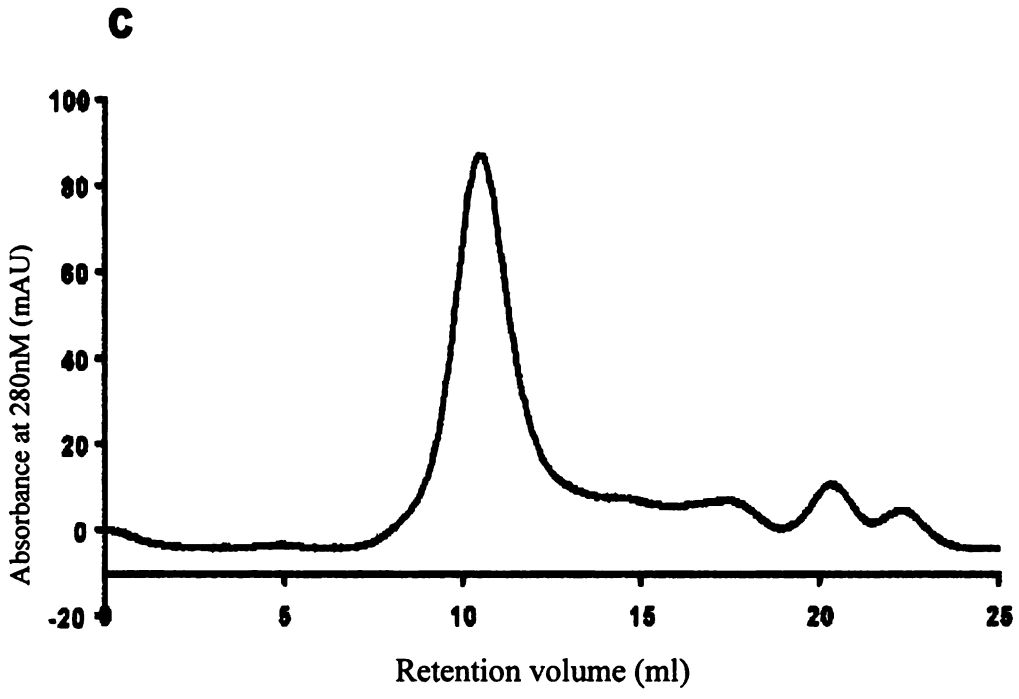

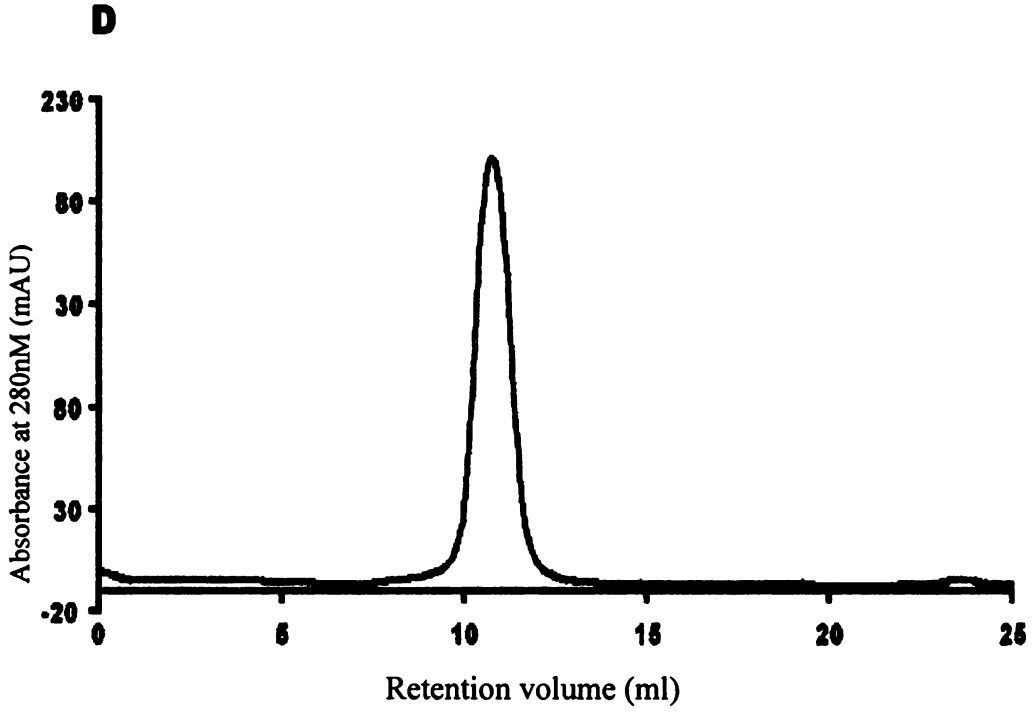

Figure 2.5 continued

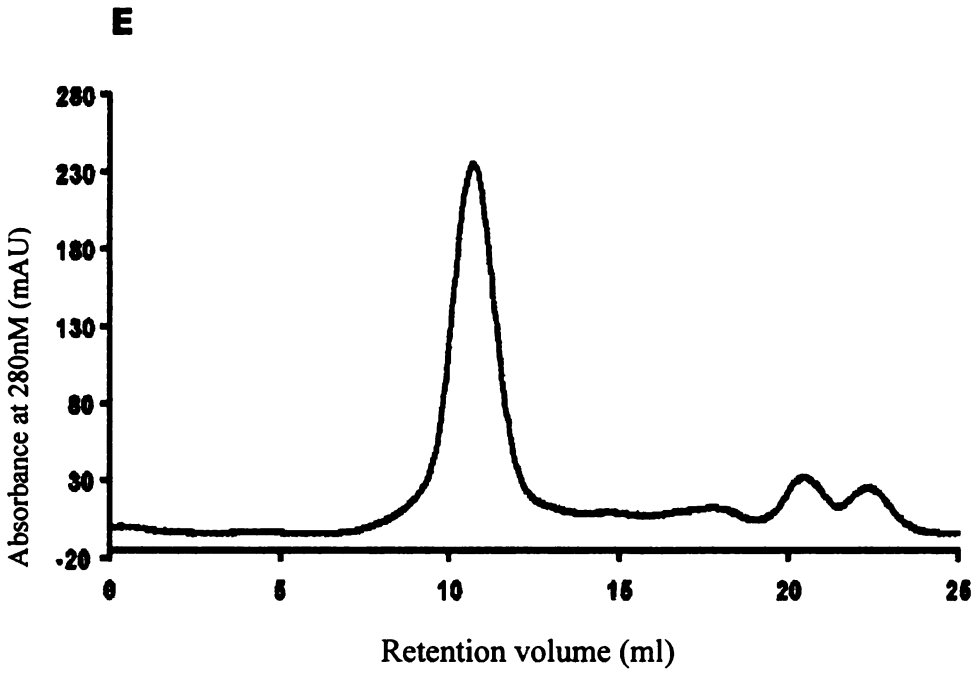

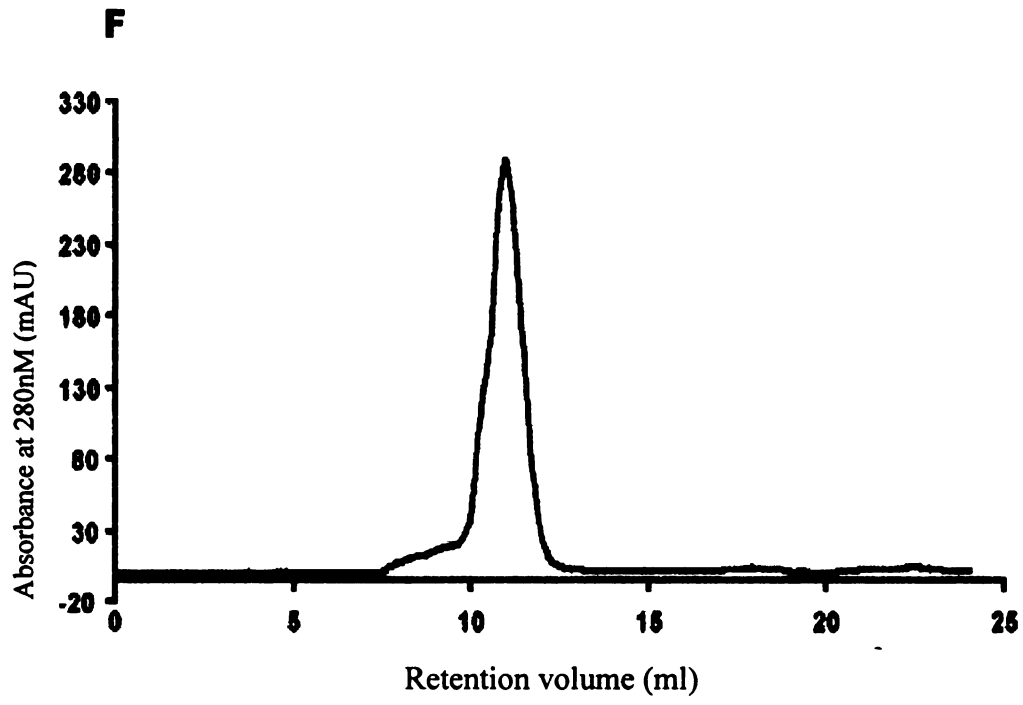

Figure 2.5 continued

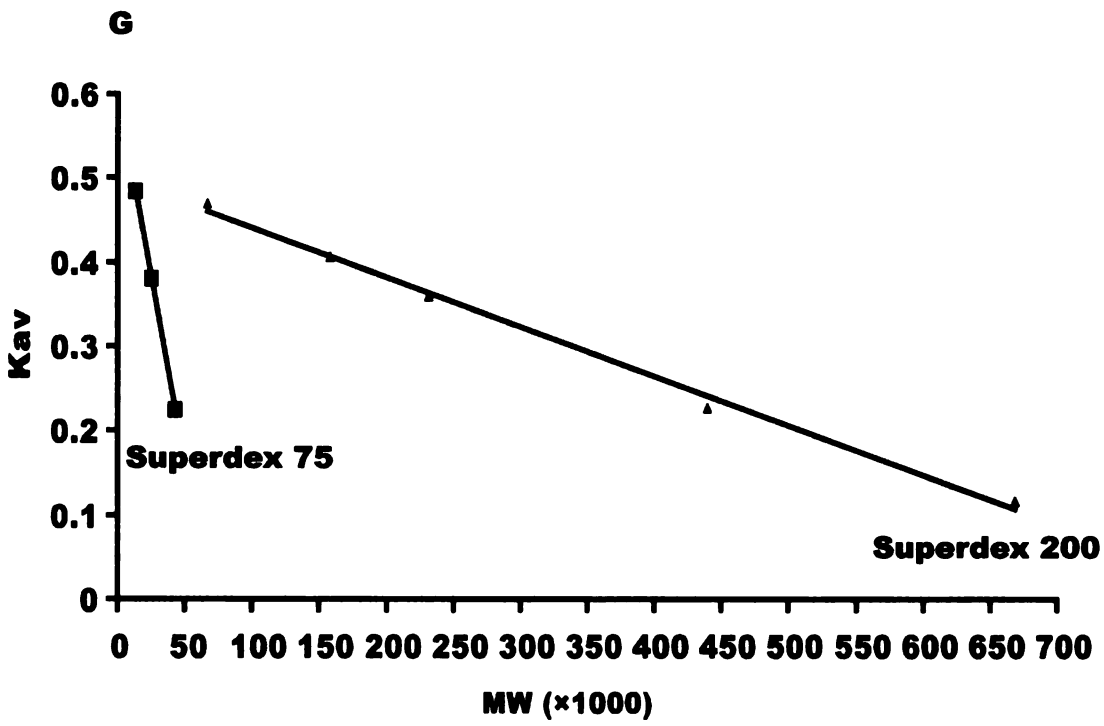

Table 2.2: Calculated molecular weight of DLP-1 WT and mutants by gel filtration. Molecular weight was based on the protein standards (Fig. 4G).

Protein	Calculated MW	Oligomeric state
DLP1 WT	350000	tetramer
DLP1_G350D	350000	tetramer
DLP1_R365S	350000	tetramer
DLP1_1-307	35000	monomer
DLP1_ΔPH	300000	tetramer
DLP1_PH-like domain	45000	tetramer

A number of research has described the GED of dynamins or related proteins as a key player in protein oligomerization and higher order structure formation (Danino and Hinshaw 2001; Praefcke and McMahon 2004). Also, the middle domain was considered to be critical for these structures (Zhang and Hinshaw 2001; Ingerman, Perkins et al. 2005; Ramachandran, Surka et al. 2007). I have attempted to expressed DLP-1 fragments with the middle domain or the GED deleted to directly study the effects of these two domains on protein oligomerization. Unfortunately, they were aggregated in non-soluble inclusion bodies in regardless of expression conditions optimized. However, this may suggest that both the middle domain and the GED are critical for the intra- and intermolecular interactions, and when lacking one of these domains, the hydrophobic regions that are supposed for the interactions are exposed to solvent and the protein aggregate. Since the GTPase domain itself is a monomer, and the PH-like domain is not essential for the protein oligomerization, our results suggest important roles of the middle domain and the GED in DLP-1 oligmerizations.

The isolated PH-like domain showed a size of about 45 kDa, a tetramer by exclusion chromatography (Fig. 2.5F and Table 2.2). At this point, although we could not exclude the PH-like domain to be involved in the protein oligomerization, the fact that the ΔPH is in stable tetrameric state suggested that the PH-like domain may not be the major determinant of DLP-1 tetramerization. The untouched quaternary protein structure without major damage on the ability of oligomerization of the ΔPH also supports our previous interpretation that inappropriate intramolecular interactions may cause the abolishment of the ΔPH GTPase activity (Fig. 2.4B).

Taken together, our results support the potential roles of the middle domain and the GED in DLP-1 intra- and intermolecular interactions.

2.3.4 *Interactions with Lipids and Membranes* - The dynamins bind to lipids, particularly to negatively charged phospholipids, primarily by their PH domains (Klein, Lee et al. 1998; Lemmon and Ferguson 2000). However, for the dynamin-related proteins, there is no obvious domain or motif indicating a typical PH domain. Usually the regions between the middle domains and the GEDs of dynamin-related proteins are physically analogous to the dynamin PH domain, and these regions also contain large content of positively charged residues that have potential to interact with negatively charged membrane lipids. For dynamin-related proteins, only Arabidopsis dynamin-like protein 2 (ADL2) was reported to bind specially to phosphatidylinositol 4-phosphate (PI(4)P) *in*

vitro without knowing which region is responsible for the binging (Kim, Park et al. 2001). DLP-1 was reported to bind and tubulate membranes (Yoon, Pitts et al. 2001). However, the specificities of the binding and what region(s) is responsible for the binding remain unclear.

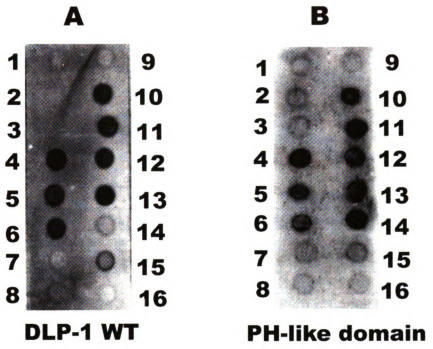

Figure 2.6: Lipids-binding of DLP-1 WT and the PH-like domain. For phospholipids that each number represents, see Tables 2.3.

Table 2.3 A: Illustration of binding strength of DLP-1 WT to phospholipids. "--", no binding; "+", binding. The strength of binding is relative to the control spot (No. 16).

Lipids	Binding	Lipids	Binding
1. Lysophosphatidic acid	--	9. Sphingosine 1-Phosphate	--
2. Lysophophatidylcholine	--	10. PtdIns(3,4)P2	++++
3. Phosphatidylinositol (PtdIns)	--	11. PtdIns(3,5)P2	+++
4. PtdIns(3)P	++++	12. PtdIns(4,5)P2	++
5. PtdIns(4)P	+++	13. PtdIns(3,4,5)P3	++++
6. PtdIns(5)P	+++	14. Phosphatidic acid	+/--
7. Phosphatidylethanolamine	--	15. Phosphatidylserine	+
8. Phosphatidylcholine	--	16. Blank	--

Table 2.3 B: Illustration of binding strength of the PH-like domain to phospholipids. Please refer to **A** for legend.

Lipids	Binding	Lipids	Binding
1. Lysophosphatidic acid	--	9. Sphingosine 1-Phosphate	--
2. Lysophophatidylcholine	--	10. PtdIns(3,4)P2	+++
3. Phosphatidylinositol (PtdIns)	--	11. PtdIns(3,5)P2	++++
4. PtdIns(3)P	++++	12. PtdIns(4,5)P2	++
5. PtdIns(4)P	++	13. PtdIns(3,4,5)P3	++
6. PtdIns(5)P	++	14. Phosphatidic acid	++++
7. Phosphatidylethanolamine	--	15. Phosphatidylserine	+/--
8. Phosphatidylcholine	--	16. Blank	--

Using Fat-Western blot assay, I found that DLP-1 wild type protein bound to free lipids, specifically to negatively charged phospholipids (Fig. 2.6A). The protein bound dominantly to phosphoinositides (PIs) with minor interactions with phosphatidylserine (PS) and phosphatidic acid (PA) (Table 2.3). Different with the ADL2 that the protein bound exclusively to PI(4)P and the dynamins that bound to PI(4,5)P2 specifically,

DLP-1 interacted with all PIs similarly without distinguishable specificities to one or a few of them. Although some reported membrane-interacting proteins seem to bind to specific lipids, binding to PIs without specificities is not uncommon to proteins that interact with membranes (DiNitto, Cronin et al. 2003; Lemmon 2007; Lemmon 2008). For example, the Annexin, epsin N-terminal homology (ENTH), AP180 N-terminal homology (ANTH), Bin/amphiphysin/Rvs (BAR), and Fer-CIP4 homology (F-BAR) domain-containing proteins bind either general acidic phopholipids or PIs without specific preferences (Lemmon 2008). However, research on a number of membrane-binding proteins indicated that, for proteins that bind lipids without specificity, if specificity exists, it could be acquired by induction of specific signals or environments (Lemmon 2008). For example, increase of calcium concentration in cytosol is a signal for some Annexin domain-containing proteins, and curved membrane environments seem to be required for the BAR domain-containing proteins to acquire PIs-binding specificity (Zimmerberg and McLaughlin 2004; Gerke, Creutz et al. 2005; Lemmon 2008). Therefore, non-specific interactions of DLP-1 with PIs do not exclude the possibilities that it binds specifically to one of the PIs at specific mitochondrial fission time or location. Meanwhile, since usually each individual PI is not abundant on the mitochondrial outer membranes, the ability to bind promiscuously to PIs or other acidic phospholipids may provide an advantage for DLP-1 to interact efficiently with membranes. Moreover, during mitochondrial fission events, the PIs may aggregate to specific fission sites to allow membranes recognition by DLP-1. However, lipid binding

does not exclude the possibility that DLP-1 interacts with other molecules such as hFis1 to form division complex onto the mitochondrial outer membranes. It is likely that the interaction of specific (or some non-specific) lipids with protein is necessary for DLP-1 to function properly in the mitochondrial fission process. Also, DLP-1 binding to PIs may serve as a signal to cytosol or to the inner mitochondrial space to further promote mitochondrial fission or other events such as apoptosis. For example, even if the DLP-1 doe not directly provide mechanical force to break the membrane, binding to the membrane may signal other molecules to facilitate the fission events. Generally speaking, our results suggested that DLP-1 may interact with membranes partially, if not totally, by binding acidic phospholipids in general and PIs preferentially.

Using the Fat-Western blot assay, the isolated PH-like domain was found to bind to lipids with a pattern that is similar with that of the wild type DLP-1, mostly to PIs with similar binding strength (Fig. 2.6B and Table 2.3). These results, to some extent, indicate that the PH-like domain may facilitate the interactions of DLP-1 with membranes, which is consistent with the three-dimensional structure of dynamin from cryo-electron micrographs that the PH domain is oriented to face the membrane directly (Zhang and Hinshaw 2001).

Although contains large content of positively charged residues, the protein sequence of the DLP-1 PH-like domain was not found to be conserved when aligned with other dyanmin-related proteins. This may suggest that function of the PH-like domains of dynamin-related proteins may not be limited to binding to membranes. They could have

evolved and acquired other functions, possibly interacting with specific proteins to facilitate the formation of protein complexes. This phenomenon is commonly observed for some lipids-bind domains such as the ENTH, ANTH, BAR, and F-BAR, which demonstrate inconspicuous preferences to specific acidic phospholipids, but are involved in other cellular functions such as curving or deforming membranes (Itoh and De Camilli 2006; Lemmon 2008). Also, the PH domain-containing proteins often have protein interacting domains such as Src homology 2, 3 (SH2, SH3) to strengthen membrane binding by interacting with other protein molecules (Schlessinger 2000). Since there is no such a domain predicted or identified in the DLP-1, the PH-like domain may be bi- or multifunctional to involve in both membranes and protein interactions.

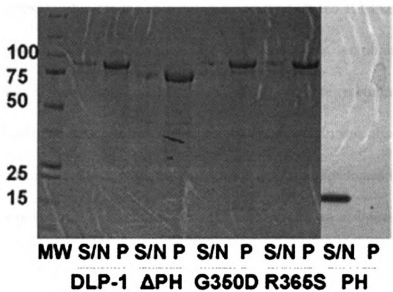

Figure 2.7: Liposome-binding of DLP-1 WT and mutants. The liposomes used in the assay were made from DOPS (see text). S/N refers to the supernatant fraction and P to the pellet.

DLP-1 has been reported to bind and tubulate lipid membranes in liposome-binding assays (Yoon, Pitts et al. 2001). I investigated whether the mutant DLP-1 species impaired the liposome-binding properties by using this assay, since liposome vesicles are good approximation of the lipid membrane structure (DiNitto, Cronin et al. 2003). The results showed that the G350D, the R365S, and the ΔPH were dominantly fractionated in the pellets as wild type DLP-1 was (Fig. 2.7), indicating that the mutations did not cause significant changes on the protein liposome-binding properties. Since these mutants also retained proper oligomeric states (Fig. 2.4), it is likely that the tetrameric structure is one of the factors required for the membranes binding. Interestingly, ΔPH still bound liposomes, indicating that besides the PH-like domain, there must be other regions in DLP-1 also are responsible for the membrane association. If the PH-like domain alone binds too weakly to lipids to drive DLP-1 to membranes, combination of other lipids-interacting regions would help cooperatively promote membranes targeting. Unexpectedly, although bound to free lipids, the PH-like domain was almost exclusively fractionated in the supernatant, indicating that it did not bind liposomes (Fig. 2.7). This contradictory results could be explained by the unique structures of liposomes that more approximate *in vivo* membrane structures than free lipids do, and the PH-like domain may need specific structural scaffolds which is provided by other domains of DLP-1 to interact with membranes. Unlike the free lipids, the membrane surface is usually curved and global which may only be associated by specific protein structures. *In vivo*, the PH-like domain may be oriented the way that one side interacts with membranes and

another side with other protein molecules. For the wild type protein, other domains may help drive membranes associations by both interacting with membranes themselves and stabilizing the PH-like domain orientation to enhance the binding. However, for isolated PH-like domain, although has lipids-interacting abilities, without other domains' support as scaffolds, the membranes interactions may not be stable given the fact that the binding may be weak or non-specific.

Taken together, the results suggested that other than the PH-like domain, DLP-1 may contain more membrane-interacting regions, and these regions may also function as a scaffold for supporting and orienting the PH-like domain for appropriate membrane targeting and protein interactions.

2.4 Conclusion

The biochemical and structural properties of recombinant full-length DLP-1 and selected mutants have been studied. The DLP-1 WT, G350D, R365S, ΔPH, GTPase domain, and PH-like domain were expressed in *E. coli* and purified to near homogeneity by a number of protein purification tools including Ni-NTA column, ion exchange, and analytical gel filtration chromatography. GTPase activity, oligomeric state, and lipid-binding properties of appropriate DLP-1 species were investigated.

Compared to the full-length DLP-1, the isolated GTPase domain exhibited a relatively lower GTPase activity, suggesting a role of the C-terminus of DLP-1 probably the GED in the full GTPase activity. The G350D and R365S mutants in the middle domain

severely impair the GTPase activity, but have no significant effects on the protein oligomeric state, indicating that these two mutations interrupted the intramolecular but not intermolecular interactions, and therefore, the middle domain of DLP-1 is important for the protein activity probably by facilitating appropriate connections between the GTPase domain and the GED.

Size exclusion chromatography showed that deletion of the PH-like domain has no significant effects on protein oligomeric state. Together with the results that the isolated GTPase is a monomer, this indicated that the GTPase domain and the PH-like domain may not be major determinants of DLP-1 tetramerization, further suggesting important roles of the middle domain and the GED in protein intermolecular interactions.

The DLP-1 and the isolated PH-like domain bound free phosphoinositides suggesting that DLP-1 may interact with membranes directly by binding acidic phospholipids preferentially phosphoinositides, and the PH-like domain may be responsible for the interactions. Although GTPase activity abolished, the ΔPH bound to liposomes suggesting in addition to the PH-like domain, other regions of DLP-1 may function as lipids-interacting enhancer as well as scaffolds for orienting the PH-like domain into appropriate membrane targeting.

References

Arechaga, I., B. Miroux, S. Karrasch, R. Huijbregts, B. de Kruijff, M. J. Runswick and J. E. Walker (2000). "Characterisation of new intracellular membranes in Escherichia coli accompanying large scale over-production of the b subunit of F1Fo ATP synthase." Febs Letters **482**(3): 215-219.

Barylko, B., D. Binns, K. M. Lin, M. A. Atkinson, D. M. Jameson, H. L. Yin and J. P. Albanesi (1998). "Synergistic activation of dynamin GTPase by Grb2 and phosphoinositides." J Biol Chem **273**(6): 3791-7.

Bhar, D., M. A. Karren, M. Babst and J. M. Shaw (2006). "Dimeric Dnm1-G385D interacts with mdv1 on mitochondria and can be stimulated to assemble into fission complexes containing Mdv1 and Fis1." Journal of Biological Chemistry **281**(25): 17312-17320.

Bridges, A., L. Gruenke, Y. T. Chang, I. A. Vakser, G. Loew and L. Waskell (1998). "Identification of the binding site on cytochrome P450 2B4 for cytochrome b5 and cytochrome P450 reductase." J Biol Chem **273**(27): 17036-49.

Danino, D. and J. E. Hinshaw (2001). "Dynamin family of mechanoenzymes." Curr Opin Cell Biol **13**(4): 454-60.

DiNitto, J. P., T. C. Cronin and D. G. Lambright (2003). "Membrane recognition and targeting by lipid-binding domains." Sci STKE **2003**(213): re16.

Fukushima, N. H., E. Brisch, B. R. Keegan, W. Bleazard and J. M. Shaw (2001). "The GTPase effector domain sequence of the Dnm1p GTPase regulates self-assembly and controls a rate-limiting step in mitochondrial fission." Mol Biol Cell **12**(9): 2756-66.

Gerke, V., C. E. Creutz and S. E. Moss (2005). "Annexins: linking Ca2+ signalling to membrane dynamics." Nat Rev Mol Cell Biol **6**(6): 449-61.

Ingerman, E., E. M. Perkins, M. Marino, J. A. Mears, J. M. McCaffery, J. E. Hinshaw and J. Nunnari (2005). "Dnm1 forms spirals that are structurally tailored to fit mitochondria." Journal of Cell Biology **170**(7): 1021-1027.

Itoh, T. and P. De Camilli (2006). "BAR, F-BAR (EFC) and ENTH/ANTH domains in the regulation of membrane-cytosol interfaces and membrane curvature." Biochim Biophys Acta **1761**(8): 897-912.

Kim, Y. W., D. S. Park, S. C. Park, S. H. Kim, G. W. Cheong and I. Hwang (2001). "Arabidopsis dynamin-like 2 that binds specifically to phosphatidylinositol 4-phosphate assembles into a high-molecular weight complex in vivo and in vitro." Plant Physiology **127**(3): 1243-1255.

Klein, D. E., A. Lee, D. W. Frank, M. S. Marks and M. A. Lemmon (1998). "The pleckstrin homology domains of dynamin isoforms require oligomerization for high affinity phosphoinositide binding." Journal of Biological Chemistry **273**(42): 27725-27733.

Lemmon, M. A. (2007). "Pleckstrin homology (PH) domains and phosphoinositides." Biochem Soc Symp(74): 81-93.

Lemmon, M. A. (2008). "Membrane recognition by phospholipid-binding domains." Nat Rev Mol Cell Biol **9**(2): 99-111.

Lemmon, M. A. and K. M. Ferguson (2000). "Signal-dependent membrane targeting by pleckstrin homology (PH) domains." Biochemical Journal **350**: 1-18.

Miroux, B. and J. E. Walker (1996). "Over-production of proteins in Escherichia coli: Mutant hosts that allow synthesis of some membrane proteins and globular proteins at high levels." Journal of Molecular Biology **260**(3): 289-298.

Muhlberg, A. B., D. E. Warnock and S. L. Schmid (1997). "Domain structure and intramolecular regulation of dynamin GTPase." Embo J **16**(22): 6676-83.

Niemann, H. H., M. L. Knetsch, A. Scherer, D. J. Manstein and F. J. Kull (2001). "Crystal structure of a dynamin GTPase domain in both nucleotide-free and GDP-bound forms." Embo J **20**(21): 5813-21.

Praefcke, G. J. and H. T. McMahon (2004). "The dynamin superfamily: universal membrane tubulation and fission molecules?" Nat Rev Mol Cell Biol **5**(2): 133-47.

Prakash, B., G. J. Praefcke, L. Renault, A. Wittinghofer and C. Herrmann (2000). "Structure of human guanylate-binding protein 1 representing a unique class of GTP-binding proteins." Nature **403**(6769): 567-71.

Prakash, B., L. Renault, G. J. Praefcke, C. Herrmann and A. Wittinghofer (2000). "Triphosphate structure of guanylate-binding protein 1 and implications for nucleotide binding and GTPase mechanism." Embo J **19**(17): 4555-64.

Ramachandran, R., M. Surka, J. S. Chappie, D. M. Fowler, T. R. Foss, B. D. Song and S. L. Schmid (2007). "The dynamin middle domain is critical for tetramerization and higher-order self-assembly." Embo Journal **26**(2): 559-566.

Reubold, T. F., S. Eschenburg, A. Becker, M. Leonard, S. L. Schmid, R. B. Vallee, F. J. Kull and D. J. Manstein (2005). "Crystal structure of the GTPase domain of rat dynamin 1." Proc Natl Acad Sci U S A **102**(37): 13093-8.

Schlessinger, J. (2000). "Cell signaling by receptor tyrosine kinases." Cell **103**(2): 211-25.

Sever, S., A. B. Muhlberg and S. L. Schmid (1999). "Impairment of dynamin's GAP domain stimulates receptor-mediated endocytosis." Nature **398**(6727): 481-6.

Shin, H. W., H. Takatsu, H. Mukai, E. Munekata, K. Murakami and K. Nakayama (1999). "Intermolecular and interdomain interactions of a dynamin-related GTP-binding protein, Dnm1p/Vps1p-like protein." J Biol Chem **274**(5): 2780-5.

Shin, H. W., H. Takatsu, H. Mukai, E. Munekata, K. Murakami and K. Nakayama (1999). "Intermolecular and interdomain interactions of a dynamin-related GTP-binding protein, Dnm1p/Vps1p-like protein." Journal of Biological Chemistry **274**(5): 2780-5.

Smirnova, E., D. L. Shurland, E. D. Newman-Smith, B. Pishvaee and A. M. van der Bliek (1999). "A model for dynamin self-assembly based on binding between three different protein domains." J Biol Chem **274**(21): 14942-7.

Stowell, M. H., B. Marks, P. Wigge and H. T. McMahon (1999). "Nucleotide-dependent conformational changes in dynamin: evidence for a mechanochemical molecular spring." Nat Cell Biol **1**(1): 27-32.

Warnock, D. E., J. E. Hinshaw and S. L. Schmid (1996). "Dynamin self-assembly stimulates its GTPase activity." J Biol Chem **271**(37): 22310-4.

Yoon, Y., K. R. Pitts and M. A. McNiven (2001). "Mammalian dynamin-like protein DLP1 tubulates membranes." Molecular Biology of the Cell **12**(9): 2894-2905.

Zhang, P. and J. E. Hinshaw (2001). "Three-dimensional reconstruction of dynamin in the constricted state." Nat Cell Biol **3**(10): 922-6.

Zhu, P. P., A. Patterson, J. Stadler, D. P. Seeburg, M. Sheng and C. Blackstone (2004).

"Intra- and intermolecular domain interactions of the C-terminal GTPase effector domain of the multimeric dynamin-like GTPase Drp1." Journal of Biological Chemistry **279**(34): 35967-35974.

Zimmerberg, J. and S. McLaughlin (2004). "Membrane curvature: how BAR domains bend bilayers." Curr Biol **14**(6): R250-2.

CHAPTER 3

Structural studies of DLP-1 and MFN-1

3.1 Introduction

Structural studies on DLP-1 and MFNs, particularly X-ray crystal structure determinations at high resolution, would provide a physical foundation for functions of these proteins, shed light on the molecular mechanisms of mitochondrial fission and fusion, and help understand some human diseases caused by mitochondria-related defects. One of the rate-limiting steps in structural biology is protein crystallization. Depending on a protein's physical nature, some proteins are relatively easy to crystallize, while, some others, such as large and complex proteins from higher organisms, are much more challenging for crystallographer. For membrane-interacting proteins, particularly integral membrane proteins, other factors such as protein expression and purification may also become rate-limiting steps for structural studies instead of the crystallization. This situation arises from the fact that membrane-interacting proteins contain hydrophobic transmembrane or membrane-interacting regions, which can interfere with folding and assembly during expression. Molecular protein engineering sometimes is a helpful tool bypassing these problems and increasing the chance of protein crystallization.

In this chapter, I will describe structural studies of DLP-1 and MFNs from the protein expression and purification through crystallization trials. Molecular engineering methods for protein crystallization enhancement are also addressed.

3.2 Crystallization trials of DLP-1

The DNA cloning, protein expression, and purification procedures of wild type DLP-1 were as described in chapter 2. Fractions of the tetrameric size of DLP-1 by size exclusion chromatography were collected and concentrated to about 10 mg/mL with a

50K Amicon Ultra centrifugal unit (Millipore) for crystallization studies. Initially, Microbatch-under-oil method with an ORYX-4 crystallization robot (Douglas Instruments) was used. With a total of at least 864 screening conditions (Hampton Research I & II, Membrane Faction I & II, Lite Screen I & II, Cryo Screens I & II, Wizard Screens I & II, Axygen Biosciences I, III, IV, & V) together with about 200 other grid screens designed by myself, 0.75 μL of purified protein and 0.75 μL precipitant reagent were mixed in each drop for crystallization.

Microbatch and hanging drop vapor diffusion are quite different methods that could lead to different patterns of crystallization results. A report that compared the two methods has shown that about 60 percent of crystals generated by the two methods have overlapped conditions, while the other 40 percent are from unique conditions (Chayen 1998). In other words, crystals grow from one method may not show up in the same condition by the other method. Therefore, hanging drop vapor diffusion was also used with the above crystallization conditions for DLP-1. Two μL of protein and 2 μL of precipitant were mixed to equilibrate against 1 mL reservoir solution.

The hGBP1 was crystallized with protein concentrations of 50-100 mg/mL (Prakash, Praefcke et al. 2000; Prakash, Renault et al. 2000) and is the only eukaryotic member in dynamin superfamily that has full-length protein crystal structure available for reference. Since DLP-1 may structurally analogous to hGBP1, protein concentration of DLP-1 was adjusted from 10 mg/mL to up to 50 mg/mL for crystallization. There was no obvious decrease of protein solubility observed in most conditions. Also, since in about 40 percent of conditions, the protein was precipitated, decreasing protein concentration to up to 2 mg/mL was attempted. The protein solubility was improved slightly with low protein

concentration.

The GTPase domain of DLP-1 contains the four conserved GTP-binding motifs. Previous structures of dynamins GTPase domains (Niemann, Knetsch et al. 2001; Reubold, Eschenburg et al. 2005) and hGBP1 (Prakash, Renault et al. 2000) indicated that the GTP/GDP binding region may be flexible if without ligands on. After GTP/GDP binding, the region is highly organized and ordered. This flexible region without ligands binding may be one of the energy barriers that hinder the protein crystallization. Thus, co-crystallization of DLP-1 with 1 mM GDP was performed. Also, since GTP is not stable substrate (which will be hydrolyzed to GDP), GTP analogues such as GppNHp were used for co-crystallization. Although proteins in the dynamin family do not require guanine nucleotide to maintain stability (unlike canonical small GTPases), I expected that binding of GDP or GTP analogues could cause a conformational change that help maintain an ordered local structure or generate new crystal contacts. Unfortunately, with all these attempts, to date, no reproducible crystals of DLP-1 protein have yet been obtained.

3.3 Protein engineering methods for crystallization enhancement

3.3.1 General introduction and rationale

It is a challenge to crystallize large complex proteins, particularly membrane-interacting proteins from higher organisms like humans, because these proteins usually contain multiple structurally independent regions or relatively flexible domains that need to interact with unknown molecular partners *in vivo*. This complexity may give rise to an energy barrier to prevent protein from forming highly ordered and aggregated crystals.

However, molecular protein engineering may help reduce this complexity and increase the chance of crystallization. With other factors such as precipitant reagents fixed, protein itself could serve as a variant in crystallization process (Dale, Oefner et al. 2003). Since the wild type DLP-1 has not yet crystallized by varying simply the solution conditions, protein engineering was performed in an effort to enhance protein crystallization.

3.3.1.1 Limited proteolysis

Large proteins from higher organisms such as plants or humans usually are composed of multiple functional regions (domains). The individual domains are relatively compact, but the whole protein is heterogeneous because of motions between domains caused by flexible domain linkers. This conformational heterogeneity often results in difficulties in protein crystallization (Koth, Orlicky et al. 2003). To solve this problem, it is effective to identify stable and crystallizable functional domains of such proteins. The challenge in this work is to identify the domain boundaries (Koth, Orlicky et al. 2003). Multiple sequence alignments and secondary structure prediction are among the ways for identifying individual domains. However, a more promising method is limited proteolysis followed by mass spectrometry and N-terminal sequencing. The rationale for limited proteolysis is that the domain-domain connection regions are highly exposed to solvents and can be recognized easier by proteases than regions within a compact domain (Koth, Orlicky et al. 2003).

3.3.1.2 Surface-entropy reduction

The basis of the surface-entropy reduction method is to reduce the entropic cost of protein crystallization by modifying the target protein using molecular protein engineering. Typically, residues with large flexible side chains in solvent-exposed loops are mutated to small amino acids (Derewenda and Vekilov 2006). For instance, highly hydrophilic residues in loop regions such as lysine or glutamate will be replaced by less hydrophilic amino acids such as alanine. Sometimes, flexible protein regions with a high degree of conformational heterogeneity have a higher entropic state and a lower propensity for crystallization. Thus, deleting or replacing the flexible regions may be helpful strategy for crystallization as it would reduce the interfering effects of the heterogeneity (Dale, Oefner et al. 2003; Schwartz, Walczak et al. 2004; Kim, Dobransky et al. 2005).

3.3.1.3 Large fusion partners as protein expression and crystallization enhancer

Large fusion tags such as maltose-binding protein (MBP) and glutathione-S-transferase (GST) have been proven to enhance the expression, improve the yield and stability, and facilitate purification of the proteins to which they are fused (Sachdev and Chirgwin 2000; Skerra and Schmidt 2000; Smith 2000). Recently, several protein crystal structures have been reported as fusion proteins (Kobe, Center et al. 1999; Liu, Manna et al. 2001; Ke, Mathias et al. 2002). The target proteins were fused in the C-terminus of *E. coli* MBP and the whole fusion proteins were used for crystallization without cleaving off the MBP. With a modified linker between the MBP and the proteins of interest, the presence of the MBP did not interfere with the native structures of the target proteins, as indicated by the

crystal structures. Several advantages of co-crystallizing a protein with fusion partner have been recognized. First, large fusion tags such as MBP enhance solubility and stability of target proteins by avoiding formation of inclusion bodies in *E. coli*. Second, since the crystal contacts of the fusion proteins are dominated by MBP/MBP or MBP/protein interactions as indicated by the crystal structures, the fusion partner could facilitate crystallization by increasing those contacts. Third, the conditions used to crystallize the native MBP and the crystal contacts found in the native MBP crystals may be used to guide the crystallization of the fusion protein. Last, but not least, the three-dimensional structure of MBP can be used as a search model to solve the crystallographic phase problem by molecular replacement.

One challenging aspect of co-crystallizing fusion proteins is modification of the linker between the tag and the target protein. The characteristic that is shared by most successfully crystallized fusion proteins is a short rigid connection such as three alanines, instead of a long flexible linker. Shorter linkers may help avoid the conformational heterogeneity introduced by flexible linkers. Since most proteins that crystallized by fusion protein method are around or less than 10 kDa, there may be a size limitation of co-crystallization with MBP. It is possible that the larger volume occupied by a large target proteins may interfere with any crystal contacts made by MBP.

An alternative large fusion tag is the monomeric DsRed (Invitrogen), which is an engineered mutant of a red fluorescent protein from Discosoma sp. reef coral. The tetrameric form of native DsRed is not a suitable crystallization carrier because fusion with an oligomeric tag may result in a chimera protein with a non-native quaternary structure of the target protein. However, monomeric form of an engineered DsRed is less

likely to affect the native quaternary structure of the target protein. A significant advantage of DsRed is that the red color of the fusion protein can be visualized directly, so that the protein expression and purification process can easily be monitored. Moreover, the red color can also be used as an indicator to differentiate the protein crystals from those of salts, which is a common problem associated with crystallization microbatch evaporation method.

3.4 Experimental procedures, results, and discussion on DLP-1

3.4.1 Fragments construction

If full-length proteins have problems on expression or crystallization, a traditional approach is to investigate the individual protein domains. Usually single domains or domain combinations are more readily expressed and crystallized, given the fact that they do not have the heterogeneity caused by motion between domains as in full-length proteins. Crystal structures of single domains or domain combinations of a protein can also give useful information on protein functional mechanisms. To determine the domain boundaries, combined with previous literature, secondary structure prediction and sequence alignments were used to ensure that conserved regions and secondary structures around domain boundaries are not interrupted.

3.4.1.1 Secondary structure prediction

Protein sequence was analyzed online by PSI-PRED and SABLE protein secondary structure predication severs, and the predictions were compared visually (Fig. 3.1). The GTPase domain of DLP-1 is consisted of combinations of helices and strands which is consistent with previous crystal structures of other dynamin GTPase domains (Prakash,

Renault et al. 2000; Niemann, Knetsch et al. 2001; Reubold, Eschenburg et al. 2005). After the GTPase domain, the structure appeared to consist of a collection of helices connected by loops. The middle and the GED domains are comprised of consecutive long helices which may needed for the intra- or intermolecular interactions. The PH-like domain does not contain specific secondary structures but only loops connected by two short helices, which indicate that it may be structurally disordered.

3.4.1.2 Sequence alignments

The protein sequences of *Apis mellifera* dynamin-like protein, *Caenorhabditis elegans* dynamin-like protein, *Homo sapiens* dynamin-like protein, and *Saccharomyces cerevisiae* dynamin-like protein were analyzed online by T-Coffee multiple sequence alignment serve, and the results were visualized by the ESPript server. The GTPase domain, the middle domain, and the GED are very conserved over the four species (Fig. 3.2). However, no conservation was found in the PH-like domain, again suggesting that this region may be flexible.

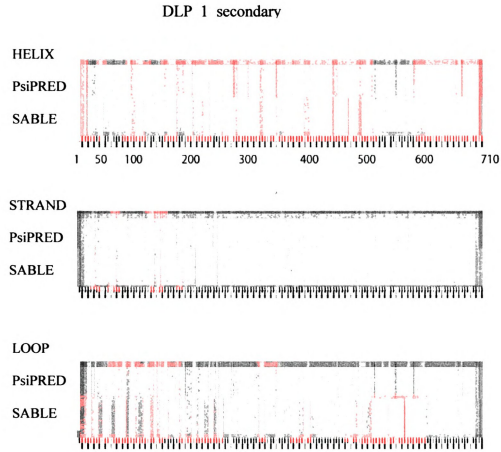

Figure 3.1: Comparison of secondary structure predictions of DLP-1 from PSI-PRED and SABLE severs by visualizing the predictions. Sequence numbers are indicated below HELIX comparison. Red color, high possibility of being an indicated as secondary structure; Blue color, low possibility of being an indicated as secondary structure. Other colors, possibility between indicated by the red and blue colors.

Figure 3.2: Multiple-sequence alignments of DLP-1. Am DLP-1, *Apis mellifera* dynamin-like protein; Ce DLP-1, *Caenorhabditis elegans* dynamin-like protein; Hs DLP-1, *Homo sapiens* dynamin-like protein; Sc DNM-1, *Saccharomyces cerevisiae* dynamin-like protein; These sequence alignments were generated by using T-Coffee and ESPript severs.

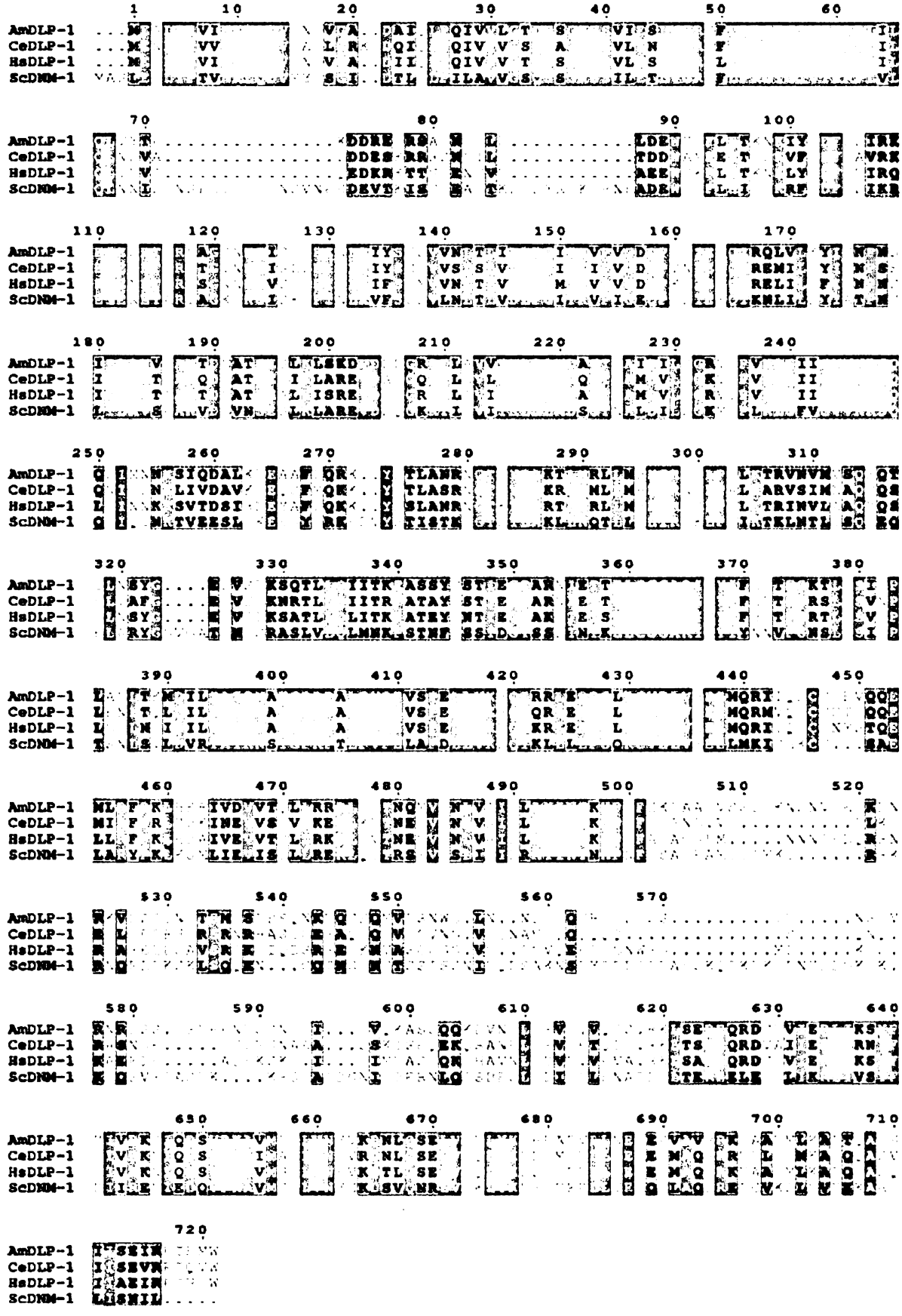
AmDLP-1
CeDLP-1
HsDLP-1
ScDNM-1

3.4.1.3 Protein expression and purification

Based on the secondary structure predictions and the multiple sequence alignments, several fragments of DLP-1 were cloned into pLW01 vector and expressed in *E. coli*. These fragments are: the GTPase domain 1 (1-307aa), the GTPase domain 2 (1-323 aa), the GTPase domain 3 (1-340 aa), the PH-like domain 1 (PH1, 497-602 aa), the PH-like domain 2 (PH2, 523-602 aa), the GTPase + Middle domain (1-500 aa), the Middle + PH-like domain + GED (330-710 aa), and the PH-like domain + GED (500-710 aa) (Fig. 3.3). The cloning, expression, and purification procedures are as described for DLP-1 full-length protein. The isolated GTPase domain 1, 2, 3, the PH1, and 2, were expressed and exhibited high or moderate solubility. However, other fragments were found exclusively in the low-speed pellets during purification, presumably inclusion bodies, in spite of various growth conditions. Attempts of solubilizing some of these fragments using denaturants from inclusion bodies failed.

Among the three isolated GTPase domain fragments, only the 1-307aa forms stable monomers (see chapter 2), while the other two fragments aggregate as measured by gel filtration. As discussed in chapter 2, the region from residue 308 to 340 of DLP-1 may be involve in the formation of helices bundle in the middle domain and inclusion of these residues into the isolated GTPase domain may cause the hydrophobic regions exposed to solvents and lead to protein aggregation.

3.4.1.4 Crystallization

Both PH-like domain fragments forms stable tetramers and remain soluble even concentrated to 50 mg/mL. Crystallization of the GTPase domain 1 and the PH-like

domain 1 and 2 were performed with procedures described before. However, no crystals have been obtained, to date.

3.4.2 Limited proteolysis

Since DLP-1 contains multiple domains, and the full-length protein failed to crystallize, limited proteolysis is applicable to this protein. The fastest way to perform limited proteolysis is the in-drop proteolysis (Gaur, Kupper et al. 2004; Johnson, Roversi et al. 2006). Different kinds of proteases such as trypsin, chymotrypsin, papain, and proteinase K were added to the solution containing the purified full-length protein before crystallization screening. Ideally, if there are crystals grown from the drops, they will be re-solubilized and subjected to N-terminal sequencing and mass spectrometry for sequence determination (Gaur, Kupper et al. 2004). However, there was no crystal observed from any screening conditions. Although the in-drop method is easy to manipulate, one of its disadvantages is that the heterogeneity resulting from the presence of other digested fragments may inhibit crystallization. Therefore, larger-scale limited proteolysis is necessary.

With larger-scale limited proteolysis, the full-length DLP-1 was digested with the proteases listed above for up to 8 hrs. At each time point, digested products were sampled for SDS-PAGE (Fig. 3.4). A common proteases-resistant band of about 50 kDa was observed from the SDS-PAGE indicating that this fragment may be a compact individual domain or domains combination. The protein band was transferred by electroboltting to PVDF membrane and sent for N-terminal sequencing. The final digested product was mixed with formic acid for mass determination using mass spectrometry.

The N-terminal sequencing showed that the first five amino acids of the fragment are ENGVE which starts from the residue number 82 of the protein. The mass spectrometry obtained a major peak of about 49 kDa (Fig. 3.5). Combined with both sequencing and mass results, the fragment was identified to be from residue 82 to 516. The N-terminus is around the second motif of the GTPase domain and the C-terminus is in the beginning of the PH-like domain. Both regions may be flexible and solvent exposed such that they are easily accessed by proteases.

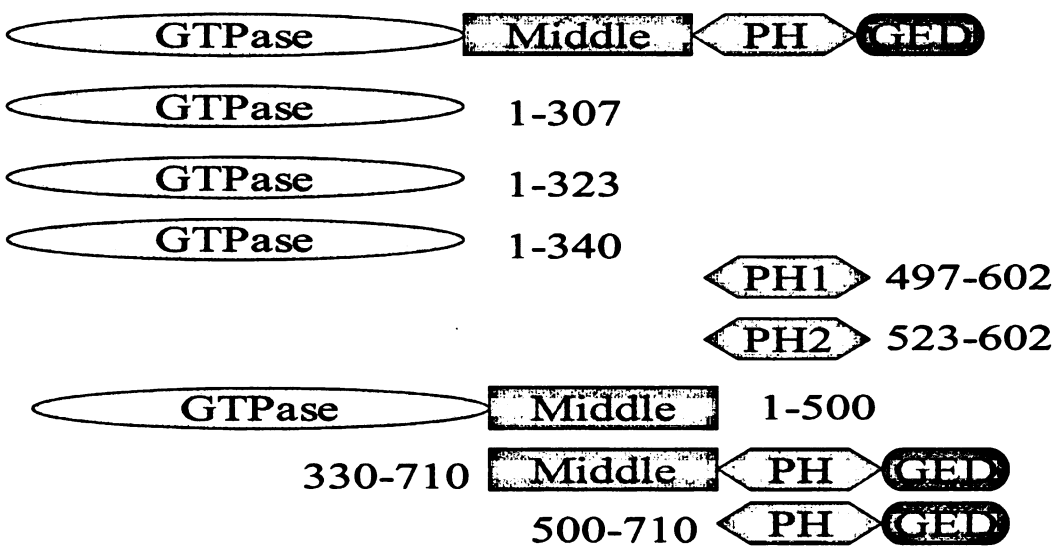

Figure 3.3: Schematic illustration of DLP-1 constructs.

The identified fragment was cloned into pLW01 expression vector and recombinant expressed in *E. coli* BL21 (DE3) cells as described for wild type DLP-1 and other fragments previously. Since the N-terminus of the fragment starts from the middle of the GTPase domain, truncation of the GTPase domain may destroy the protein structure. Therefore, another fragment encoding residues from 1 to 516, which includes the entire

GTPase domain, was also cloned. However, both fragments were expressed in inclusion bodies in regardless of application of methods to lower the protein synthesis rate during expression.

One possible reason that these fragments are not soluble may be the disruption of the intra- and intermolecular interactions. It is purported that the GED folds back to interact with the middle domain; the results from chapter 2 support this idea. The cleavage in the flexible PH-like domain removed all the C-terminus including the GED. Therefore, the middle domain could no longer interact with the GED, leading to disrupted intra- and intermolecular interactions and an increased exposure of the hydrophobic regions of the middle domain. It is necessary to consider a way to balance the maintenance of critical interactions, while removing some protein flexibility.

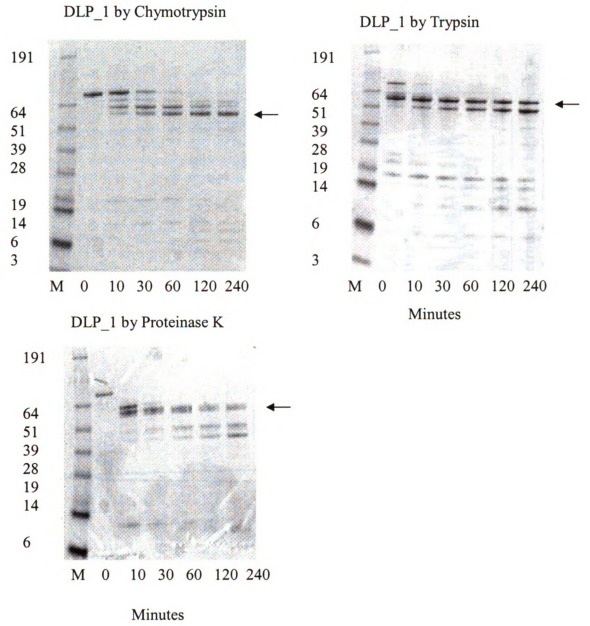

Figure 3.4: SDS-PAGE analysis of Limited proteolysis of DLP-1 by different proteases. Purified DLP-1 and protease were incubated at room temperature at a ratio of 1000:1 (w:w). The reaction was stopped at each time points by adding PMSF. Proteolytic products were resolved by SDS-PAGE. Arrows indicate similar size of proteolytic products.

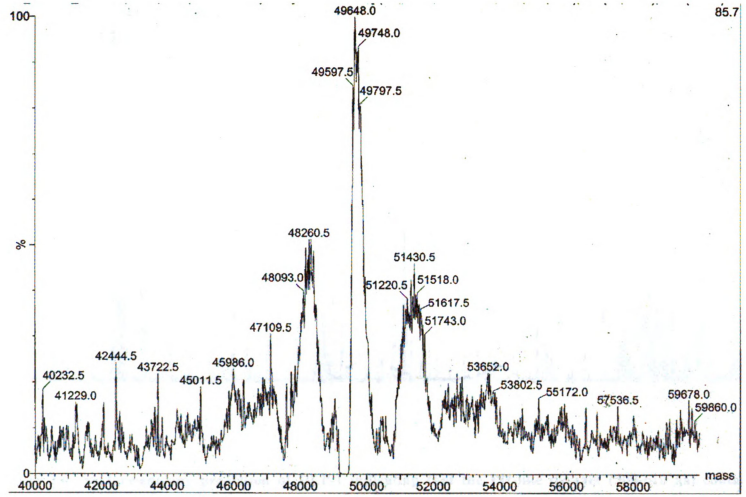

Figure 3.5: Mass determination of the DLP-1 proteolytic fragment by mass spectrometry. The highest peak in the middle shows a size of about 49 kDa, indicating the size of the protease-resistant fragment.

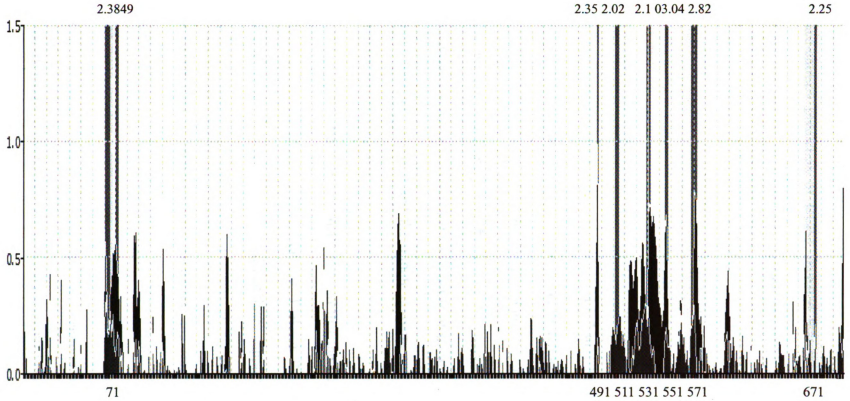

Figure 3.6: Surface-entropy prediction of DLP-1 indicating that the PH-like domain (500-610 aa) contains many residue clusters with high conformational entropy (green lines). X-axis, residue numbers of DLP-1; Y-axis, the side chain entropy scores for each residue. Green lines indicate high entropy clusters that are candidates for mutation to low entropy residues to aid in crystallization. This prediction was generated using Surface Entropy Reduction Prediction Sever (http://nihserver.mbi.ucla.edu/SER/).

3.4.3 Surface-entropy reduction

Surface-entropy prediction of DLP-1 revealed that the high ratio of charged and flexible residue clusters in the PH-like domain causes high surface entropy (Fig. 3.6). Secondary structure predictions showed that the PH-like domain does not have a regular secondary structure and probably forms a large solvent-exposed loop (Fig. 3.1). Sequence comparison of DLP-1 with the crystallized hGBP1 showed that hGBP1 lacks the PH-like domain between the conserved middle domain and the GED (data not shown). These analyses indicated that the PH-like domain of DLP-1 may be highly flexible causing an energy barrier for crystal formation. Therefore, combined with the previous limited proteolysis results, replacement of the PH-like domain with a shorter, but less mobile linker by protein engineering may be a way to enhance the likelihood of DLP-1 crystallization. Whatever our designed construct is, it should capture the domain-domain interactions between the GED and the middle domain, and the GED and the GTPase domain in the crystal structure.

The X-ray crystal structure of hGBP1 showed that the GED forms a long helix and interacts with the middle and GTPase domain (Prakash, Praefcke et al. 2000; Prakash, Renault et al. 2000). For DLP-1, biochemical analyses supported these interactions (Shin, Takatsu et al. 1999; Zhu, Patterson et al. 2004). If the PH-like domain of DLP-1 is a flexible region that is recognized by proteases, the fragments obtained by limited proteolysis method would likely to be the GTPase domain plus the middle domain, and the GED alone, but not a combination of both. Therefore, replacing the PH-like domain of DLP-1 may be the best way to enhance the likelihood of crystallization as well as obtain the structural information of the domain-domain interactions particularly that of

the middle domain and the GED. Furthermore, once the domain interactions are met, it is also possible to reduce the formation of inclusion bodies as described for the limited proteolysis fragment.

The DLP-1 ΔPH was designed, cloned, expressed, and purified, as described in chapter 2. The protein was less soluble *in vivo* than the wild type mainly because of lacking of the hydrophilic PH-like domain. The solubility problem was solved by expressing the protein at low temperature (18 °C) and low IPTG (0.02 mM) induction. At least 1 mg purified protein was obtained after the final step of purification from 1 L bacterial culture. However, no crystals have yet been observed with the screening conditions as described above.

Figure 3.7: Illustration of designed RMG series expression vectors. (A) pRMG-*pfu*MBP; (B) pRMG-*pfu*MBP-c2X; (C) pRMG_*eco*MBP; (D) pRMG_DsRed_M.

Figure 3.7 continued

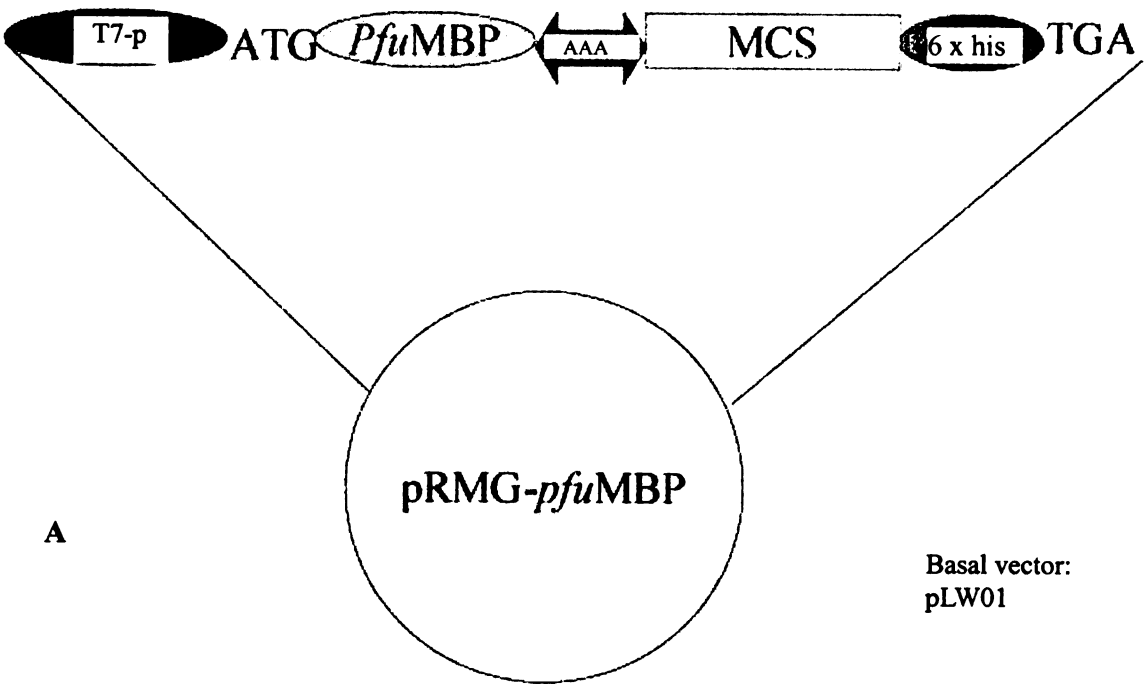

A

Basal vector:
pLW01

Figure 3.7 continued

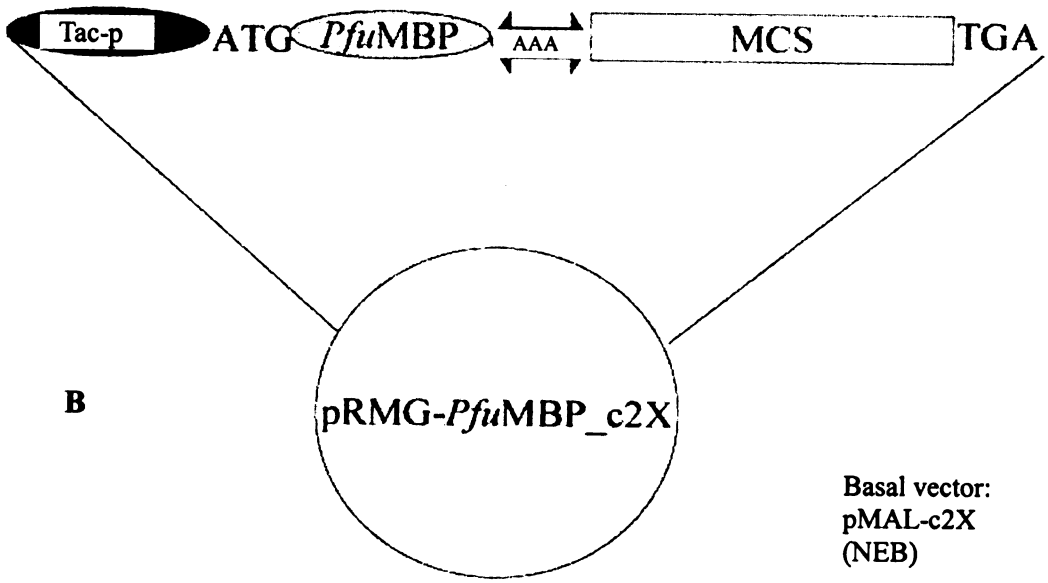

Figure 3.7 continued

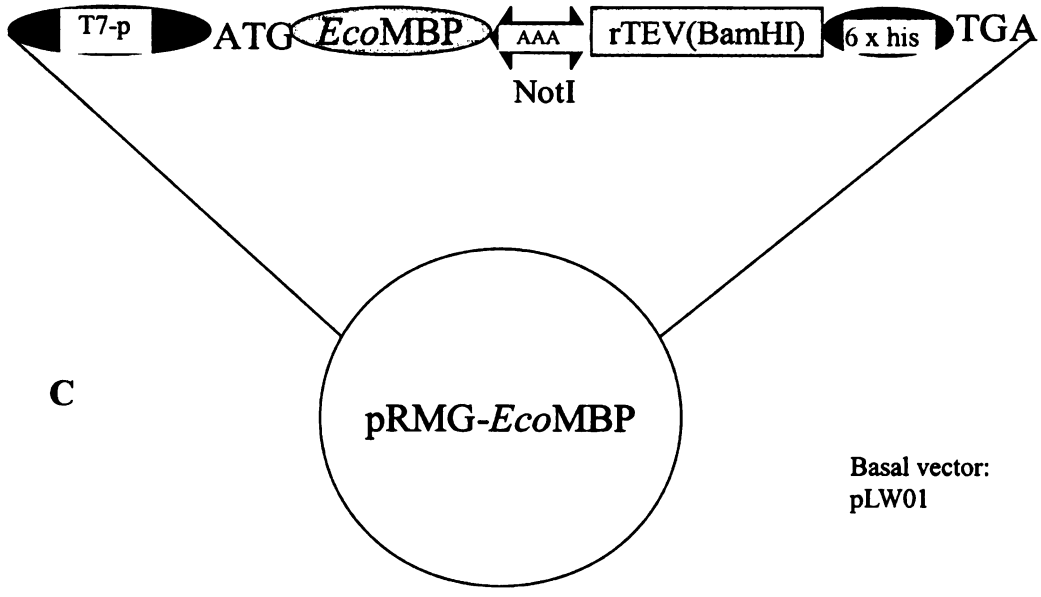

Figure 3.7 continued

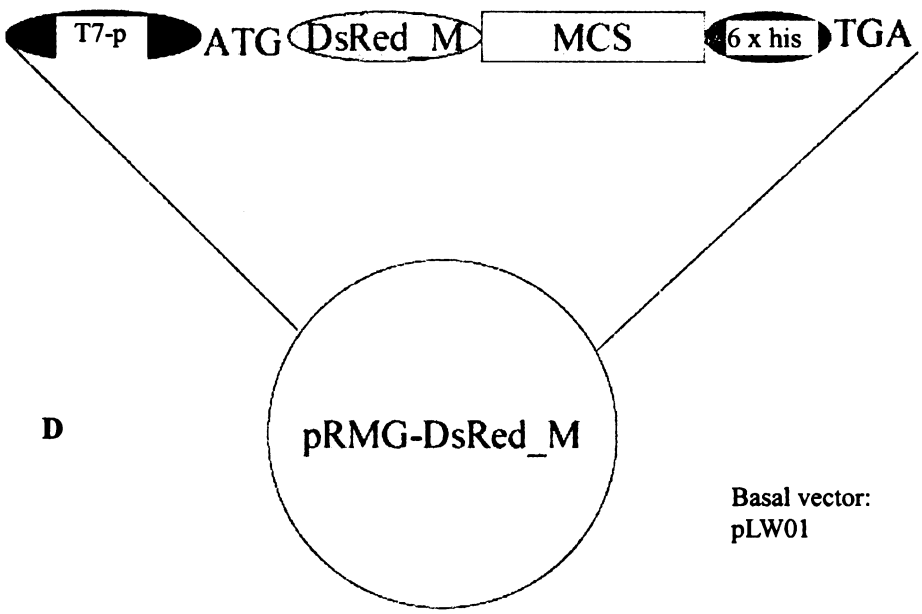

3.4.4 Fusion proteins for crystallization aids

3.4.4.1 Development of expression vectors for P. furiosus MBP

The *Pyrococcus furiosus* (*pfu*) MBP was showed to be a more efficient solubilizing partner than the *E. coli* MBP (Fox, Routzahn et al. 2003), although currently it is not widely used for protein solubilization and co-crystallization. With the crystal structure available, the *pfu* MBP would serve as an alternative choice of protein expression and crystallization enhancer (Evdokimov, Anderson et al. 2001).

The *pfu* MBP was cloned into pLW01 and pMAL-c2X vectors creating pRMG_*pfu*MBP and pRMG_*pfu*MBP_c2X expression vectors, respectively (Fig. 3.7A and B). Briefly, the gene encoding the *pfu* MBP was amplified from genomic cDNA by PCR. The reaction was comprised of 35 cycles of denaturing at 94 °C for 30 s, annealing

at 55 °C for 45 sec, and elongation at 72 °C for 1 min and 20 sec followed by 72 °C for 10 min. For the pRMG_*pfu*MBP vector, the PCR products were digested with restriction enzymes Afl III and BamHI, and the pLW01 vector was digested with NcoI (compatible with Afl III) and BamHI. For the pRMG_*pfu*MBP_c2X vector, both PCR products and the pMAL-c2X vector were digested with NdeI and BamHI. The digestion products were ligated and transformed into *E. coli* DH5α competent cells. Positive clones growing from LB plates containing antibiotics were picked and sequenced.

3.4.4.2 Development of expression vectors for E. coli MBP

The *E. coli* (*eco*) MBP was cloned into pLW01 vector creating pRMG_*eco*MBP expression vector (Fig. 3.7C). The detailed procedure for vector construction was similar as described for the *pfu* MBP. In the C-terminus of MBP, a three-alanine linker was added by modification of restriction enzyme NotI for co-crystallization purpose. Another advantage of this vector is that an rTEV site with a BamHI site was inserted behind the linker. If only the target protein is wanted for function-structure studies, the TEV protease can be used to cleave off the MBP and the linker, leaving entire target protein. With this vector, researchers can choose different restriction enzyme sites depending on whether the purpose is to co-crystallization or protein solubilization, or both. For instance, if only for solubilization enhancement was desired, the BamHI is utilized so that the MBP could be cleaved after purification. For both co-crystallization and solubilization, NotI site should be used because the linker between the MBP and target proteins will be a short three-alanine stretch.

3.4.4.3 Monomeric DsRed

The monomeric DsRed was cloned into pLW01 vector using NcoI and BamHI sites creating pRMG_DsRed_M expression vector (Fig. 3.7D). The gene encoding DsRed-monomer was amplified from pDsRed-Monomer vector (BD Biosciences). The procedure for vector construction was similar as described for the *pfu* MBP.

3.4.4.4 More applications of the expression vectors

Besides the advantages described before of using the expression vectors such as enhancing protein expression, solubility, and co-crystallization, guiding crystallographic phase, and monitoring protein purification by color, fusion target proteins with MBPs or DsRed can be applied to other research efforts such as identifying protein-protein interactions *in vitro* or providing diagnostics for a protein's oligomeric state.

Protein-protein interactions can be determined *in vitro* by immobilizing one protein onto a column matrix and letting the putative partner flow through the column. If the two proteins interact, the second protein will bind to the column. Upon elution of immobilized protein, the putative partner can be detected by SDS-PAGE or Western blotting. With our vectors, we can fuse one protein with MBP and a second one with DsRed. The MBP fusion will be immobilized onto an amylose column, and binding of the second DsRed fusion protein will turn the column red. For a more quantitative measurement, the fluorescence of the elution fractions can be monitored to detect the amount of bound partner.

Since both the MBPs and the DsRed are monomeric, they can also be used to diagnose the target protein oligomeric state. Several crystallographic studies have showed that

MBP does not affect the target protein oligomeric state, and the target proteins are the major factor drives fusion protein to oligomerization if the target proteins are oligomeric (Kobe, Center et al. 1999; Liu, Manna et al. 2001; Ke, Mathias et al. 2002). Therefore, for proteins with poor solubility that could not be purified without solubilizing aids, we can fuse them with the MBPs or the DsRed to increase the solubility. And the oligomeric states of the purified fusion proteins will reflect those of the target proteins.

Researchers who have used our expression vectors in their research have obtained quite successful results. For example, when attempting to measure the ATPase activity of a protein target *in vitro*, the Benning group could not obtain recombinant protein because of the poor solubility. By fusion the target protein with MBP, the fusion protein was soluble enough to be purified and the activities were measured (Lu, Xu et al. 2007). The Benning group tried to examine phosphatidic acid (PA) binding by a putative lipid transporter component, but solubility problems and non-specific lipid binding plagued most fusion constructs. When the pRMG_DsRed_M vector was used to fuse DsRed with the target protein, the resulting fusion protein had improved solubility and made the determination of PA binding much more facile (Lu and Benning 2009). Another example of a success application for these expression vectors is the use of the pRMG-*eco*MBP by Thines et al. (Thines, Katsir et al. 2007) to express recombinant plant proteins for protein-protein interaction assays.

3.4.4.5 DLP-1 fusion proteins expression, purification, and crystallization

The DLP-1 GTPase domain, the PH-like domain, and the GED were cloned into the pRMG-*eco*MBP vector. Since the purpose of these experiments were to co-crystallize the

fusion proteins, the NotI and XhoI restriction enzyme sites were use for cloning by which the linker between the MBP and the target proteins was the three-alanine. The GED fusion protein appeared exclusively in inclusion bodies, while other two fusions are quite soluble. As there is 6x-His tag in the C-terminus of the fusion proteins, the Ni-NTA column was used for protein purification. Although the amylose column is often the preferred means for purification tool, MBP-fusion proteins may sometimes display weaker binding to the amylose column, which causes protein loss in the washing fraction. Moreover, MBP binding to the amylose column is also markedly diminished in the presence of detergents. Thus, the C-terminal 6x-His tag ensures a means to rapidly purify the fusion protein.

Both the PH-like domain and the GTPase domain fusion proteins were further purified to near homogeneity by ion exchange chromatography. No crystals for the PH-like domain and the GTPase domain fusion proteins have yet been observed in the initial rounds of crystallization trials. The DsRed fusions of the same fragments exhibited similar behavior in crystallization trial as those of MBP fusions. A number of factors may have led to this situation. The GTPase domain may be a little too large for co-crystallization with MBP, such that MBP may not dominate in the formation of ordered crystal contacts. For the PH-like domain, which is of protein size suitable for co-crystallization, the domain may be too flexible for crystallization. Another explanation is that the linker lengths and conformation may not yet be suitable for crystallization. Additional experiments are being attempted to explore this situation in greater depth.

3.4.5 Homology model of the GTPase domain of DLP-1

3.4.5.1 Experimental procedures and the model

If protein crystal structures are not available, one can predict the 3-D protein structure of a target protein empirically using homology modeling. A homology model is useful for functional predictions and the design of mutagenic experiments. The bottleneck for this experiment is the availability of a suitable crystal structure that is highly homologous to the target protein. Without high protein sequence homology, the model will not be reliable, particularly in the non-conserved regions. The crystal structure of the GTPase domain of rat dynamin was solved and the domain shares greater than 70% sequence homology with the GTPase domain of DLP-1 (Reubold, Eschenburg et al. 2005). Thus, it is suitable to make a homology model to get a general overview about the 3-D structure of the DLP-1 GTPase domain.

The protein sequences of the GTPase domains of DLP-1 and the rat dynamin were sent to http://proteins.msu.edu/servers/homologymodelingserve/construct_homology_PDB. The initial model was modified by Pymol software to visualize conserved residues. The GTPase domain model is a compact core containing seven helices and eight strands. The sheets are inside the core and surrounded by the helices. Six sheets are parallel and two are anti-parallel (Fig. 3.8).

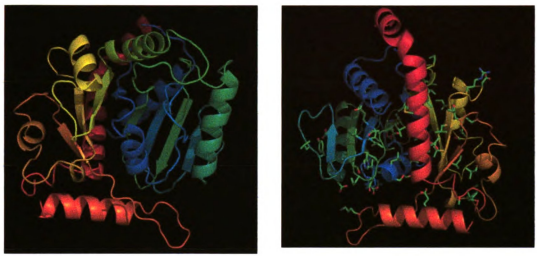

A B

Figure 3.8: Homology model of the GTPase domain of DLP-1. This model was created using the crystal structure of the GTPase domain of *Rattus norvegicus* dynamin 1 (PDB: 2AKA) as a template. (A) Front view. (B) Back view. In **B**, identical residues are highlighted by showing the side chains.

3.5 MFNs experimental procedures and results

3.5.1 Protein expression and purification

The DNAs encoding for human MFN-1 and MFN-2 were amplified from cDNAs IMAGE (clone ID 5270347 and 3901235, respectively) by PCR. The PCR amplification was comprised of 35 cycles of denaturing at 94 °C for 30 sec, annealing at 55 °C for 45 sec, and elongation at 72 °C for 2 min and 30 sec followed by 72 °C for 10 min. The PCR products were purified by QIAquick PCR purification kit (QIAGEN), digested with restriction enzymes BamHI and XhoI for ligation with pRMG-N-FLAG vector, and NcoI

and BamHI for pRMG-C-FLAG vector. The digestion product was ligated and transformed into *E. coli* DH5α competent cells. Positive clones growing from LB plates containing 100 μg/mL ampicillin were picked, and plasmid DNAs were isolated and sequenced.

The sequenced plasmids were transformed into expression host *E. coli* C41 (DE3) competent cells. Fresh single colonies from selection plates were inoculated into 100 ml LB media containing 100 μg/mL ampicillin at 37 °C with shaking at 200 rpm overnight. Twenty mL of this culture was transferred into 1 L fresh LB media and the cells were grown at 37 °C to an A_{600} of 0.8-1.0. The cells were then induced by adding 0.05 mM IPTG and incubated with shaking at 18 °C for 36 hrs. Cells were harvested by centrifugation and stored at –80 °C.

To purify MFN-1, cell pellets were resuspended in Buffer A (50 mM sodium phosphate, 300 mM NaCl, 250 mM sucrose, 10% glycerol, 10 mM β-mecaptoethanol, pH 8.0), and the crude cell extract was sonicated and centrifuged at 4 °C for 20 min at 12,000×g (low-speed centrifugation). The supernatant was further centrifuged for one hour at 45,000×g at 4 °C (high-speed centrifugation) to separate the cell membrane fragments from the soluble proteins. The supernatant of the high-speed centrifugation was saved for SDS-PAGE analysis, and the pellet of high-speed centrifugation were re-suspended and incubated in Buffer A with 1% detergent (octyl glucoside or dodecyl maltoside) at 4 °C for one hour. After another high-speed centrifugation, the supernatant was loaded onto a Ni-NTA column. The protocol for column wash and elution was the same as described for DLP-1 except that the all buffers contain 0.1% detergent. However, less then 0.1 mg of MFN-1 was obtained from 1 L culture, which is an insufficient amount at this time for

structural studies. SDS-PAGE and Western-blot analyses have shown that the MFN-1 was produced at high levels, but present in the pellet following low-speed centrifugation, probably inclusion bodies (Fig. 3.9). Since most inclusion bodies were formed because of high rate of protein synthesis, protein expression conditions such as growth temperature and IPTG induction, went through more optimization. However, the systematic alteration of growth and induction conditions failed to produce soluble MFN-1. Attempts of using nonionic detergents to solubilize MFN-1 from inclusion bodies were unsuccessful.

The low amount of MFN-1 purified from the low-speed supernatant was loaded to analytic gel filtration for size determination. The procedure was similar as described for DLP-1 except that the running buffer contains 0.1% detergent. Most protein was eluted in the void volume, and some were in a later peak, which corresponds a tetrameric size of MFN-1. The aggregation problem can be solved by adding 10 mM DTT into elution buffer and gel filtration running buffer (Fig. 3.10), indicating that the aggregation of MFN-1 is partially caused by disulfide bonds. The MFN-2 expression was not detected under a number of different expression conditions.

3.5.2 MFN fragment construction

3.5.2.1 Secondary structure prediction and sequence alignments

The secondary structure prediction (Fig. 3.11) and sequence alignments of MFN-1 and -2 were performed, as described for DLP-1. Like DLP-1, the secondary structure of MFNs is comprised of combinations of helices and strands in the GTPase domain, exclusively long helices in the HR1 and HR2, and a region predicted to be transmembrane segments. The major difference is that there is a long helix in the N-

terminus before the GTPase domain that is functionally unknown. The crystal structure of a bacterial dynamin-like protein (BDLP) shows that this helix is involved in the formation of helix bundles with the HR1 and HR2 (Low and Lowe 2006).

The protein sequences of *Saccharomyces cerevisiae* dynamin-like protein, *Homo sapiens* mitofusin-2, *Danio rerio* mitofusion-1; *Homo sapiens* mitofusin-1; *Xenopus laevis* mitofusin; *Caenorhabditis elegans* fuzzy onions protein (homologue of human mitofusins) were used for multiple sequence alignment (Fig. 3.12). The GTPase domain, the HR1, and the HR2 are highly conserved over these species. The only less conserved region is the transmembrane domains.

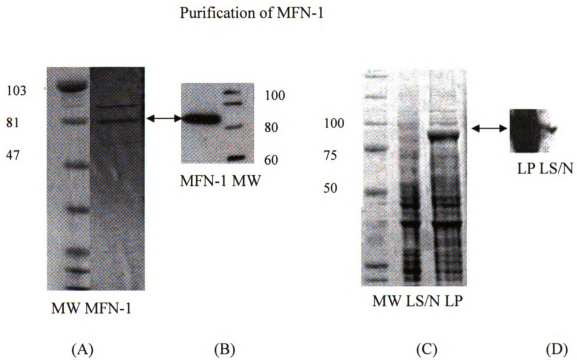

Figure 3.9: Expression and purification of MFN-1 in *E. coli*. The arrows indicate MFN-1. (A) and (B) SDS-PAGE and Western-blot analysis of purified MFN-1. (A) SDS-PAGE analysis. (C) and (D) SDS-PAGE and Western-blot analysis showing that most MFN-1 is present in pellet of low speed-centrifugation, presumably inclusion bodies. (C) SDS-PAGE analysis. MW, molecular weight markers; LS/N, supernatant of low-speed centrifugation; LP, pellet of low-speed centrifugation; (D) Western-blot analysis using anti-6×his antibody.

3.5.2.2 Protein expression and purification

Based on the secondary structure predictions and the multiple sequence alignments, several fragments of MFN-1 were cloned into pLW01 vector and expressed in *E. coli*. These fragments are: the GTPase domain (1-352 aa), the GTPase domain + HR1 (1-572 aa), the HR1 + TM + HR2 (354-741 aa) (Fig. 13). The cloning, expression, and purification procedures are as described for DLP-1 fragments. Unfortunately, all fragments were expressed exclusively in inclusion bodies, in spite of various adjusted growth conditions. Attempts of solubilizing some of these fragments using denaturants from inclusion bodies were not successful.

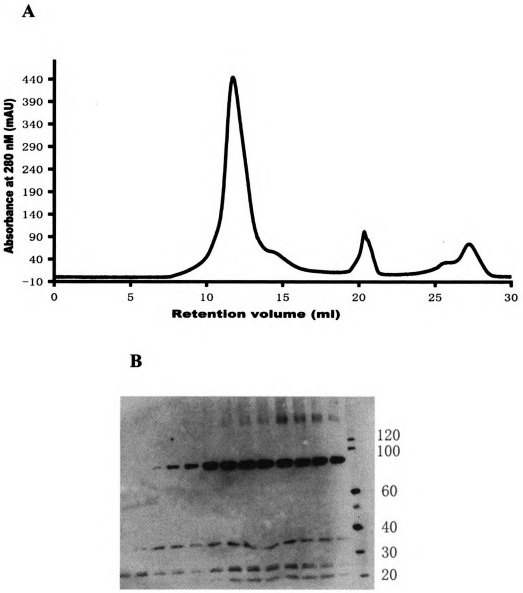

Figure 3.10: Size exclusion chromatography of MFN-1 by a Superdex 200 10/30 column. (A) chromatograph showing the tetrameric form of MFN-1 in the major peak. (B) Western blotting of the major peak fractions by anti-FLAG antibody. The protein molecular weight was calculated as for DLP-1 described in chapter 2.

Figure 3.11: Multiple-sequence alignments of MFN-1 by T-Coffee and ESPript. Hs MFN-2, *Homo sapiens* mitofusin-2; Dr MFN-1, *Danio rerio* mitofusion-1; Hs MFN-1, *Homo sapiens* mitofusin-1; Xl MFN, *Xenopus laevis* mitofusion; Ce Fzo, *Caenorhabditis elegans* fuzzy onions protein (homologue of human mitofusions).

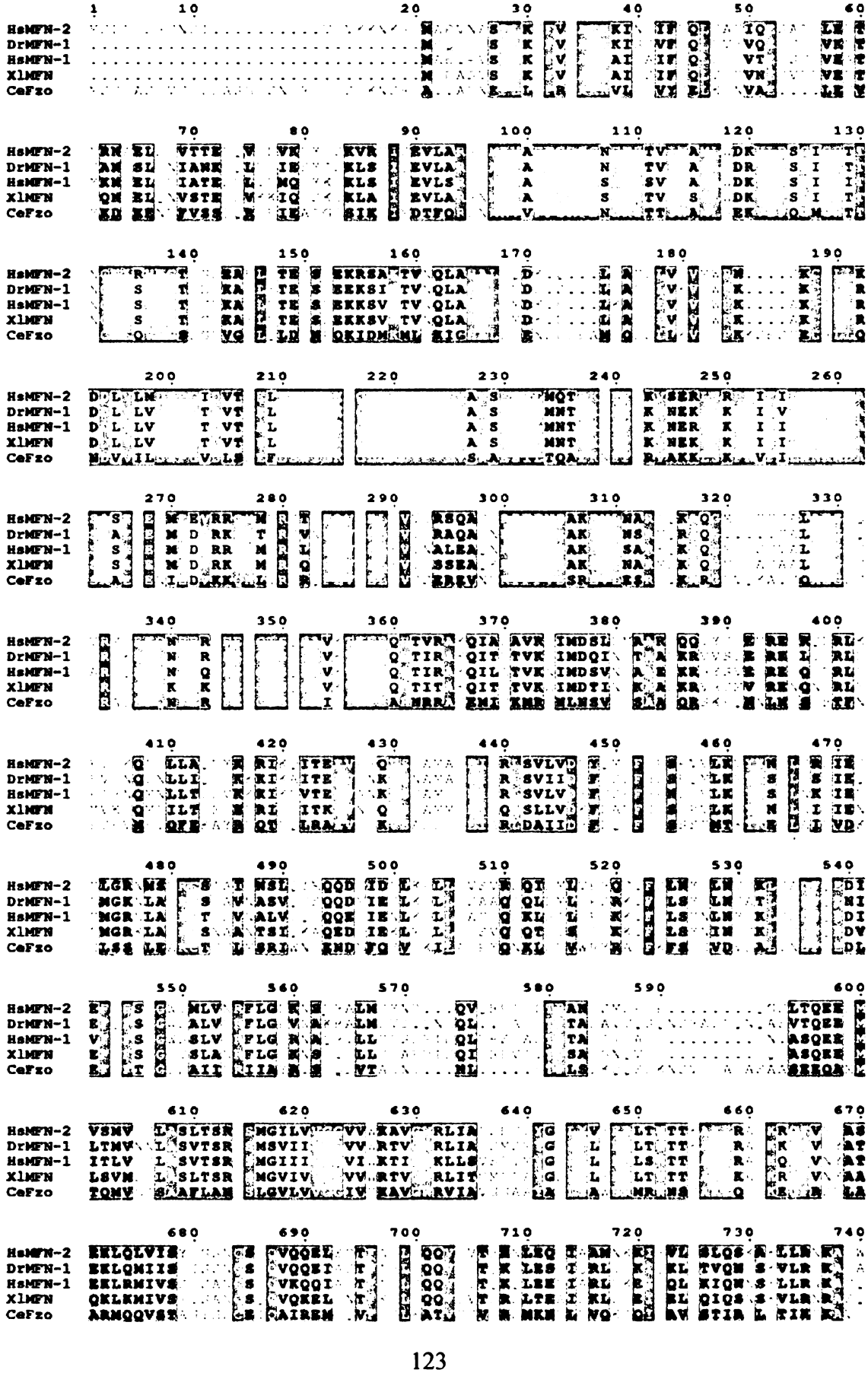
HsMFN-2
DrMFN-1
HsMFN-1
XlMFN
CeFzo

Figure 3.11 continued

The full-length MFN-1 and MFN-2 proteins were also cloned into the pRMG-*eco*MBP vector using BamHI and XhoI sites. The major purpose of this experiment was to increase the solubility of MFNs. The solubility was increased but not good enough to get purified proteins. Since MBP is mostly used with soluble proteins, membrane proteins may not be good candidates for MBP fusion.

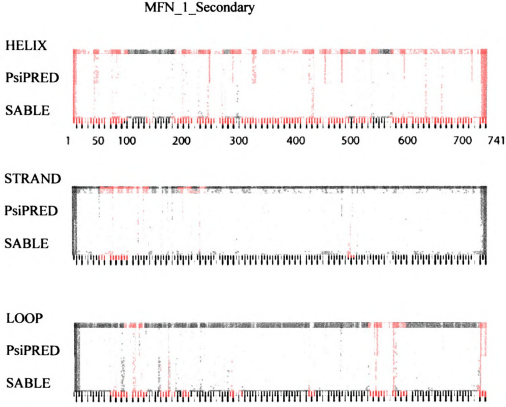

Figure 3.12: Comparison of secondary structure predictions of MFN-1 from PSI-PRED and SABLE severs by visualizing the predictions. Sequence numbers are indicated below HELIX comparison. Probabilities that each color represents are as in Fig. 3.1.

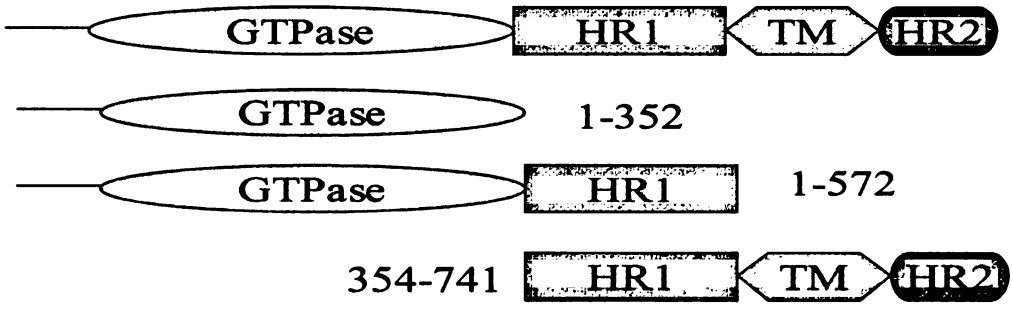

Figure 3.13: Schematic illustration of MFN-1 constructs.

3.5.3 Protein re-naturation

Previous results have shown that recombinant MFN-1 tended to form inclusion bodies. To obtain large amounts of well-folded MFN-1 for structural studies, protein re-naturation methods were explored. However, MFN-1 aggregated in the middle of the re-naturation process with either guanidine hydrochloride or urea as the denaturation reagents.

With failure of classical renaturation methods, we generated non-classical inclusion bodies of MFN-1 to try protein renaturation using ionic detergents. Expressing proteins at low temperature has been shown to produce readily solubilized "non-classical" inclusion bodies (Jevsevar, Gaberc-Porekar et al. 2005) containing large amounts of partially folded protein. Instead of using strong denaturants such as guanidine hydrochloride or urea, the non-classical inclusion bodies can be solubilized by non-denaturing solvents or low concentration of ionic detergents such as N-lauryl-sarcosine (sarcosyl). Another reason that sarcosyl was selected as a solubilizing agent is that it was

reported to successfully solubilize integral membrane proteins from inclusion bodies (Bruckner, Gunyuzlu et al. 2003).

MFN-1 was expressed in *E. coli* at 15 °C and the inclusion body was re-solubilized by 0.2 % sarcosyl. For further biochemical analysis, the protein was purified by Ni-NTA column and sarcosyl was replaced with non-ionic detergent dodecyl maltoside by gel filtration column. A wide peak in the void volume and a peak of the size of tetrameric MFN-1 size appeared in the gel filtration chromatogram. Although the renatured MFN-1 had no detectable GTPase activity, there is no report in the literature of recombinant MFN-1 exhibiting GTPase activity in *in vitro* assays. With the current preparation of renatured MFN-1, no crystals have yet been observed.

3.6 Summary

A total of at least 1064 screening conditions of precipitants were used for DLP-1 with microbatch and hanging drop vapor diffusion crystallization methods. Molecular protein engineering was designed and performed using limited proteolysis, surface-entropy reduction, and large fusion tags, to increase the likelihood of protein crystallization. A total of at least 32 protein fragments of DLP-1 were cloned, expressed, and purified for crystallization purpose. However, no crystals have yet been obtained. Homology model of the GTPase domain of DLP-1 were made for structural overview.

MFN-1 was expressed mostly in inclusion bodies. Protein renatured using ionic detergent method yielded solubilized protein, but *in vitro* GTPase activity was not observed. A total of at least 13 full-length or fragments of MFN-1 and -2 were cloned and expressed with different DNA vectors or *E. coli* cell lines. However, no crystals have

yet been obtained after the initial rounds of crystallization screening.

Nonetheless, several expression vectors containing large fusion partners were designed and constructed. Enhancing protein expression, solubility, and co-crystallization, guiding crystallographic phase, monitoring protein purification by color, detecting protein-protein interactions, and diagnosing protein oligomeric state, are among the advantages of using these vectors.

References

Bruckner, R. C., P. L. Gunyuzlu and R. L. Stein (2003). "Coupled kinetics of ATP and peptide hydrolysis by Escherichia coli FtsH protease." Biochemistry **42**(36): 10843-52.

Chayen, N. E. (1998). "Comparative studies of protein crystallization by vapour-diffusion and microbatch techniques." Acta Crystallogr D Biol Crystallogr **54**(Pt 1): 8-15.

Dale, G. E., C. Oefner and A. D'Arcy (2003). "The protein as a variable in protein crystallization." J Struct Biol **142**(1): 88-97.

Derewenda, Z. S. and P. G. Vekilov (2006). "Entropy and surface engineering in protein crystallization." Acta Crystallogr D Biol Crystallogr **62**(Pt 1): 116-24.

Evdokimov, A. G., D. E. Anderson, K. M. Routzahn and D. S. Waugh (2001). "Structural basis for oligosaccharide recognition by Pyrococcus furiosus maltodextrin-binding protein." J Mol Biol **305**(4): 891-904.

Fox, J. D., K. M. Routzahn, M. H. Bucher and D. S. Waugh (2003). "Maltodextrin-binding proteins from diverse bacteria and archaea are potent solubility enhancers." FEBS Lett **537**(1-3): 53-7.

Gaur, R. K., M. B. Kupper, R. Fischer and K. M. Hoffmann (2004). "Preliminary X-ray analysis of a human V(H) fragment at 1.8 A resolution." Acta Crystallogr D Biol Crystallogr **60**(Pt 5): 965-7.

Jevsevar, S., V. Gaberc-Porekar, I. Fonda, B. Podobnik, J. Grdadolnik and V. Menart (2005). "Production of nonclassical inclusion bodies from which correctly folded protein can be extracted." Biotechnol Prog **21**(2): 632-9.

Johnson, S., P. Roversi, M. Espina, J. E. Deane, S. Birket, W. D. Picking, A. Blocker, W. L. Picking and S. M. Lea (2006). "Expression, limited proteolysis and preliminary crystallographic analysis of IpaD, a component of the Shigella flexneri type III secretion system." Acta Crystallogr Sect F Struct Biol Cryst Commun **62**(Pt 9): 865-8.

Ke, A., J. R. Mathias, A. K. Vershon and C. Wolberger (2002). "Structural and thermodynamic characterization of the DNA binding properties of a triple alanine mutant of MATalpha2." Structure **10**(7): 961-71.

Kim, A. R., T. Dobransky, R. J. Rylett and B. H. Shilton (2005). "Surface-entropy reduction used in the crystallization of human choline acetyltransferase." Acta Crystallogr D Biol Crystallogr **61**(Pt 9): 1306-10.

Kobe, B., R. J. Center, B. E. Kemp and P. Poumbourios (1999). "Crystal structure of human T cell leukemia virus type 1 gp21 ectodomain crystallized as a maltose-

binding protein chimera reveals structural evolution of retroviral transmembrane proteins." Proc Natl Acad Sci U S A **96**(8): 4319-24.

Koth, C. M., S. M. Orlicky, S. M. Larson and A. M. Edwards (2003). "Use of limited proteolysis to identify protein domains suitable for structural analysis." Methods Enzymol **368**: 77-84.

Liu, Y., A. Manna, R. Li, W. E. Martin, R. C. Murphy, A. L. Cheung and G. Zhang (2001). "Crystal structure of the SarR protein from Staphylococcus aureus." Proc Natl Acad Sci U S A **98**(12): 6877-82.

Low, H. H. and J. Lowe (2006). "A bacterial dynamin-like protein." Nature **444**(7120): 766-9.

Lu, B. and C. Benning (2009). "A 25-amino acid sequence of the Arabidopsis TGD2 protein is sufficient for specific binding of phosphatidic acid." J Biol Chem **284**(26): 17420-7.

Lu, B., C. Xu, K. Awai, A. D. Jones and C. Benning (2007). "A small ATPase protein of Arabidopsis, TGD3, involved in chloroplast lipid import." J Biol Chem **282**(49): 35945-53.

Niemann, H. H., M. L. Knetsch, A. Scherer, D. J. Manstein and F. J. Kull (2001). "Crystal structure of a dynamin GTPase domain in both nucleotide-free and GDP-bound forms." Embo J **20**(21): 5813-21.

Prakash, B., G. J. Praefcke, L. Renault, A. Wittinghofer and C. Herrmann (2000). "Structure of human guanylate-binding protein 1 representing a unique class of GTP-binding proteins." Nature **403**(6769): 567-71.

Prakash, B., L. Renault, G. J. Praefcke, C. Herrmann and A. Wittinghofer (2000). "Triphosphate structure of guanylate-binding protein 1 and implications for nucleotide binding and GTPase mechanism." Embo J **19**(17): 4555-64.

Reubold, T. F., S. Eschenburg, A. Becker, M. Leonard, S. L. Schmid, R. B. Vallee, F. J. Kull and D. J. Manstein (2005). "Crystal structure of the GTPase domain of rat dynamin 1." Proc Natl Acad Sci U S A **102**(37): 13093-8.

Sachdev, D. and J. M. Chirgwin (2000). "Fusions to maltose-binding protein: control of folding and solubility in protein purification." Methods Enzymol **326**: 312-21.

Schwartz, T. U., R. Walczak and G. Blobel (2004). "Circular permutation as a tool to reduce surface entropy triggers crystallization of the signal recognition particle receptor beta subunit." Protein Sci **13**(10): 2814-8.

Shin, H. W., H. Takatsu, H. Mukai, E. Munekata, K. Murakami and K. Nakayama (1999).

"Intermolecular and interdomain interactions of a dynamin-related GTP-binding protein, Dnm1p/Vps1p-like protein." J Biol Chem **274**(5): 2780-5.

Skerra, A. and T. G. Schmidt (2000). "Use of the Strep-Tag and streptavidin for detection and purification of recombinant proteins." Methods Enzymol **326**: 271-304.

Smith, D. B. (2000). "Generating fusions to glutathione S-transferase for protein studies." Methods Enzymol **326**: 254-70.

Thines, B., L. Katsir, M. Melotto, Y. Niu, A. Mandaokar, G. Liu, K. Nomura, S. Y. He, G. A. Howe and J. Browse (2007). "JAZ repressor proteins are targets of the SCF(COI1) complex during jasmonate signalling." Nature **448**(7154): 661-5.

Zhu, P. P., A. Patterson, J. Stadler, D. P. Seeburg, M. Sheng and C. Blackstone (2004). "Intra- and intermolecular domain interactions of the C-terminal GTPase effector domain of the multimeric dynamin-like GTPase Drp1." J Biol Chem **279**(34): 35967-74.

CHAPTER 4

Studies on the (pro)renin receptor and the promyelocytic zinc finger protein

4.1 Introduction

The cytoplasmic tail of the (P)RR is short, but functionally important for the pivotal roles of the (P)RR in blood pressure and cardiovascular regulation. Since the tail is the only region that is exposed to the cytosol, it should be the direct mediator for the signal transduction pathways that activated by binding of (pro)renin to (P)RR. Structural studies on the cytoplasmic tail might shed light on the functions of the (P)RR in the downstream signal transduction.

PLZF has been identified as one of the protein molecules that interact with the (P)RR and transduce (pro)renin signals. When (pro)renin binds (P)RR, the PLZF is activated and translocated to the nucleus to be recruited to the *cis* element of the (P)RR promoter (Schefe, Menk et al. 2006). The transcription of the (P)RR is then repressed by the activated PLZF, creating a short negative feedback loop. Direct interaction of PLZF with the cytoplasmic domain of the (P)RR was confirmed by the yeast two-hybrid study and coimmunoprecipitation with truncated (P)RR proteins (Schefe, Menk et al. 2006). However, which region(s) of the PLZF is responsible for the interaction remains unclear.

Since the cytoplasmic tail of the (P)RR is short (19 residues), the MBP fusion method was chosen for simplifying the protein expression and purification, to generate a unique chimeric protein for binding studies, and to enhance the potential for protein crystallization. This chapter describes the structural determination of the cytoplasmic tail of the (P)RR with MBP fusion method. Heterologous expression of PLZF truncated proteins was perform for structural studies as well as investigation of which specific

region(s) of the protein is responsible for the interaction with the (P)RR.

4.2 (P)RR wild type protein

4.2.1 Secondary structure and hydropathy prediction

The secondary structure of the (P)RR was predicted using the *PSI-PRED* online server. The outcome showed that the protein is comprised of a mixture of helices and stands connected by loops. Two major loops are located in the residues from 50 to 100, and from 160 to 175 which may be potential active sites for the (pro)renin binding. The cytoplasmic tail forms a loop structure. The hydropathy prediction was performed by the *TMHMM* online serve 2.0. Two major hydrophobic regions were revealed by the predication. One is in the first 20 amino acids, the signal peptides. The other is between residues 300 and 330, the transmembrane domain.

4.2.2 Expression and purification

The DNA encoding for the (P)RR was cloned into the pLW01 vector. Sequenced plasmid was transformed into *E. coli* C41 (DE3) competent cells for expression. The expression procedure was similar with that for MFN-1 described in chapter 3. In short, single colonies were inoculated into 20 ml 2YT media with shaking at 37 °C overnight. The culture was transferred into 1 L 2YT media and the cells were grown at 37 °C until the OD600 reached to 1.0. IPTG was added into the culture at final concentration of 1 mM for induction and the cells were grown at 18 °C for 20 hrs.

To purify the (P)RR, cell pellets were re-suspended in buffer A (50 mM Tris, 300 mM Sucrose, pH 8.0), and the crude cell extract was sonicated and centrifuged at 4 °C for 20 min at 12,000 g (low-speed centrifugation). The supernatant was further centrifuged for one hour at 45,000 g at 4 °C (high-speed centrifugation) to separate the cell membranes from the soluble lysate. The supernatant of the high-speed centrifugation was saved for SDS-PAGE analysis. And the pellet of high-speed centrifugation were re-suspended in buffer B (50 mM sodium phosphate, 300 mM NaCl, 10% glycerol, pH 8.0) and incubated with 0.75% dodecyl maltoside at 4 °C for one hour. After another high-speed centrifugation, the supernatant was added with 10 mM imidazole and loaded onto a Ni-NTA column. The gradients of lysis, washing, and elution buffer were same as those for DLP-1 purification (chapter 2) except that all buffers contained 0.05% dodecyl maltoside and the concentration of imidazole in the washing buffer was 38 mM.

The purified protein was loaded to analytic gel filtration for size determination. The procedure was similar with that for DLP-1 (chapter 2) except that the column running buffer was 30 mM Tris, 300 mM NaCl, 0.2% decyl maltoside. Most protein was eluted in the void volume, indicating a size greater than the limit of the column, 1300 kDa. Since there are detergents present in the buffer, conclusion could not be drawn whether the large size was caused by protein aggregation or whether it is higher order structure of (P)RR formed when binding to detergent micelles.

4.2.3 Crystallization

The purified (P)RR protein was concentrated with a 30K Amicon Ultra centrifugal unit (Millipore) to about 10 mg/mL. Initial screens were performed by microbatch-under-oil method with an ORYX crystallization robot (Douglas Instruments). A total of 198 conditions (Hampton Research screen I & II; Cryo screen I & II) were applied by combining 0.75 μL of purified protein with 0.75 μL screen solutions. Within 30 days, small crystals grew from conditions of 28% PEG 400, 0.2 M $CaCl_2$, 0.1 M HEPES, pH 7.5. Since there was detergent in the protein solution, sitting drop vapor diffusion method, which is less affected by the lower surface tension of detergent solutions, was used for crystal optimization. A matrix including different concentration of major precipitates, additives, and pH ranges were designed in order to obtain large and single crystal suitable for X-ray diffraction. With this designing matrix, putative crystals grew from most of the conditions. However, the crystals are small and not in perfect shapes (Fig. 4.1). Further efforts to optimize the crystallization conditions are underway.

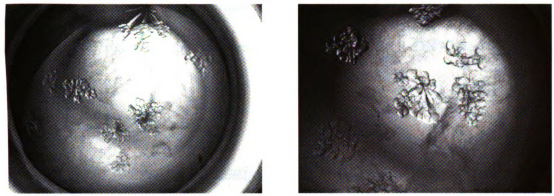

Figure 4.1: Putative crystals of the (pro)renin receptor in hanging drops. The crystals growing condition was 28% PEG 400, 0.2 M $CaCl_2$, 0.1 M HEPES, pH 7.5.

4.3 Structural determination of the cytoplasmic tail of the (P)RR

4.3.1 Experimental procedure

4.3.1.1 Cloning design - The DNA encoding the cytoplasmic domain of (pro)renin receptor was engineered into pRMG-*eco*MBP vector with three alanines as a linker. In short, two oligonucleotides encoding the 19 amino acids flanking with designed restriction enzyme sites were synthesized. The sequences of the complementary oligonucleotides are:

5'-GGCCGCCGATCCTGGATATGATAGCATCATTTATAGGATGACAAACCAGAAG ATTCGAATGGAT*TGA* -3' and 5'-TCGAG*TCA*ATCCATTCGAATCTTCTGGTTTGTCATCCTATAAATGATGCTATCATA TCCAGGATC -3'. The oligonucleotides were annealed by slowly cooling down after incubating at 95 °C, and then phosphorylated by polynucleotide kinase at 37 °C. The product was ligated to pre-cut pRMG-MBP vector into the Not I and Xho I sites and

transformed into *E. coli* DH5α competent cells. Positive clones growing from LB plates containing 100 μg/mL ampicillin were picked, and plasmid DNA were isolated and sequenced.

4.3.1.2 Protein expression and purification - The sequenced plasmids encoding the fusion protein (MBP-(P)RR19) were transformed into the expression host *E. coli* BL21 (DE3) competent cells. A fresh single colony from a selection plate was inoculated into 100 ml LB media with 100 μg/mL ampicillin. After shaking at 37 °C with 200 rpm overnight, 20 ml of this culture was transferred into 1 L fresh LB media with antibiotics. When an OD_{600} reached to about 0.8-1.0, IPTG was added into the culture with a final concentration of 0.05 mM. The growing temperature was reduced to 24 °C and the cells were continuously shaken for 17 hours. The cells were harvested by centrifugation and stored at –80 °C.

Cell pellets were re-suspended in Buffer A (20 mM Tris-HCl, pH 7.4, 0.2 M NaCl, 1 mM EDTA, 10 mM β-mercaptoethanol). The crude cell extract obtained by sonication was centrifuged at 24 °C at 12,000×g for 20 min. The supernatant was mixed with 10 ml amylose resin (New England Biolabs) pre-equilibrated with buffer A and incubated at 4 °C for 5 hrs with shaking. The mixture was loaded onto a column to allow unbound proteins to flow through. The column was then washed with 10 column volumes of buffer A. These washing eluants were considered as the fusion protein-containing fractions and were pooled and concentrated to 1 ml using an Amicon Ultra centrifugal unit (Millipore).

The protein was loaded onto a 1 ml HiTrap Q ion exchanger (Amersham Biosciences), eluted with a gradient generated by using buffer B (20 mM Tris-HCl, pH 8.5) and buffer C (20 mM Tris-HCl, 1 M NaCl, pH 8.5) at a flow rate of 1 ml/min. The peak fractions were pooled and concentrated. The buffer was exchanged with buffer D (20 mM Tris-HCl, pH 7.4, 0.1 M NaCl) by passing two 5-ml spin columns with sephadexTM G-25 coarse (GE healthcare). The protein was analyzed by SDS-PAGE and the concentration was determined using a BCA assay (Thermo Scientific).

The oligomeric state of the MBP-(P)RR19 was determined by size exclusion chromatography. A Superdex 200 10/30 GL column was pre-equilibrated with buffer D. The purified fusion protein was loaded onto the column and eluted at a rate of 0.5 ml/min. Fractions containing fusion protein was analyzed by SDS-PAGE and Western blot.

4.3.1.3 Mass spectrometry - The molecular weight of the purified MBP-(P)RR19 was analyzed by a Waters LCT Premier time-of-flight mass spectrometer which is coupled with Shimadzu LC-20AD HPLC pumps and a SIL-5000 autosampler. Separation was performed using a Thermo BetaBasic cyano column (1 x 10 mm) with a gradient generated by 0.15% aqueous formic acid and 75% acetonitrile for online desalting and elution. Instrument control, data acquisition, and processing were provided by the MassLynx data system (Waters Ltd, Manchester, UK, version 4.1). Molecular weight was calculated based on spectrum deconvolution using MaxEnt1 software.

4.3.1.4 Crystallization - Prior to crystallization, the apo-fusion protein was adjusted to 20 mg/mL. Preliminary crystallization screen was performed at 20°C by microbatch-under-oil method using an ORYX crystallization robot (Douglas Instruments). With crystal screens (HR2-110 and HR2-112, Hampton Research), 0.75 μL protein solution and 0.75 μL crystallization reagent were mixed in each drop. After finding initial crystallization conditions, crystal growth was scaled up by hanging-drop vapour diffusion method at 20°C (2 μl protein solution and 2 μl reservoir solution equilibrated against 1 ml reservoir solution). The precipitant concentration and the pH were optimized and the best crystals were obtained using solutions consisting of 20% (w/v) PEG 4000, 0.2 M $MgCl_2$ and 0.1 M Tris, pH 8.5. Final crystal dimensions were 0.4 × 0.3 × 0.04 mm. To occupy the ligand-bound sites with maltose, 0.5 mM maltose were added into the fusion protein and the mixture was incubate at 4 °C for at least 3 hrs before crystallization trials as described above for the apo-fusion protein. The crystals of the ligand-bound protein was optimized to a size of 0.2 × 0.2 × 0.08 mm with the condition of 26% (w/v) PEG 4000, 0.2 M $MgCl_2$, and 0.1 M Na Cacodylate, pH 6.5.

4.3.1.5 Cryoprotection and data collection - Crystals for X-ray diffraction studies were transferred stepwise into cryoprotectant solutions with increasing concentrations of glycerol. The apo-fusion protein crystals were flash-cooled in the final cryoprotectant solution consisted of 20 mM Tris-HCl (pH 7.4), 0.1 M Tris-HCl (pH 8.5), 0.1 M NaCl, 20% PEG 4000 (w/v), 0.2 M $MgCl_2$, and 15% glycerol (v/v). And the ligand-bound

protein crystals were in the final cryoprotectant solution consisted of 20 mM Tris-HCl (pH 7.4), 0.1 M Na Cacodylate (pH 6.5), 0.1 M NaCl, 26% PEG 4000 (w/v), 0.2 M $MgCl_2$, and 15% glycerol (v/v). X-ray diffraction data were collected at –173 °C on 21-ID beamline (LS-CAT) using a MAR CCD detector at Advanced Photon Sources (Argonne, IL). Complete datasets were collected from single crystals with a crystal-to-detector distance of 250 mm and an exposure time of 1 sec per 1° oscillation under the wavelength of the synchrotron radiation at 0.98 Å. All diffraction images were processed using *DENZO* and integrated intensities were scaled using the *SCALEPACK* from the *HKL-2000* program package (Otwinowski and Minor 1997).

4.3.1.6 Structural determination and refinement - The structure of the fusion protein was determined by molecular replacement using the programs from *CCP4* suite (1994), with the known structures of *E. coli* MBP as search models. Structure with PDB code of 1JW4 (Residues 1-363) (Duan and Quiocho 2002) was used for apo-fusion protein and 1ANF (Residues 1-363) (Quiocho, Spurlino et al. 1997) was for ligand-bound protein. Models building were performed in *Coot* (Emsley and Cowtan 2004) using the 2*F*o-*F*c and *F*o-*F*c electron-density maps. Translation/Libration/Screw (TLS) (Winn, Isupov et al. 2001) motion determination using both domains of MBP as TLS group and non-crystallographic symmetry (NCS) were used for model refinement. The quality of the models were evaluated using the program *PROCHECK*. The graphical figures were visualized using the program *PyMOL*.

4.3.2 Results and discussion

4.3.2.1 Protein expression and purification

4.3.2.1.1 Rationale of strategies

Like many effector regions of receptors on membranes, the cytoplasmic tail of the (P)RR is short and has only about 19 amino acids. We initially thought about synthesizing the 19-residue peptides for structural studies. However, such peptides may not be well behaved enough or be in the appropriate conformation for crystallization. Therefore, I used the traditional method of recombinant expression in *E. coli*, but considered that 19 residues may be too short to be observed in both agarose gel and SDS-PAGE, which would cause problems during DNA cloning and protein purification. Also, if we try to express the 19 amino acids alone in *E. coli*, the protein may have solubility problem, which is common for truncated protein fragments. Therefore, an expression and purification aid is necessary to create the recombinant fusion protein with the cytoplasmic tail. Maltose binding protein (MBP) from *E. coli* is commonly used to enhance the expression, improve the yield and stability, and facilitate the purification and crystallization. Most importantly, with an appropriate linker, MBP is a good crystallization aid without affecting the native structure of target proteins (for details, please refer to chapter 3).

Due to the short DNA sequence encoding for the 19 amino acids, it would be extremely difficult to clone the gene into expression vectors by PCR. For traditional DNA cloning using PCR, sequence shorter than 100 bp would cause a decrease of the success

rate. If shorter than 70 bp, PCR method may not be the best because of the problem of recovering DNA from agarose gels. Thus, I used the oligonucleotide annealing method, which allows the manipulation of relatively short DNA from 10 bp up to 100 bp. The trick is that each oligonucleotide should be designed with sticky ends so that after annealing, they resemble the structure that is cut by restriction enzymes and are able to ligate to pre-cut vectors. This method can also be used for designing and constructing DNA vectors particularly when require inserting short DNA sequences such as a promotor sequence or a new restriction enzyme site (Brummelkamp, Bernards et al. 2002).

Another possible problem due to the short target protein is that it would be hard to separate and distinguish the endogenous *E. coli* MBP with the MBP-(P)RR19 during protein purification. Both MBPs would bind to the amylose column and they would also be difficult to separate by ion exchange chromatography because the fusion of 19 residues in the C-terminus may not cause a significant change on MBP biophysical and biochemical properties. I assumed that the MBP-(P)RR19 would affect the binding affinity of MBP to amylose column that it would not bind the amylose resin as tight as that of the endogenous native MBP that requires 10mM maltose to be eluted from the column. Thus, I used large volume of washing buffer (10 column volume) without maltose in it to wash the fusion protein off the amylose column and considered this fraction as relatively pure MBP-(P)RR19. The elution fraction that was eluted with 10 mM maltose was considered as the mixture of fusion and endogenous MBPs and was

discarded.

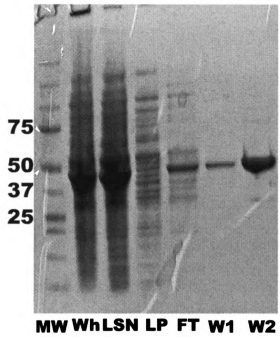

Figure 4.2: SDS-PAGE of MBP-(P)RR19 purification by amylose column. Incubating for 5~6 hrs with amylose and washing with about 10 column volumes would yield highest amount and pure protein. MW, molecular weight standard; Wh, whole cells; LSN, supernatant of low-speed centrifugation; LP, pellets of low-speed centrifugation; FT, flow through; W1, wash fraction 1; W2, wash fraction 2.

4.3.2.1.2 Protein purification

I have screened different incubation time of the MBP-(P)RR19 with amylose and different volume of washing fractions and found that incubating at 4 ^{o}C for 5~6 hrs and washing with about 10 column volumn would be a balance between yield and purity of the MBP-(P)RR19 (Fig. 4.2). Shorter incubation time or larger volume of washing caused impurity of the fusion protein because the endogenous MBP did not bind the column tight

enough. While, longer incubation time or less volume of washing caused low yield of fusion protein because more fusion protein would bind the column and would not eluted until with maltose.

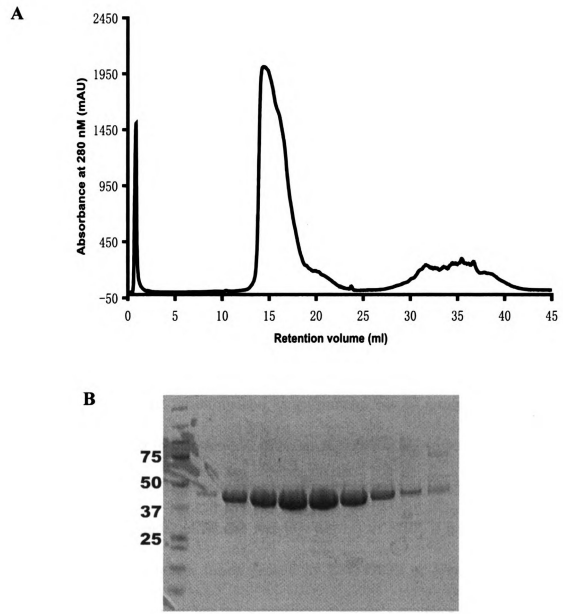

Figure 4.3: Purification of the MBP-(P)RR19 by ion exchange chromatography. (A) In the ion exchange chromatogram, the protein was eluted in the major peak at an ionic strength between 0.25 and 0.35 M NaCl. (B) SDS-PAGE of fractions corresponding to the major peak in panel A.

The theoretical isoelectric point of the MBP-(P)RR19 is 4.99. Therefore, anion exchange is appropriate for further protein purification. The MBP-(P)RR was eluted in a single peak at the ionic strength between 0.25 to 0.35 mM NaCl. Based on previous chromatographic experience from the current laboratory, endogenous MBP usually is eluted behind but closed to the peak of fusion proteins. In the MBP-(P)RR19 case, there were no other peaks showing up in the chromatogram (Fig. 4.3) indicating the fusion protein was homogeneous. Meanwhile, it supports our assumption that the fusion protein may have less affinity to the amylase resin than the endogenous MBP and the strategy of collecting the washing fraction during purification. Judging from SDS-PAGE, the MBP-(P)RR19 was greater than 98% pure after ion exchange purification (Fig. 4.3). About 8 mg of purified protein was obtained from 500 ml culture for structural studies.

4.3.2.1.3 Mass spectrometry

Occasionally, with the fusion method, target proteins can be unexpectedly "cleaved" off the MBP, leaving truncated fusions. Although the reasons are unclear, it may be due to interrupted protein translation *in vivo* or protease cleavage during purification. Since the MBP-(P)RR19 has similar molecular weight with that of MBP, it is hard to determine expression of the full-length fusion protein by SDS-PAGE or Western blotting. The ESI-TOF mass spectrometry has the accuracy to measure a protein's molecular mass to within one amino acid. The mass spectrometry results on purified MBP-(P)RR19 showed that the fusion protein mass is 42488.5 Da (Fig. 4.4), with an error range of 10 Da. The

theoretical mass of MBP-(P)RR19 is 42497 Da.

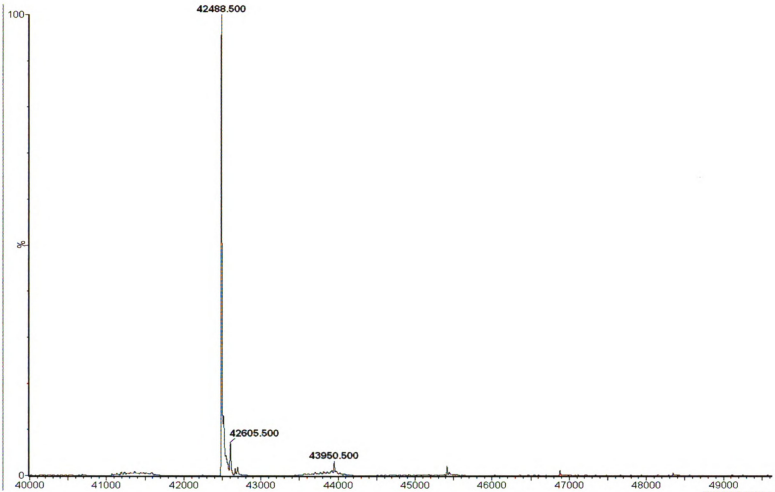

Figure 4.4: Accurate molecular weight of purified MBP-(P)RR19 measured by mass spectrometry. The major peak indicated that the protein mass is 42488.5 Da which is within the system error range of 10 Da of the theoretical mass, 42497 Da.

4.3.2.2 Crystallization

4.3.2.2.1 Apo-MBP-(P)RR19

Before crystallization, the MBP-(P)RR19 was buffer exchanged with 20 mM Tris, 100 mM NaCl, pH 7.4 to remove excess salts from ion exchange chromatography. Initial screens were performed by microbatch-under-oil method with an ORYX crystallization robot (Douglas Instruments). A total of 198 conditions (Hampton Research screen I & II; Cryo screen I & II) were applied by combining 0.75 μL of purified protein with 0.75 μL screen solutions. Within 30 days, clustered large crystals grew from conditions of 30% PEG 4000, 0.2 M $MgCl_2$, 0.1 M Tris pH 8.5 and 25% PEG monomethyl ether (PEGmme) 550, 0.01 M $ZnSO_4$, 0.1 M MES pH 6.5. Hanging drop vapor diffusion was used to optimize the conditions of the initial hits. A matrix including different concentration of major precipitates, additives, and pH ranges were designed in order to obtain large and single crystal suitable for X-ray diffraction. With this designed matrix, crystals precipitated by PEGmme 550 were still highly clustered and no single crystal could be picked for data collection. Whereas, with a concentration gradient of PEG 4000 from 18% to 30%, nice and single crystals grew about four days after the setup from 20% PEG 4000, 0.2 M $MgCl_2$, and 0.1 M Tris 8.5 (Fig. 4.5).

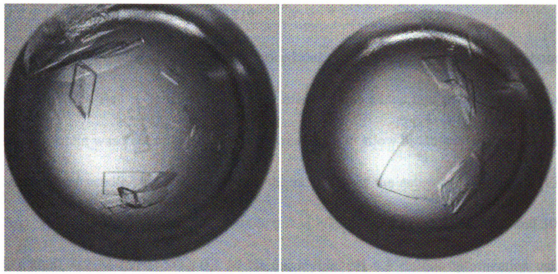

Figure 4.5: Crystals of apo-MBP-(P)RR19 from hanging drop vapor diffusion. The optimized condition is 20% PEG 4000, 0.2 M $MgCl_2$, and 0.1 M Tris 8.5.

Glycerol was added to the mother liquor as a cryoprotectant. As adding too much cryoprotectant increases the chances that the crystals would crack. It is necessary to find the lowest amount of glycerol that would avoid the formation of ice but not cause crystal damage. About 15% of glycerol was determined to be the best concentration for the MBP-(P)RR19 crystals. Because there was no glycerol in the crystallization conditions, the procedure of introduction was in a stepwise manner. Adding a high concentration of cryoprotectant at one time can cause a sudden change of solution environment and damage crystals. Therefore, crystals were first transferred into stabilizing buffer containing 2% glycerol to let them adapt to the new glycerol environment. Then, the glycerol concentrations was increased to 5%, 10%, and finally to 15%. There was no obvious damage observed on surface of the crystals in the final cryoprotectant solution.

4.3.2.2.2 Ligand-bound MBP-(P)RR19

Same crystallization and freezing procedures were applied to the ligand-bound MBP-(P)RR19. Before screenings, 0.5 mM maltose was added into the protein solution and the protein was kept on ice for at least three hours to allow binding of ligands. Highly clustered and needle-shape crystals grew the next day of the setup by microbatch (Fig. 4.6A). The conditions are 30% PEG 4000, 0.2 M NH_4AC, 0.1 M NaAC pH 4.6 and 30% PEG 8000, 0.2 M $(NH_4)_2SO_4$, 0.1 M Na cacodylate pH 6.5. Initial optimization using hanging drop method generated similar clustered crystals. However, conditions by matrix designing yielded much better crystals that are suitable for data collection with the condition of 26% PEG 4000, 0.2 M $MgCl_2$, 0.1 M Na Cacodylate, pH 6.5 (Fig. 4.6B).

A

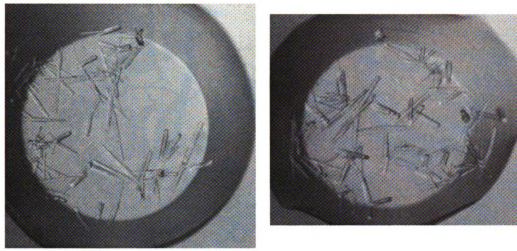

B

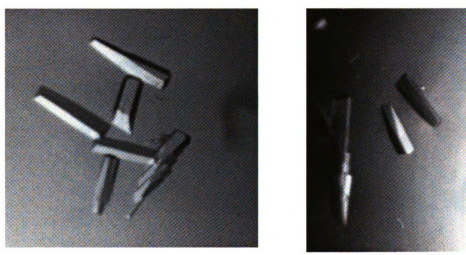

Figure 4.6: Crystals of ligand-bound MBP-(P)RR19. (A) Crystals from microbatch with conditions of 30% PEG 4000, 0.2 M NH_4AC, 0.1 M Na acetate pH 4.6 (left) and 30% PEG 8000, 0.2 M $(NH_4)_2SO_4$, 0.1 M Na cacodylate pH 6.5 (right). (B) Crystals from hanging drop with optimized condition of 26% PEG 4000, 0.2 M $MgCl_2$, 0.1 M Na Cacodylate, pH 6.5.

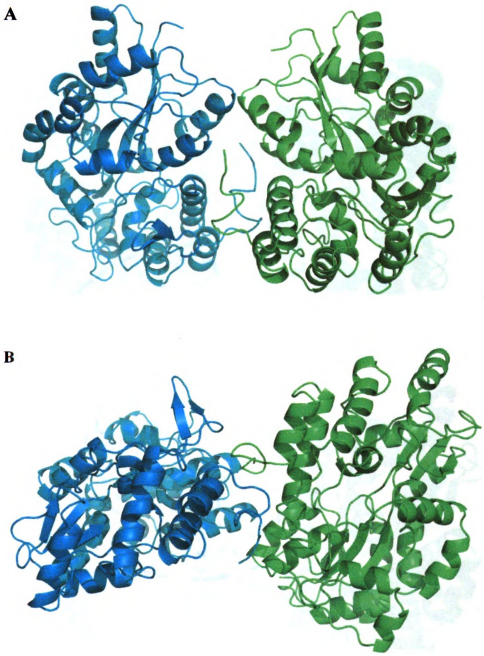

Figure 4.7: Structure of MBP-(P)RR19 with maltose bound. (A) Front view. (B) Side view.

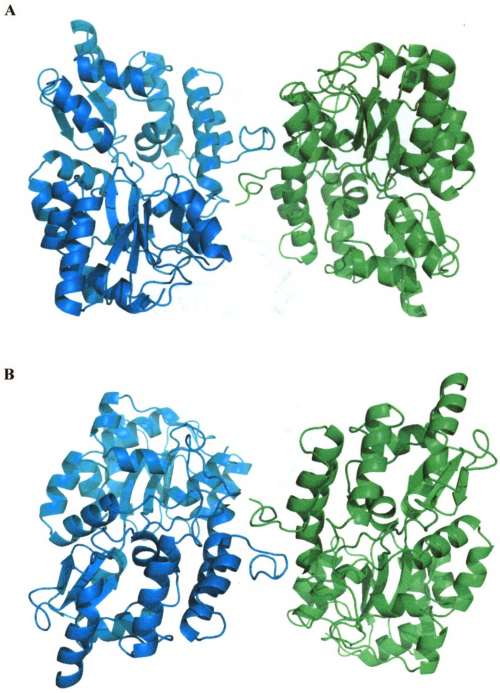

Figure 4.8: Structure of MBP-(P)RR19 without maltose. (A) Front view. (B) Back view.

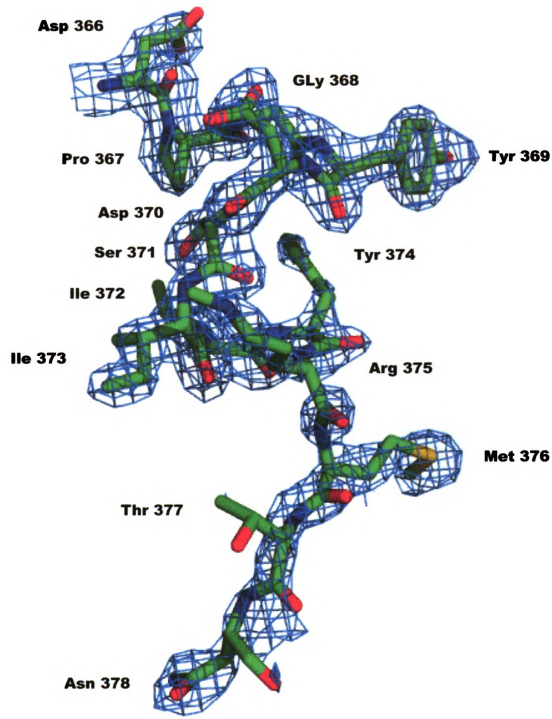

Figure 4.9: The (P)RR19 in a *2Fo-Fc* electron-density map contoured at one standard deviation above the mean density. Residues 366-378 (from left top to bottom) of molecule B with maltose bound are shown in sticks representation.

Figure 4.10: Dimeric interface of apo-MBP-(P)RR19 is mediated by hydrogen bonds formed by residues from (P)RR19 peptide. Hydrogen bonds are highlighted by red dashes. (A) Overview of hydrogen bonding pattern. (B) Detailed hydrogen bonds.

A

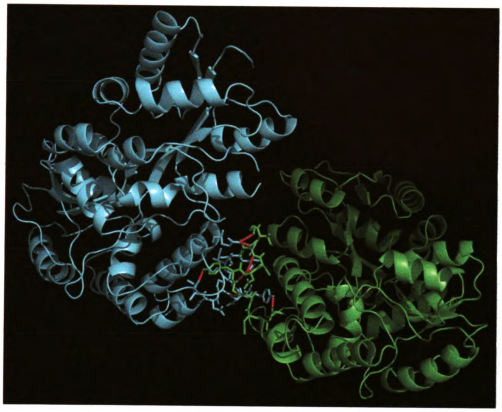

Figure 4.10 continued

B

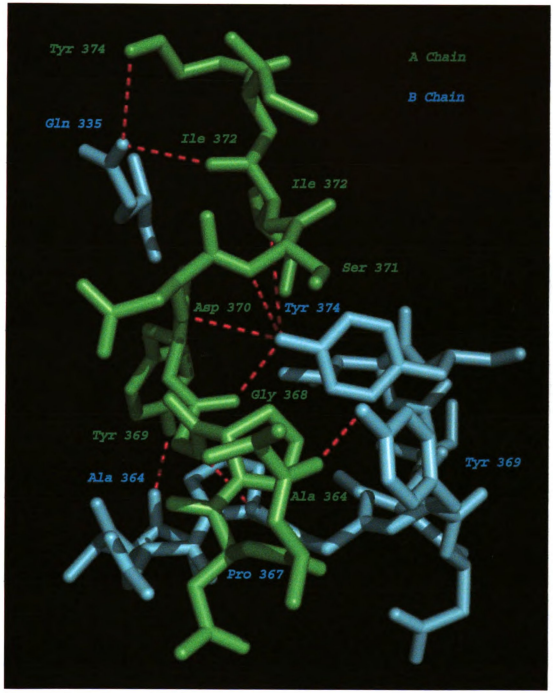

Figure 4.11: Dimeric interface of ligand-bound-MBP-(P)RR19 is predominated by hydrogen bonds formed by residues from (P)RR19 peptide. Hydrogen bonds are highlighted by red dashes. (A) Overview of hydrogen bonding pattern. (B) Detailed hydrogen bonds.

A

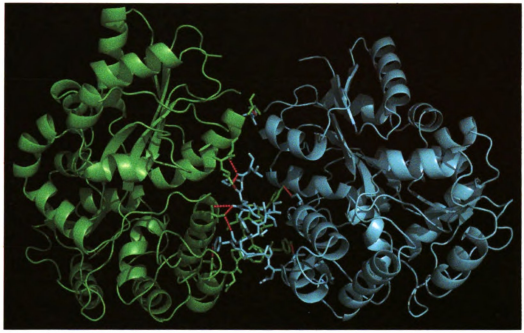

Figure 4.11 continued

B

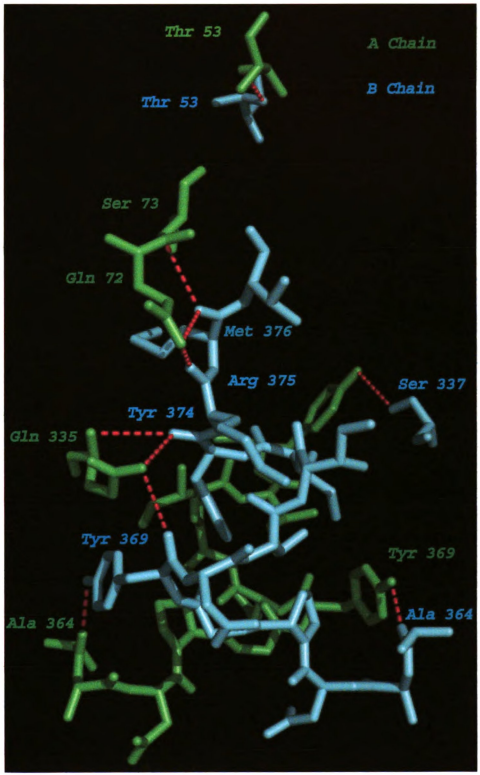

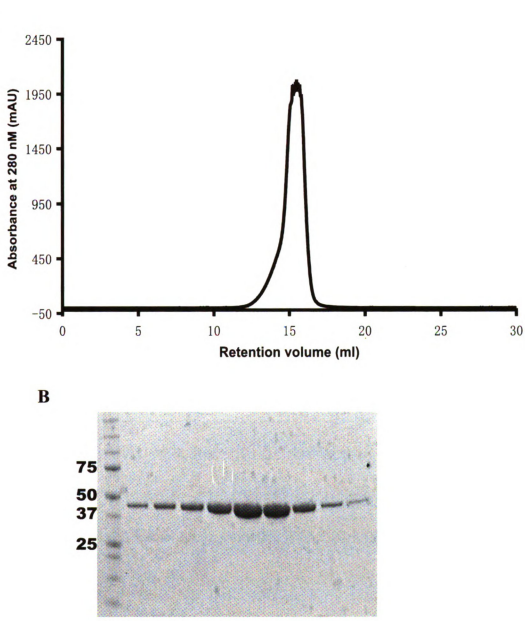

Figure 4.12: Size exclusion chromatography of MBP-(P)RR19. (A) Chromatography. The major peak is corresponding to a size of 42 kDa. (B) SDS-PAGE of fractions of the major peak showed in A.

4.3.2.3 Crystal structure

4.3.2.3.1 Overall structure

The MBP-(P)RR19 crystals with and without maltose bound have the space group symmetry $P2_12_12_1$. The MBP-(P)RR19 apo-crystals have the unit-cell parameters a = 47.78, b = 112.70, c = 175.11 Å; the MBP-(P)RR19 crystals with maltoses have the unit-cell parameters a = 41.95 , b = 96.78, c = 191.45. A close examination of the unit cell parameters clear suggests that the two crystal forms are probably not identical, perhaps arising from different molecular packings, despite the fact that they have the same space group symmetry.

Table 4.1: Data-collection and processing statistics.

Crystals	without maltose	with maltose
Space group	$P2_12_12_1$	$P2_12_12_1$
Unit-cell parameters		
a(Å)	47.78	41.95
b(Å)	112.70	96.78
c(Å)	175.11	191.45
$\alpha = \beta = \gamma$ (°)	90	90
No. of molecules per ASU	2	2
Data collection		
Wavelength (Å)	0.979338	0.979338
Resolution (Å)	50.0–2.0	50.0-1.996
Unique reflections	61694	50067
Multiplicity	6.2	6.1
Completeness (%)	97.8 (98.9)	95.3(85.6)
Refinement statistics		
R work	0.19	0.22
R free	0.26	0.29
B factor	26.79	34.52
R.m.s.d. bond lengths (Å)	0.018	0.024
R.m.s.d. bond angles (°)	2.13	1.58

Both structures were solved by molecular replacement and refined to 2.0 Å resolution (Fig. 4.7 and 4.8). The statistics of the crystallographic data were summarized in Table 4.1. There are two chains in the asymmetric unit for both structures. In the starting model, residues 1 to 363 are the MBP, and residues 364 and 365 are the short alanine linker. The last 19 amino acids of the (P)RR cytoplasmic tail start from residue 366. The final model of the apo-MBP-(P)RR19 contained 748 amino-acid residues including 373 amino acids in chain A and 375 amino acids in chain B, 712 water molecules, and 11 magnesium ions per asymmetric unit. The electron-density for residue 1 of MBP was poor in both chains such that these residues could not be modeled into the structure. The final model of the

ligand-bound MBP-(P)RR19 is similar and contains 751 amino-acid residues including 375 amino acids in chain A and 376 amino acids in chain B, 683 water molecules, and 3 magnesium ions per asymmetric unit. The first residue in chain A and the first two residues in chain B of the N-terminus of MBP were not included in the model due to weak electron-densities. The ligand-bound model contained one maltose molecule in each of the active sites of MBP per asymmetric unit. Only the first thirteen and eleven residues of the (P)RR cytoplasmic tail were observed in the chain B and A, respectively, of the ligand-bound protein, and the first eleven and nine residues were observed in chain B and chain A of the apo-protein, respectively (Fig. 4.9). The rest residues are disordered and could not be included in either model. It is likely that a portion of the C-terminus of the (P)RR cytoplasmic tail is unstructured because the mass spectrometry experiment clearly shows the presence of the 19 amino acids in the fusion protein. Since the (P)RR cytoplasmic tail may interact with multiple proteins in different signal transduction pathways, having an unstructured C-terminus may provide an advantage of interconvertibility for adapting to multiple receptor/signaling molecules. However, the unstructured C-terminus observed from this study does not exclude the possibility that this region may become ordered when stimulated by specific signals such as (pro)renin binding, protein modifications, and protein interactions.

4.3.2.3.2 The molecular packing interaction: evidence for a (P)RR induced dimer

What was unusual about the two MBP-(P)RR19 crystal structures is that the dimeric

arrangement of the MBP molecules within the asymmetric unit. The formation of "symmetric oligomers" in crystals is not uncommon and may arise coincidently from the crystal symmetry. To verify whether the "symmetric oligomers" arise from interactions between the molecules in the asymmetric unit and not from crystal symmetry, a closer look at the molecular packing was done.

Using the *LSQKAB* program from *CCP4* (1994), two monomers in asymmetric unit were superimposed by rotating one monomer through a series of angles. When using spherical polar coordinates *omega*, *phi*, *chi* to achieve the superposition, the *chi* angle can be used to detect near perfect rotations (e.g., ~180° is a 2-fold or ~120° is a 3-fold). For the apo-protein model, when chain A was superimposed onto chain B, the *chi* angle was, 176.31°, a value near 180°. For the ligand-bound model, the superimposition of chain A onto chain B yielded a *chi* angle of 179.7°. Since the angle between rotation axis and centroid vector is near to 90° (88.69° and 90.92° for apo- and ligand-bound models, respectively), the superimposition most likely represented a pure rotation. These analyses support the contention that the two molecules in the asymmetric unit are forming a molecular dimer.

MBP exist as a monomer, in solution and in crystal structures, unless the assembly into higher order oligomers is induced by a protein fusion. Interfacial contacts in asymmetric unit of some dimeric or trimeric forms of MBP-fusions were predominately driven by target proteins instead of MBPs (Kobe, Center et al. 1999; Liu, Manna et al. 2001). Since the MBP-(P)RR19 forms dimer, it led to the hypothesis that the 19 amino acid tail

promotes the dimerization of the fusion protein, and the major dimeric contacts should be found in the peptide regions. Using the *PISA* online sever (http://www.ebi.ac.uk/msd-srv/prot_int/pistart.html), protein interfaces analyses showed that hydrogen bonds formed by the peptide amino acids, especially by the Tyr369 and Tyr374, predominated in the dimer interface. No water-mediated hydrogen bonds, salt bridges, disulfide bonds, or covalent bonds were observed in the *PISA* interface analyses.

For the apo-MBP-(P)RR19, the dimeric interface resulted in 756.3 Å of buried surface area, which corresponds to 4.7% of monomeric surface. The solvation free energy gain upon formation of the dimeric interface is –11.2 kcal/M, indicating an energy favorable state. Nine potential hydrogen bonds were found between the two monomers at the interface, all of which are mediated by residues in (P)RR19 peptide with the Tyr 369 and Tyr 374 involved in seven of them (Fig. 4.10 and Table 4.2A). The side chain OH group of Tyr 369 from each chain protruded from the peptide main chain and interact with the main chain O atom of the linker Ala 364 from the other chain. The side chain OH group of Tyr 374 in chain B is hydrogen bonding with the main chain O atom of Gly 368, the main chain N atoms of Asp 370, Ser 371, and Ile 372, respectively. Since the side chain of Tyr 374 in chain A was not included in the model due to weak electron-density map, similar interaction was not observed in chain B. In the interface, contact is also made between the main chain O atom of Ile 372 and the Nε2 atom of Gln 335, and between the main chain N atom of Gly 368 and the main chain O atom of Pro367.

For the ligand-bound MBP-(P)RR19, the dimeric interface caused a 1148.9 Å of buried

area which corresponds to 7.3% of monomeric surface. The solvation free energy gain upon formation of the dimeric interface is –17.1 kcal/M, indicating an energy favorable state. The ligand-bound structure had the similar overall interface arrangement where the major potential contacts were mediated by the (P)RR19 peptide residues, particularly by the Tyr 369 and Tyr 374 (Fig. 4.11 and Table 4.2B). Similar to the apo-protein structure, the side chain OH group of Tyr 369 from each chain protruded from the peptide main chain and interacted the main chain O atom of the linker Ala 364 from the other chain. Residue Thr53 in chain A is 29 Å away from its counterpart in chain B in the "open" apo-protein structure. With ligands bound, the MBP represents a "closed" structure, which brings the two Thr53 residues together to form a hydrogen bond.

The (P)RR19 peptide residues have more contact with the MBP in the more compact "closed" form than in the "open" form. Several hydrogen pairs between the (P)RR19 peptide and MBP occur in dimer interface: the O atom of Thr377 and the main chain O atom of Gln72, the main chain O atom of Arg 375 and the Nε2 atom of Gln 72, the main chain O atom of Met376 and the main chain N atom of the Ser73, and the main chain O atom of Tyr 369 and the side chain Nε2 atom of Gln 335. Although the Tyr 374 is involved in formation of hydrogen bonds, the bonding pattern is different than that of the apo-protein. In chain A, the OH group of Tyr374 interacts with the Oγ atom of Ser337 of chain B. Surprisingly, the main chain O atom of Tyr 374 in chain B hydrogen bonds with the main chain N atom and side chain Nε2 atom of Gln 335, but the hydroxyl of Tyr 374 makes no obvious interactions with other side chains. The distances between the OH

group of Tyr 374 in chain B with other side chains no shorter than 5 Å. However, the electron density around Tyr374 in chain B is very weak compared to that of other tyrosines observed in the structure. It is therefore possible that these interactions were not observed due to the poor quality of the electron density in this region. The compact "closed" MBP structure then yields contradictory observations: the MBP-(P)RR19 dimer is more "symmetric" overall, but "closed" MBP structure provides less space in between two monomers, which may cause some localized disorder blurring the detailed conformation of the peptide.

The size exclusion chromatography of the MBP-(P)RR19 showed a peak that was estimated to about 42 kDa (Fig. 4.12), indicating that the protein exists as a monomer in solution. Since the protein concentration for crystallization is much higher than that in solution for gel filtration, it is possible that the dimerization of the MBP-(P)RR19 is concentration-dependent. In addition, if the hydrophobic interactions are the major force bringing two monomers together, some fraction of dimeric MBP-(P)RR19 should exist in solution. Therefore, the monomeric form in solution excludes the possibility that the dimers observed in the crystal structures were caused by the pure hydrophobic interactions in the peptide region.

Table 4.2 A: Potential hydrogen bonds formed between two MBP-(P)RR19 monomers of apo-MBP-(P)RR19. The online server EBI Pisa (http://www.ebi.ac.uk/msd-srv/prot_int/pistart.html) and software PyMOL was used for find these contacts.

Molecule 1	Distance (Å)	Molecule 2
B: Gln 335 (Nε2)	3.2	A: Ile 372 (O)
B: Gln 335 (Nε2)	3.3	A: Ala 374 (O)
B: Tyr 369 (OH)	2.6	A: Ala 364 (O)
B: Tyr 374 (OH)	2.6	A: Gly 368 (O)
B: Ala 364 (O)	2.4	A: Tyr 369 (OH)
B: Tyr 374 (OH)	3.5	A: Asp 370 (N)
B: Tyr 374 (OH)	3.2	A: Ser 371 (N)
B: Tyr 374 (OH)	3.8	A: Ile 372 (N)
B: Pro 367 (O)	3.1	A: Gly368 (N)

Table 4.2 A: Potential hydrogen bonds formed between two MBP-(P)RR19 monomers of maltose-bound-MBP-(P)RR19. Please refer **A** for legend.

Molecule 1	Distance (Å)	Molecule 2
B: Thr 53 (Oγ)	3.7	A: Thr 53 (Oγ)
B: Thr 377 (Oγ)	3.8	A: Gln 72 (O)
B: Tyr 369 (OH)	2.7	A: Ala 364 (O)
B: Ser 337 (Oγ)	3.8	A: Tyr 374 (OH)
B: Arg 375 (O)	3.2	A: Gln 72 (Nε2)
B: Met 376 (O)	3.7	A: Ser 73 (N)
B: Tyr 374 (O)	3.4	A: Gln 335 (Nε2)
B: Ala 364 (O)	2.6	A: Tyr 369 (OH)
B: Tyr 374 (O)	3.8	A: Gln 335 (N)
B: Tyr 369 (O)	3.7	A: Gln 335 (Nε2)

4.3.2.3.3 Description of the (P)RR cytoplasmic tail structure

The MBP-(P)RR19 contains the full 19 amino acids of the cytoplasmic tail as determined by the mass spectrometry sequencing analysis (Fig. 4.4). In the models, the first 13 and 11 residues out of 19 were observed in the ligand-bound structure chains B

and A, respectively; in the apo-structure, the first 11 and 9 residues were clearly observed in chains B and chain A, respectively. Absence of the electron density for the remaining residues indicates that this region of the cytoplasmic tail may be disordered. The observed residues have a structure of relatively flexible loop without obvious secondary structure (Fig. 4.13). The linker region of the Ala364 and Ala365 is involved in formation of the C-terminus of the helix of the MBP. The loop region from residue Asp366 to Tyr369 is relatively smooth and straight. A turn occurs between the Tyr369 and the Asp 370 and leads into a spiral-like structure from residue Asp 370 through Arg 375. A few hydrogen bonds were formed among the residues in this region. Then the loop straightens out again and extends into the space in between the two monomers until no more electron density is observed.

Figure 4.13: Structure of the (P)RR cytoplasmic tail. The residual 366-378 is shown from top to bottom.

The crystal structures of the MBP-(P)RR19 both in with and without maltose provide a

overview of the protein structure of the (P)RR cytoplasmic tail. The dimeric nature of the complex in the crystal, for both forms, indicate that the (P)RR19 is the driving force for the dimerization of monomeric MBP. Although in the maltose-bound form, the Thr 53 was also involved in interactions at interface, the predominate interactions were made by hydrogen bonds from residues in the (P)RR19 peptide to MBP. These results suggested a possible role of the (P)RR19 in the dimerization of full-length (P)RR protein, since the (P)RR was reported to exist as a dimer (Schefe, Menk et al. 2006). Without additional experimental evidence on other regions of the (P)RR, we cannot not yet conclude about structural roles of the N-terminus and transmembrane domain. However, the structural results of the (P)RR19 suggested that besides interacting with other signaling molecules, the cytoplasmic tail may at least partially involved in protein oligomerization.

4.3.2.3.4 N-terminal fusion

Since no more than 13 out of 19 amino acids of the (P)RR cytoplasmic tail were observed in the MBP C-terminus fusion, it is necessary to consider other fusion methods to get a better structure for (P)RR19. Although it is likely that some of the residues in (P)RR19 are flexible and do not form an ordered structure, fusing the 19 amino acids to the N-terminus of the MBP may be an alternative way to test it.

The annealing DNA cloning method was used for the 19 amino acids fusion to the MBP N-terminus. Since there is 6×his tag in the C-terminus of the MBP in the expression vector, the Ni-NTA column was used for initial protein purification. Further ion exchange

purification showed the protein was eluted at the same ionic strength range of 0.25 M to 0.35 M NaCl and the protein was purified to homogeneity.

Unfortunately, there was no crystals have yet been obtained in conditions with or without maltose. One possible reason may be that the C-terminus of the 19 amino acids is flexible and causes an energy barrier for crystallization when it is in between its N-terminus and the MBP N-terminus. Since the N-terminus of the MBP is crucial to the protein folding, it is also possible that the N-terminus fusion disrupt the MBP protein structure and further impact the crystallization. Currently, to my knowledge, no crystal structure of fusion protein in N-terminus of MBP was reported indicating that N-terminus fusion may not be an applicable method for protein crystallization aid.

4.4 Cloning and expression of the promyelocytic zinc finger protein (PLZF)

4.4.1 Experimental procedures

4.4.1.1 DNA Cloning of PLZF and truncated proteins - The DNA encoding for the full-length PLZF, the BTB domain (1-132aa), the center domain (137-377aa), and the zinc fingers domain (378-673aa) were amplified from cDNA by PCR. The PCR amplification was comprised of 35 cycles of denaturing at 94°C for 30 sec, annealing at 55°C for 45 sec, and elongation at 72°C for 2 min and 10 sec for the full-length PLZF; 40 sec for the BTB domain; 1 min for the center domain; and 1 min 30 sec for the zinc

fingers domain, followed by 72°C for 10 min. The PCR products were purified by QIAquick PCR purification kit (QIAGEN), and digested with restriction enzymes BamHI and XhoI for ligation with pRMG-*eco*MBP vector, and NcoI and XhoI for pLW01 vector. Ligation products were transformed into *E.coli* DH5α competent cells. Positive clones growing from LB plates containing 100 μg/ml ampicillin were picked, and plasmid DNAs were isolated and sequenced.

4.4.1.2 Protein Expression and Purification - The protein expression procedures were same as described for that of DLP-1 in chapter 2, except that the *E. coli* BL21 (DE3) was used as expression host cells. To purify the PLZF full-length and truncated proteins, the cell pellets were re-suspended in Buffer A (50 mM sodium phosphate, 300 mM NaCl, 0.1 mM EDTA, pH 8.0). After sonication, the crude cell extract was centrifuged at 4℃ for 20 min at 12,000×g. The supernatant was loaded onto a pre-equilibrated column containing 20 ml Ni-NTA agarose slurry. The column was washed with buffer B (50 mM sodium phosphate, 300 mM NaCl, 20 mM imidazole, pH 8.0). Protein bound column was eluted by Buffer C (50 mM sodium phosphate, 300 mM NaCl, 200 mM imidazole, pH 8.0). The protein eluates were pooled and concentrated to 1 ml by Amicon ultra centrifugal filter molecular cutoff (Millipore).

Ion exchange chromatography was performed to further purify target proteins and remove contaminants. The pooled and concentrated eluates from Ni-NTA were loaded onto a 1 ml HiTrap Q ion exchanger (Amersham Biosciences) pre-equilibrated with

Buffer D (20 mM Tris-HCl, pH 8.5). Protein was eluted off the column with a linear concentration gradient of NaCl from 0 to 1 M, at a flow rate of 1 ml/min. The peak fractions containing highly purified target protein were pooled and concentrated. Protein concentration was estimated by Bradford assay using bovine serum albumin as standard.

Figure 4.14: Purification of PLZF fragments by Ni-NTA column. (A) Full-length PLZF. (B) BTB domain. (C) RD2 domain. (D) Zinc finger domain. Protein molecular weigh marker was labeled at left (kDa). MW, Molecular weight standard; Wh, Whole cells; LSN, Supernatant of low-speed centrifugation; FT, Flow through fraction; Wa, Wahsing fraction; E1 and E2, Elution fractions.

A

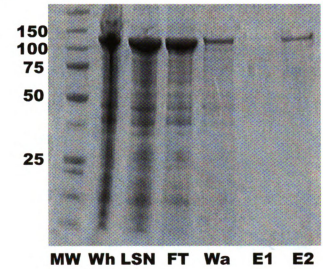

B

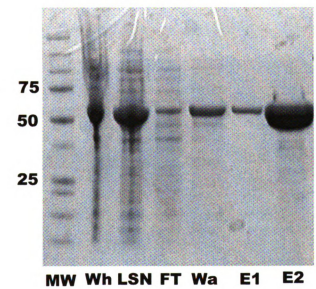

Figure 4.14 continued

C

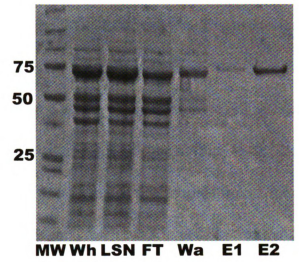

D

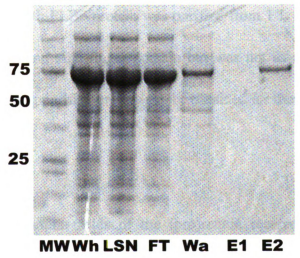

4.4.2 Results and discussion

4.4.2.1 Protein expression and purification

The full-length PLZF, the BTB, RD2, and zinc finger domains were cloned into the pRMG-*eco*MBP vector with restriction enzyme sites of BamHI and XhoI. With expression and purification conditions optimized as described in chapter 2 for DLP-1, all fusion proteins were purified by Ni-NTA column (Fig. 4.14). The BTB domains had the highest yield with greater than 20 mg protein purified from 1 L culture. However, for the full-length PLZF, although the protein was in soluble fraction (supernatant fraction of low-speed centrifugation), most protein did not bind the Ni-NTA column, indicating that the protein may be moderately aggregated and/or the 6×his is not accessible. Only about less than 1 mg full-length PLZF protein was purified from 1 L culture. Similar problem occurred for the RD2 and zinc finger domain but was not as severe as the full-length protein and about 3-4 mg purified protein can be obtained for these two fragments.

4.5 Conclusion

The C-terminal 19 amino acids of the (pro)rennin receptor corresponding to the cytoplasmic tail were fused into the C-terminus of *E. coli* maltose binding protein (MBP), creating the MBP-(P)RR19 fusion protein. The chimera was expressed in *E. coli* and purified to homogeneity. Protein crystals that are both in presence and in absence of the MBP ligand, maltose, were obtained and X-ray diffraction data were collected. The crystals were diffracted to a resolution of up to 1.996 Å and belong to the space group

$P2_12_12_1$. Depending on the presence or absence of maltose, the crystals have significantly different unit-cell dimensions and molecular packing arrangements for the MBP-(P)RR19 fusion protein.

Structures in both forms were determined by molecular replacement using the available MBP structures as phasing models. Despite of significantly different unit-cell dimensions and molecular packing arrangements, there are two monomers in asymmetric unit for both structures. The first 13 and 11 residues of the (P)RR cytoplasmic tail were included in chain B and chain A in the ligand-bound model, respectively. And the first 11 and 9 residues were observed in the apo-structure chain B and chain A, respectively. Absence of the strong electron density for the remaining residues suggested that this region of the cytoplasmic tail may be disordered. The available residues showed a structure of relatively flexible loop without obvious helices or stands presented. The major non-crystallographic interactions were predominated by the residues in the cytoplasmic tail, particularly by the Tyr 369 and Tyr 374, suggesting roles of the cytoplasmic tail in protein oligomerization.

The PLZF full-length and individual domains have been cloned into expression vectors by fusing the *E. coli* MBP in their N-terminus as expression aids. These PLZF species have been expressed in *E. coli* and have been purified. The protein-protein interactions of the PLZF individual domains with the (P)RR cytoplasmic tail have been investigated. Please refer to "Appendix" for preliminary binding results.

References

(1994). "The CCP4 suite: programs for protein crystallography." Acta Crystallogr D Biol Crystallogr **50**(Pt 5): 760-3.

Brummelkamp, T. R., R. Bernards and R. Agami (2002). "A system for stable expression of short interfering RNAs in mammalian cells." Science **296**(5567): 550-3.

Duan, X. and F. A. Quiocho (2002). "Structural evidence for a dominant role of nonpolar interactions in the binding of a transport/chemosensory receptor to its highly polar ligands." Biochemistry **41**(3): 706-12.

Emsley, P. and K. Cowtan (2004). "Coot: model-building tools for molecular graphics." Acta Crystallogr D Biol Crystallogr **60**(Pt 12 Pt 1): 2126-32.

Kobe, B., R. J. Center, B. E. Kemp and P. Poumbourios (1999). "Crystal structure of human T cell leukemia virus type 1 gp21 ectodomain crystallized as a maltose-binding protein chimera reveals structural evolution of retroviral transmembrane proteins." Proc Natl Acad Sci U S A **96**(8): 4319-24.

Liu, Y., A. Manna, R. Li, W. E. Martin, R. C. Murphy, A. L. Cheung and G. Zhang (2001). "Crystal structure of the SarR protein from Staphylococcus aureus." Proc Natl Acad Sci U S A **98**(12): 6877-82.

Otwinowski, Z. and W. Minor (1997). "Processing of X-ray diffraction data collected in oscillation mode." Macromolecular Crystallography, Pt A **276**: 307-326.

Quiocho, F. A., J. C. Spurlino and L. E. Rodseth (1997). "Extensive features of tight oligosaccharide binding revealed in high-resolution structures of the maltodextrin transport/chemosensory receptor." Structure **5**(8): 997-1015.

Schefe, J. H., M. Menk, J. Reinemund, K. Effertz, R. M. Hobbs, P. P. Pandolfi, P. Ruiz, T. Unger and H. Funke-Kaiser (2006). "A novel signal transduction cascade involving direct physical interaction of the renin/prorenin receptor with the transcription factor promyelocytic zinc finger protein." Circ Res **99**(12): 1355-66.

Winn, M. D., M. N. Isupov and G. N. Murshudov (2001). "Use of TLS parameters to model anisotropic displacements in macromolecular refinement." Acta Crystallogr D Biol Crystallogr **57**(Pt 1): 122-33.

CHAPTER 5

Future directions

The biochemical and structural properties of DLP-1 and selected mutants have been characterized, and the major functions of individual domains on GTPase activities, intra- and intermolecular interactions, and membrane targeting have been identified or confirmed in this thesis. However, more direct evidence from high-resolution crystal structures is needed to elucidate functions of DLP-1 in more detail and reveal the molecular mechanisms of mitochondrial fission and fusion. This need for structural information of DLP-1 and MFNs has become a much more critical issue. As protein-engineering methods have not yet yielded successful routes to solve DLP-1 and MFN-1 structure, alternative strategies and methods will need to be explored in the future to obtain protein crystals.

5.1 Alternative protein expression systems and crystallization screening methods

DLP-1 and MFNs, which are both eukaryotic proteins, were expressed in *E. coli* mostly for easy manipulation and low-cost purposes. Although it is common to express eukaryotic proteins for structural studies in prokaryotic expression systems, alternative eukaryotic expression systems may be more appropriate for DLP-1 and MFNs, particularly for ensuring proper folding and membrane insertion. As MFN-1 was expressed mainly as inclusion bodies in *E. coli*, other expression systems may improve the yield of folded and soluble protein. However, since the overexpression of DLP-1 or MFN-1 in yeast, insect, or mammalian cells might seriously disrupt mitochondrial fission or fusion, it may markedly compromise cell viability. Baculoviral-driven expression in

insect cells might be a suitable alternative expression system as the infected insect cells need to survive for 24-72 hours during a normal protein expression experiment.

DLP-1 is a membrane-interacting protein, which probably requires lipids to stabilize its local structures such as the PH-like domain. Therefore, crystallization screening with a much wider range of detergents may be necessary to trap an ordered DLP-1 protein conformation that promotes crystallization. Although non-ionic detergents such as dodecyl maltoside, decyl maltoside, and octyl glucoside have been attempted, there are many more nonionic and zwitterionic detergents that might lead to DLP-1 crystallization. Usually detergents screening is performed after initial hits were found to optimize further the crystal growth conditions. This scenario is the most efficient as it minimizes the screening strategies, which in turn reduces the workload. Since there are currently no potential crystallization condition found for DLP-1 or DLP-1 fragments, and DLP-1 fusions, large scale brute-force screening with 10-20 different detergent types may need to be performed. The up-coming acquisition of a new crystallization robot will make this rather daunting task much more tractable.

For the purified MFNs, an alternative membrane protein crystallization method, lipidic cubic phase, also called "in meso" method, can be used. Several membrane proteins have been crystallized for high-resolution structure determination by using this method (Kolbe, Besir et al. 2000; Luecke, Schobert et al. 2001; Gordeliy, Labahn et al. 2002; Katona, Andreasson et al. 2003; Johansson, Wohri et al. 2009). In the cubic phase, the lipidic compartments are interpenetrated by a freely communicating system of aqueous channels

(Landau and Rosenbusch 1996). Although the exact mechanism of "in meso" crystallization remains unclear, the cubic phase may provide a lipid bilayer that is an environment similar to the biological membranes. The membrane protein may reconstitute into the bilayer and crystals nucleate and grow upon addition of precipitants (Caffrey 2003). In addition, several recently crystallized membrane proteins have led the lipidic bicelle as another alternative tool for crystallizing MFNs (Faham, Boulting et al. 2005; Rasmussen, Choi et al. 2007; Luecke, Schobert et al. 2008; Ujwal, Cascio et al. 2008). The bicelle method could be considered a combination of the cubic phase and the traditional detergent crystallization method. The bicelles are generated by mixing lipids dimyristoyl phosphatidylcholine (DMPC) or ditridecanoyl phosphatidylcholine (DTPC) with the detergent CHAPSO or nonyl maltoside (Johansson, Wohri et al. 2009). Like the cubic phase, the bicelles provide a more bilayer-like environment for membrane proteins than detergents. Given the relatively large amount of refolded, recombinant MFN-1 that we have in hand, we intend to use the lipidic cubic phase and the bicelle methods to screen for crystallization conditions for MFN-1.

5.2 Further structural studies on (P)RR and roles of tyrosines on the cytoplasmic tail in protein oligomerization and signal transduction

The crystal structure of the cytoplasmic tail of (P)RR has been determined using MBP fusion method and part of its function has been suggested by the structure. However, the cytoplasmic domain is only a small portion of (P)RR. We need to determine more of the

(P)RR structure to elucidate more function and roles of (P)RR in blood pressure regulation and organelle functions. Therefore, optimization of the crystal growth conditions for the full-length (P)RR aiming to obtain better crystals suitable for X-ray diffraction would be one of the major future directions. Since the (P)RR is an integral membrane protein, screening different detergents may help shield hydrophobic regions and produce less aggregated species and also promote better crystals. Meanwhile, the lipidic cubic phase and bicelle method are applicable for (P)RR. In addition, if the poor crystals of (P)RR are due to disordered or flexible regions, protein engineering may be used to explore compact functional domains for structural studies. Currently, the most promising fragments we have been considering would be the N-terminal extracelluar domain.

Although some structural information was obtained for the MBP-(P)RR19 crystals, the last six residues of the cytoplasmic tail were not observed in the electron-density maps. To resolve the disordered regions in the MBP-(P)RR19 crystals, we are now exploring the use of alternative crystal freezing methods such as dehydration and reannealing to reduce conformational flexibility of the protein termini in the MBP-(P)RR19 fusion. In addition, since the two tyrosines were observed in the crystal structures of the MBP-(P)RR19 to be important for dimeric interactions, more evidence from functional and genetic studies such as site-directed mutagenesis may be pursued to support the functions of the two tyrosines in protein oligomerization. For example, the protein oligomeric state can be investigated be size exclusion chromatographic and

crystallographic studies after the tyrosines are mutated to functional-unrelated residues. Also, (P)RR with these two tyrosines mutated can be transformed into mammalian cells to study their roles in signal transduction by measuring the levels of activations of the downstream signal pathways.

References

Caffrey, M. (2003). "Membrane protein crystallization." J Struct Biol **142**(1): 108-32.

Faham, S., G. L. Boulting, E. A. Massey, S. Yohannan, D. Yang and J. U. Bowie (2005). "Crystallization of bacteriorhodopsin from bicelle formulations at room temperature." Protein Sci **14**(3): 836-40.

Gordeliy, V. I., J. Labahn, R. Moukhametzianov, R. Efremov, J. Granzin, R. Schlesinger, G. Buldt, T. Savopol, A. J. Scheidig, J. P. Klare and M. Engelhard (2002). "Molecular basis of transmembrane signalling by sensory rhodopsin II-transducer complex." Nature **419**(6906): 484-7.

Johansson, L. C., A. B. Wohri, G. Katona, S. Engstrom and R. Neutze (2009). "Membrane protein crystallization from lipidic phases." Curr Opin Struct Biol **19**(4): 372-8.

Katona, G., U. Andreasson, E. M. Landau, L. E. Andreasson and R. Neutze (2003). "Lipidic cubic phase crystal structure of the photosynthetic reaction centre from Rhodobacter sphaeroides at 2.35A resolution." J Mol Biol **331**(3): 681-92.

Kolbe, M., H. Besir, L. O. Essen and D. Oesterhelt (2000). "Structure of the light-driven chloride pump halorhodopsin at 1.8 A resolution." Science **288**(5470): 1390-6.

Landau, E. M. and J. P. Rosenbusch (1996). "Lipidic cubic phases: a novel concept for the crystallization of membrane proteins." Proc Natl Acad Sci U S A **93**(25): 14532-5.

Luecke, H., B. Schobert, J. K. Lanyi, E. N. Spudich and J. L. Spudich (2001). "Crystal structure of sensory rhodopsin II at 2.4 angstroms: insights into color tuning and transducer interaction." Science **293**(5534): 1499-503.

Luecke, H., B. Schobert, J. Stagno, E. S. Imasheva, J. M. Wang, S. P. Balashov and J. K. Lanyi (2008). "Crystallographic structure of xanthorhodopsin, the light-driven proton pump with a dual chromophore." Proc Natl Acad Sci U S A **105**(43): 16561-5.

Rasmussen, S. G., H. J. Choi, D. M. Rosenbaum, T. S. Kobilka, F. S. Thian, P. C. Edwards, M. Burghammer, V. R. Ratnala, R. Sanishvili, R. F. Fischetti, G. F. Schertler, W. I. Weis and B. K. Kobilka (2007). "Crystal structure of the human beta2 adrenergic G-protein-coupled receptor." Nature **450**(7168): 383-7.

Ujwal, R., D. Cascio, J. P. Colletier, S. Faham, J. Zhang, L. Toro, P. Ping and J. Abramson (2008). "The crystal structure of mouse VDAC1 at 2.3 A resolution reveals mechanistic insights into metabolite gating." Proc Natl Acad Sci U S A **105**(46): 17742-7.

CHAPTER 5

Future directions

The biochemical and structural properties of DLP-1 and selected mutants have been characterized, and the major functions of individual domains on GTPase activities, intra- and intermolecular interactions, and membrane targeting have been identified or confirmed in this thesis. However, more direct evidence from high-resolution crystal structures is needed to elucidate functions of DLP-1 in more detail and reveal the molecular mechanisms of mitochondrial fission and fusion. This need for structural information of DLP-1 and MFNs has become a much more critical issue. As protein-engineering methods have not yet yielded successful routes to solve DLP-1 and MFN-1 structure, alternative strategies and methods will need to be explored in the future to obtain protein crystals.

5.1 Alternative protein expression systems and crystallization screening methods

DLP-1 and MFNs, which are both eukaryotic proteins, were expressed in *E. coli* mostly for easy manipulation and low-cost purposes. Although it is common to express eukaryotic proteins for structural studies in prokaryotic expression systems, alternative eukaryotic expression systems may be more appropriate for DLP-1 and MFNs, particularly for ensuring proper folding and membrane insertion. As MFN-1 was expressed mainly as inclusion bodies in *E. coli*, other expression systems may improve the yield of folded and soluble protein. However, since the overexpression of DLP-1 or MFN-1 in yeast, insect, or mammalian cells might seriously disrupt mitochondrial fission or fusion, it may markedly compromise cell viability. Baculoviral-driven expression in

insect cells might be a suitable alternative expression system as the infected insect cells need to survive for 24-72 hours during a normal protein expression experiment.

DLP-1 is a membrane-interacting protein, which probably requires lipids to stabilize its local structures such as the PH-like domain. Therefore, crystallization screening with a much wider range of detergents may be necessary to trap an ordered DLP-1 protein conformation that promotes crystallization. Although non-ionic detergents such as dodecyl maltoside, decyl maltoside, and octyl glucoside have been attempted, there are many more nonionic and zwitterionic detergents that might lead to DLP-1 crystallization. Usually detergents screening is performed after initial hits were found to optimize further the crystal growth conditions. This scenario is the most efficient as it minimizes the screening strategies, which in turn reduces the workload. Since there are currently no potential crystallization condition found for DLP-1 or DLP-1 fragments, and DLP-1 fusions, large scale brute-force screening with 10-20 different detergent types may need to be performed. The up-coming acquisition of a new crystallization robot will make this rather daunting task much more tractable.

For the purified MFNs, an alternative membrane protein crystallization method, lipidic cubic phase, also called "in meso" method, can be used. Several membrane proteins have been crystallized for high-resolution structure determination by using this method (Kolbe, Besir et al. 2000; Luecke, Schobert et al. 2001; Gordeliy, Labahn et al. 2002; Katona, Andreasson et al. 2003; Johansson, Wohri et al. 2009). In the cubic phase, the lipidic compartments are interpenetrated by a freely communicating system of aqueous channels

(Landau and Rosenbusch 1996). Although the exact mechanism of "in meso" crystallization remains unclear, the cubic phase may provide a lipid bilayer that is an environment similar to the biological membranes. The membrane protein may reconstitute into the bilayer and crystals nucleate and grow upon addition of precipitants (Caffrey 2003). In addition, several recently crystallized membrane proteins have led the lipidic bicelle as another alternative tool for crystallizing MFNs (Faham, Boulting et al. 2005; Rasmussen, Choi et al. 2007; Luecke, Schobert et al. 2008; Ujwal, Cascio et al. 2008). The bicelle method could be considered a combination of the cubic phase and the traditional detergent crystallization method. The bicelles are generated by mixing lipids dimyristoyl phosphatidylcholine (DMPC) or ditridecanoyl phosphatidylcholine (DTPC) with the detergent CHAPSO or nonyl maltoside (Johansson, Wohri et al. 2009). Like the cubic phase, the bicelles provide a more bilayer-like environment for membrane proteins than detergents. Given the relatively large amount of refolded, recombinant MFN-1 that we have in hand, we intend to use the lipidic cubic phase and the bicelle methods to screen for crystallization conditions for MFN-1.

5.2 Further structural studies on (P)RR and roles of tyrosines on the cytoplasmic tail in protein oligomerization and signal transduction

The crystal structure of the cytoplasmic tail of (P)RR has been determined using MBP fusion method and part of its function has been suggested by the structure. However, the cytoplasmic domain is only a small portion of (P)RR. We need to determine more of the

(P)RR structure to elucidate more function and roles of (P)RR in blood pressure regulation and organelle functions. Therefore, optimization of the crystal growth conditions for the full-length (P)RR aiming to obtain better crystals suitable for X-ray diffraction would be one of the major future directions. Since the (P)RR is an integral membrane protein, screening different detergents may help shield hydrophobic regions and produce less aggregated species and also promote better crystals. Meanwhile, the lipidic cubic phase and bicelle method are applicable for (P)RR. In addition, if the poor crystals of (P)RR are due to disordered or flexible regions, protein engineering may be used to explore compact functional domains for structural studies. Currently, the most promising fragments we have been considering would be the N-terminal extracelluar domain.

Although some structural information was obtained for the MBP-(P)RR19 crystals, the last six residues of the cytoplasmic tail were not observed in the electron-density maps. To resolve the disordered regions in the MBP-(P)RR19 crystals, we are now exploring the use of alternative crystal freezing methods such as dehydration and reannealing to reduce conformational flexibility of the protein termini in the MBP-(P)RR19 fusion. In addition, since the two tyrosines were observed in the crystal structures of the MBP-(P)RR19 to be important for dimeric interactions, more evidence from functional and genetic studies such as site-directed mutagenesis may be pursued to support the functions of the two tyrosines in protein oligomerization. For example, the protein oligomeric state can be investigated be size exclusion chromatographic and

crystallographic studies after the tyrosines are mutated to functional-unrelated residues. Also, (P)RR with these two tyrosines mutated can be transformed into mammalian cells to study their roles in signal transduction by measuring the levels of activations of the downstream signal pathways.

References

Caffrey, M. (2003). "Membrane protein crystallization." J Struct Biol **142**(1): 108-32.

Faham, S., G. L. Boulting, E. A. Massey, S. Yohannan, D. Yang and J. U. Bowie (2005). "Crystallization of bacteriorhodopsin from bicelle formulations at room temperature." Protein Sci **14**(3): 836-40.

Gordeliy, V. I., J. Labahn, R. Moukhametzianov, R. Efremov, J. Granzin, R. Schlesinger, G. Buldt, T. Savopol, A. J. Scheidig, J. P. Klare and M. Engelhard (2002). "Molecular basis of transmembrane signalling by sensory rhodopsin II-transducer complex." Nature **419**(6906): 484-7.

Johansson, L. C., A. B. Wohri, G. Katona, S. Engstrom and R. Neutze (2009). "Membrane protein crystallization from lipidic phases." Curr Opin Struct Biol **19**(4): 372-8.

Katona, G., U. Andreasson, E. M. Landau, L. E. Andreasson and R. Neutze (2003). "Lipidic cubic phase crystal structure of the photosynthetic reaction centre from Rhodobacter sphaeroides at 2.35A resolution." J Mol Biol **331**(3): 681-92.

Kolbe, M., H. Besir, L. O. Essen and D. Oesterhelt (2000). "Structure of the light-driven chloride pump halorhodopsin at 1.8 A resolution." Science **288**(5470): 1390-6.

Landau, E. M. and J. P. Rosenbusch (1996). "Lipidic cubic phases: a novel concept for the crystallization of membrane proteins." Proc Natl Acad Sci U S A **93**(25): 14532-5.

Luecke, H., B. Schobert, J. K. Lanyi, E. N. Spudich and J. L. Spudich (2001). "Crystal structure of sensory rhodopsin II at 2.4 angstroms: insights into color tuning and transducer interaction." Science **293**(5534): 1499-503.

Luecke, H., B. Schobert, J. Stagno, E. S. Imasheva, J. M. Wang, S. P. Balashov and J. K. Lanyi (2008). "Crystallographic structure of xanthorhodopsin, the light-driven proton pump with a dual chromophore." Proc Natl Acad Sci U S A **105**(43): 16561-5.

Rasmussen, S. G., H. J. Choi, D. M. Rosenbaum, T. S. Kobilka, F. S. Thian, P. C. Edwards, M. Burghammer, V. R. Ratnala, R. Sanishvili, R. F. Fischetti, G. F. Schertler, W. I. Weis and B. K. Kobilka (2007). "Crystal structure of the human beta2 adrenergic G-protein-coupled receptor." Nature **450**(7168): 383-7.

Ujwal, R., D. Cascio, J. P. Colletier, S. Faham, J. Zhang, L. Toro, P. Ping and J. Abramson (2008). "The crystal structure of mouse VDAC1 at 2.3 A resolution reveals mechanistic insights into metabolite gating." Proc Natl Acad Sci U S A **105**(46): 17742-7.

Appendix: Preliminary mapping of PLZF fragments binding to the (P)RR cytoplasmic tail

A.1 Methods

Protein-protein interaction assays - The purified PLZF full-length or individual domains were buffer exchanged to buffer A (50 mM sodium phosphate, 300 mM NaCl, pH 8.0) and mixed with purified MBP fusion protein containing the C-terminus 19 amino acids of the (P)RR (MBP-(P)RR19). The mixture was incubated at room temperature for 8 hrs with shaking to allow maximal protein-protein interactions. The 1 ml solution was loaded onto a column containing 2 ml Ni-NTA agarose slurry pre-equilibrated with Buffer B (50 mM sodium phosphate, 300 mM NaCl, 0.1 mM EDTA, pH 8.0) to allow unbound protein to flow through. The column was then washed with buffer C (50 mM sodium phosphate, 300 mM NaCl, 20 mM imidazole, pH 8.0) for over 20 column volume. Proteins bound column was eluted by Buffer D (50 mM sodium phosphate, 300 mM NaCl, 200 mM imidazole, pH 8.0) and the composition of the eluants was analyzed by SDS-PAGE and Western-blot assays.

A.2 Results and discussion

A.2.1 Preliminary results of PLZF binding to the cytoplasmic tail of the (P)RR – The PLZF fragments were tagged with both MBP and 6×his and the (P)RR19 was tagged with only MBP. Therefore, when incubating the binding mixture onto a Ni-NTA column, the

PLZF fragments can be immobilized onto the column, and the MBP-(P)RR19 will flow through unless binds PLZF fragments. The binding can be detected by SDS-PAGE and Western blotting using anti-MBP antibody. Since the full-length PLZF protein was purified to low level that was not sufficient for binding assays, I directly tested the available individual domains for binding to the (P)RR cytoplasmic domain. The SDS-PAGE and Western blotting showed considerable amount of MBP-(P)RR19 presented in the elution fraction of the binding assay together with the PLZF RD2 domain (Fig. A1). Much less amount of MBP-(P)RR19 was observed together with the BTB domain (Fig. A2) and negligible amount was present together with the zinc finger domain (Fig. A3). To eliminate the possibilities that the RD2 domain interact with MBP in the MBP-(P)RR19, MBP protein without any tags on was expressed and purified (Fig. A4). And the MBP did not show any binding to the RD2 domain (Fig. A5). All these results indicated that the RD2 domain is probably the major region of PLZF that is responsible for interactions with the (P)RR cytoplasmic domain.

A.2.2 Future directions – Since there is a Proline-rich region in the PLZF RD2 domain, a motif that is commonly involved in protein-protein interactions, it is possible that this region plays important roles in interacting with the (P)RR cytoplasmic domain. Therefore, in the future, investigating roles of this motif by binding assays with the MBP-(P)RR19 may be necessary.

In addition, co-structure of the PLZF RD2 domain with the cytoplasmic tail of the

(P)RR would provide structural information for the molecular mechanisms of the functions of both the PLZF and the (P)RR. Therefore, co-crystallization of the PLZF RD2 domain (or possibly the BTB domain) with the (P)RR19 peptide may be another future dictions for studies on the (P)RR-PLZF signal transduction pathway.

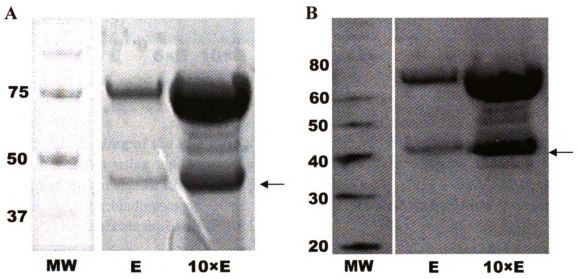

Figure A1: Binding of the PLZF RD2 domain to the MBP-(P)RR19. (A) SDS-PAGE. (B) Western-blot using anti-MBP as primary antibody (New England Biolabs). MW, Molecular weight standard; E, Elution from the binding assay; 10×E, 10 times concentrated elution form the binding assay. Arrows indicate the MBP-(P)RR19.

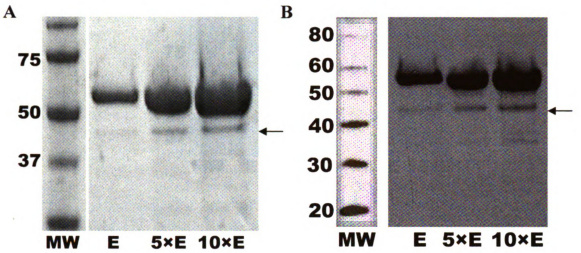

Figure A2: Binding of the PLZF BTB domain to the MBP-(P)RR19. (A) SDS-PAGE. (B) Western-blot using anti-MBP as primary antibody (New England Biolabs). MW, Molecular weight standard; E, Elution from the binding assay; 5×E, 5 times concentrated elution form the binding assay. 10×E, 10 times concentrated elution form the binding assay. Arrows indicate the MBP-(P)RR19.

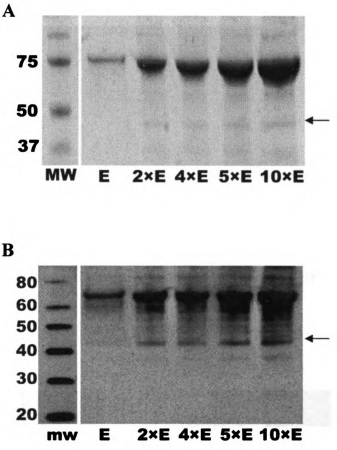

Figure A3: Binding of the PLZF zinc finger domain to the MBP-(P)RR19. (A) SDS-PAGE. (B) Western-blot using anti-MBP as primary antibody (New England Biolabs). MW, Molecular weight standard; E, Elution from the binding assay; 2×E, 4×E, 5×E, and 10×E, 2, 4, 5, and 10 times, respectively, concentrated elution form the binding assay. Arrows indicate the MBP-(P)RR19.

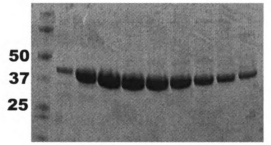

Figure A4: Purification of *E. coli* maltose-binding protein (MBP) by ion exchange chromatography. The elution from amylose column was concentrated and used for further purification on an anionic exchange column. The left lane shows molecular weight standard. Other lanes show the fractions containing purified MBP.

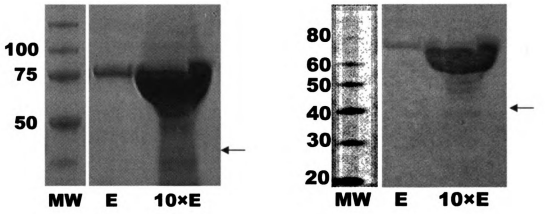

Figure A5: Binding of the PLZF RD2 domain to the MBP. (A) SDS-PAGE. (B) Western-blot using anti-MBP as primary antibody (New England Biolabs). MW, Molecular weight standard; E, Elution from the binding assay; 10×E, 10 times concentrated elution form the binding assay. Arrows indicate the size of MBP.